

**Improving Lithium-Ion Battery Management Systems
Using Equivalent Circuit Models, Cloud Platforms,
and Machine Learning Estimation Techniques**

by

Manh-Kien Tran

A thesis

presented to the University of Waterloo

in fulfillment of the

thesis requirement for the degree of

Doctor of Philosophy

in

Chemical Engineering

Waterloo, Ontario, Canada, 2024

© Manh-Kien Tran 2024

Examining Committee Membership

The following served on the Examining Committee for this thesis. The decision of the Examining Committee is by majority vote.

External Examiner	Professor Sheldon Williamson Electrical, Computer and Software Engineering University of Ontario Institute of Technology
Supervisor	Professor Michael Fowler Chemical Engineering University of Waterloo
Internal Member	Professor Ali Elkamel Chemical Engineering University of Waterloo
Internal Member	Professor Yverick Pascal Rangom Chemical Engineering University of Waterloo
Internal-external Member	Professor XiaoYu Wu Mechanical and Mechatronics Engineering University of Waterloo

Author's Declaration

This thesis consists of material all of which I authored or co-authored: see Statement of Contributions included in the thesis. This is a true copy of the thesis, including any required final revisions, as accepted by my examiners.

I understand that my thesis may be made electronically available to the public.

Statement of Contributions

In Chapter 3, the author was responsible for designing the experiments, developing Matlab scripts, performing data analysis, and preparing the results, graphs, and manuscript. Andre DaCosta and Anosh Mevawalla assisted with the experimental setup and procedure, while Satyam Panchal and Michael Fowler offered advice and guidance on the research [1].

In Chapter 4, the author was responsible for developing the comprehensive equivalent circuit model, designing the experiments, collecting and analyzing data, and preparing the results, graphs, and manuscript. Manoj Mathew and Stefan Janhunen offered assistance with the experimental setup and manuscript reviewing, while Satyam Panchal, Kaamran Raahemifar, Roydon Fraser, and Michael Fowler offered advice and guidance on the research [2].

In Chapter 5, the author was responsible for creating the manuscript synopsis, collecting and analyzing concepts and data from the literature, and primarily writing the manuscript. Tran Dinh Khang and Kirti Panchal assisted with writing and reviewing the manuscript, while Satyam Panchal, Roydon Fraser, and Michael Fowler offered advice and guidance on the research [3].

In Chapter 6, the author was responsible for developing Matlab simulation scripts, collecting and analyzing data, and preparing the results, graphs, and manuscript. Carlo Cunanan assisted with developing and running Matlab simulation scripts, while Satyam Panchal, Roydon Fraser, and Michael Fowler offered advice and guidance on the research [4].

Finally, in Chapter 7, the author was responsible for creating the manuscript synopsis, collecting and processing data from the literature, developing the methodology and algorithms, and preparing the results, graphs, and manuscript. Tran Phuc Manh Linh assisted with processing data and running the machine learning algorithms, while Tran Dinh Khang, Satyam Panchal, and Michael Fowler offered advice and guidance on the research.

Abstract

Building a future that preserves the environment and reduces dependence on fossil fuels is an imperative undertaking, and it greatly hinges on the global transition to renewable energy. Energy storage plays an important role in the adoption of renewable energy to help solve climate change problems. Lithium-ion (Li-ion) batteries are an excellent solution for energy storage due to their properties including high energy density, high power density, long cycle life, low self-discharge rate, no memory effects, and low environmental pollution. In order to ensure the safety and efficient operation of Li-ion battery systems, battery management systems (BMSs) are required. However, the current design and functionality of the BMS suffer from a few critical drawbacks including its low computational capability and limited data storage. The work in this thesis focuses on improving the BMS by investigating and improving the equivalent circuit model (ECM) which is often the core battery model used in practical BMS, researching and developing a smart BMS utilizing the cloud platform, and proposing potential applications of the cloud-based smart BMS such as cell replacement or SOH estimation using machine learning.

One of the main focuses of this work is on the critical role of accurate battery modeling for safe and effective operation. The first contribution of this research is an investigation into the performance of three ECMs—1RC, 2RC, and 1RC with hysteresis—across four common Li-ion chemistries: LFP, NMC, LMO, and NCA. Experimental results demonstrate that all three models can be applied to these chemistries with low error rates, particularly under dynamic current profiles. The findings indicate that the 1RC with hysteresis ECM performs best for LFP and NCA chemistries, while the 1RC ECM is most suitable for NMC and LMO chemistries. These insights are crucial for optimizing BMS applications in real-world scenarios, highlighting the need to tailor ECM selection to specific battery chemistries.

This work also seeks to add further to the improvement of the ECM used in the BMS, as another novel contribution. Its next research delves into the effects of state of charge (SOC), temperature, and state of health (SOH) on the parameters of the ECM, particularly the Thevenin model. While SOC and temperature are well-integrated into ECMs, the impact of SOH has been less explored. Through a series of experiments, it was found that as SOH decreases, both the ohmic and polarization resistances increase, while the polarization capacitance decreases. An empirical

model was developed to represent the combined effects of SOH, SOC, and temperature on ECM parameters. This model was validated experimentally and showed significant improvements in accuracy without increasing complexity. The proposed model offers a practical solution for real-world BMS applications, enhancing the precision of battery monitoring and control.

As part of the next steps in the research, the concept and development of cloud-based smart BMSs were discussed in detail. Traditional BMSs are limited by computational capacity and data storage, which can hinder the development of advanced battery management algorithms. A cloud-based BMS can address these issues by offloading computation and storage to the cloud, enabling more sophisticated and reliable battery algorithms. The study discusses the design, functionality, and benefits of cloud-based BMSs, including improved reliability and performance of Li-ion battery systems. It also explores the division of tasks between local and cloud functions, emphasizing the potential for significant advancements in battery management through cloud integration. This innovation is expected to play a pivotal role in advancing renewable energy technologies.

Once the development of the cloud-based smart BMS has been discussed, the practical applications of such innovation are then examined. As the optimization of Li-ion battery pack usage becomes increasingly more necessary and given the inevitable degradation of Li-ion batteries, recent research has focused on maximizing the utilization of battery cells within packs. Another study, which is the next novel contribution of this work, investigates the feasibility and benefits of cell replacement within battery packs, using a simulation framework based on cell voltage and degradation models. The cloud-based BMS, with more data storage, shall be able to advance the cell replacement application by providing significantly more battery historical data. The study, conducted using MATLAB, simulates the life cycles of battery packs with varied cell configurations. Results show that cell replacement can significantly extend the lifespan of battery packs and is economically advantageous compared to a full pack replacement. For practical implementation, the design criteria include individual cell monitoring and easy accessibility for cell replacement, underscoring the potential for more efficient battery usage strategies.

Another practical application of the cloud-based BMS with improved computational and memory capability is battery state estimation, specifically complex algorithms such as SOH estimation. A part of this work, its final novel contribution, develops a novel SOH estimation

approach, which is crucial for the effective operation of Li-ion battery systems. Existing methods have limitations in adaptability and real-time application. This study introduces a machine learning-based approach for online SOH estimation during fast charging cycles. Using a dataset of 124 cells, with various machine learning algorithms tested, the neural network algorithm demonstrated superior accuracy with an RMSE of 9.50mAh and a MAPE of 0.69%. The methodology, which utilizes partial charge metrics without needing historical data, is highly suitable for real-time BMS integration. This approach enhances the reliability and performance of Li-ion battery systems, contributing to the broader adoption of electric vehicles (EVs) and renewable energy technologies.

Overall, this thesis presents significant advancements in the field of battery management systems, particularly through the improvement of the ECM, the introduction of cloud-based smart BMSs, and the development of innovative cell replacement and SOH estimation methods. The cloud-based BMS would be able to solve the problems of limited computational capability and data storage. It would also lead to more accurate and reliable battery algorithms and allow the development of other complex BMS functions. The cloud-based smart BMS is expected to improve the reliability and overall performance of Li-ion battery systems, contributing to the mass adoption of EVs and renewable energy.

Acknowledgments

I would like to thank my family, friends, colleagues, professors and mentors who have helped me throughout my university career.

Firstly, I would like to express my sincere gratitude to my academic supervisor Michael Fowler for his continuous support and guidance during my entire PhD program. In addition to the great deal of technical knowledge I have acquired under his supervision, I have also learned how to think critically, how to conduct myself professionally, and how to approach any challenge with fortitude and determination. I received an incredible amount of support and guidance from him that I will forever be grateful for. I would also like to thank Dr. Ali Elkamel, Dr. XiaoYu Wu, Dr. Yverick Pascal Rangom, and Dr. Sheldon Williamson for their constructive feedback on my thesis.

I would also like to acknowledge Dr. Satyam Panchal and Dr. Manoj Mathew who have been my “go-to” throughout my PhD study. Their expertise on the subject helped guide me through the projects which eventually became my thesis. Thank you to all the co-ops for their help with running experiments and collecting data to assist my research.

Thank you to my friends and family – Minh, Olsi, Jack, Sky, Brandon, Matt, and many others – for all the unforgettable memories we have made together over the years. My deepest gratitude goes to my wonderful partner, Lucie, whose unwavering support and encouragement were my guiding light. I truly could not have completed this thesis without her by my side.

Finally, I would like to express my very profound gratitude to my parents for providing me with unfailing support and continuous encouragement throughout my years of study. They are my ultimate role models.

Table of Contents

Examining Committee Membership	ii
Author’s Declaration	iii
Statement of Contributions	iv
Abstract.....	v
Acknowledgments	viii
List of Figures.....	xiii
List of Tables	xv
List of Abbreviations	xvi
Chapter 1 : Introduction	1
1.1. Motivation	1
1.2. Research Objectives	3
1.3. Thesis Outline	4
Chapter 2 : Background and Literature Review	6
2.1. Lithium-Ion Battery.....	6
2.1.1. Basic Concept of Battery	6
2.1.2. Battery Terminologies	10
2.1.3. Battery Degradation	12
2.1.4. Battery Faults	14
2.2. Battery Management System	16
2.2.1. Common Functionalities	16
2.2.2. Battery Modeling	20
2.2.3. Current Drawbacks of BMS.....	21
2.3. Cloud Platform and Machine Learning.....	22
2.3.1. Cloud Platform.....	22

2.3.2. Machine Learning	23
Chapter 3 : Investigation of Equivalent Circuit Models Performance in Various Lithium-ion Batteries.....	25
3.1. Introduction	25
3.2. Background	27
3.2.1. Lithium-ion battery chemistries.....	27
3.2.2. Equivalent circuit models for lithium-ion batteries	30
3.3. Experimental	32
3.3.1. Cell characterization experiments.....	34
3.3.2. Model validation experiments.....	35
3.4. Results	36
3.4.1. Cell characterization results.....	36
3.4.2. Model validation results.....	40
3.4.3. Comparative discussion of models and battery chemistries	41
3.5. Conclusions	43
Chapter 4 : Comprehensive Equivalent Circuit Model Development for Lithium-ion Battery.....	44
4.1. Introduction	44
4.2. Experimental and Trend Analysis	46
4.2.1. Experimental.....	46
4.2.2. Trend Analysis	49
4.3. Model Development and Validation	52
4.4. Conclusions	58
Chapter 5 : Cloud-Based BMS Design and Functionalities.....	59
5.1. Current Design of the BMS.....	59
5.2. Proposed Design of the Cloud-Based BMS	61

5.3.	Functionalities of the Cloud-based BMS	64
5.4.	Conclusions	66
Chapter 6 : Analysis of Cell Replacement in Lithium-Ion Battery Packs.....		67
6.1.	Introduction	67
6.2.	Experimental	69
6.3.	Modeling and Simulation.....	71
6.3.1.	Cell voltage model	71
6.3.2.	Cell degradation model	74
6.3.3.	Pack voltage model	75
6.3.4.	Cell replacement simulation framework.....	76
6.4.	Results and Discussion.....	79
6.4.1.	Cell replacement concept simulation and results.....	79
6.4.2.	Battery pack design requirements for cell replacement concept	81
6.4.3.	Economic feasibility of cell replacement concept	81
6.5.	Conclusions	83
Chapter 7 : Online Lithium-ion Battery State of Health Estimation Using Machine Learning.....		85
7.1.	Introduction	85
7.2.	Methodology	89
7.2.1.	Dataset description.....	89
7.2.2.	Development of SOH estimation approach	89
7.3.	Proposed machine learning algorithms	91
7.3.1.	Neural network.....	93
7.3.2.	Classification and regression trees (CART)	93
7.3.3.	Light gradient boosting machine (LightGBM).....	94

7.3.4.	Extreme gradient boosting (XGBoost)	94
7.3.5.	Categorical boosting (CatBoost).....	94
7.3.6.	Random forest.....	95
7.4.	Results and analysis	95
7.5.	Conclusions	103
Chapter 8 : Conclusions and Recommendations		104
8.1.	Conclusions and Contributions	104
8.1.1.	Contribution to Battery Modeling 1.....	104
8.1.2.	Contribution to Battery Modeling 2.....	104
8.1.3.	Contribution to Cloud-Based BMS.....	105
8.1.4.	Contribution to Analysis of Cell Replacement Strategies	105
8.1.5.	Contribution to State of Health Estimation.....	105
8.2.	Recommendations and Future Work.....	106
References		109

List of Figures

Figure 1.1: Projected global battery demand from 2020 to 2030, by application [16]..... 1

Figure 2.1: Electrochemical operation of a cell during discharge (left) and charge (right) [27].... 7

Figure 2.2: Ragone plot for different cell chemistry [29]. 8

Figure 2.3: Reactions within Li-ion battery cell. 9

Figure 2.4: Schematic of Li-ion cell in the process of discharge and charge [29]. 9

Figure 2.5: Causes for battery aging and their effects. 14

Figure 2.6: Internal and external Li-ion battery faults and their causes. 15

Figure 2.7: Structure of a typical BMS for battery applications [53]. 17

Figure 2.8: Various functions of the BMS..... 20

Figure 3.1: Equivalent circuit model diagrams, (a) first-order (1RC), and (b) second-order (2RC).
..... 30

Figure 3.2: Four lithium-ion battery cells with different chemistries tested in the study. 33

Figure 3.3: Experimental setup, including (a) battery tester setup, and (b) schematic of setup. .. 33

Figure 3.4: HPPC test profile for the NCA cell. 35

Figure 3.5: Validation current profiles for the four batteries, (a) UDDS cycle, and (b) ND cycle.
..... 36

Figure 3.6: SOC-OCV curves for each lithium-ion battery chemistry tested; (a) LFP, (b) NMC,
(c) LMO, and (d) NCA. 37

Figure 3.7: Model validation results from the LFP cell using first-order ECM at 0.6 SOC; (a)
UDDS cycle, and (b) ND cycle..... 41

Figure 3.8: Model validation performance of different equivalent circuit models for various
lithium-ion cell chemistries under the UDDS cycles..... 41

Figure 3.9: Model validation performance of different equivalent circuit models for various
lithium-ion cell chemistries under the ND cycles..... 42

Figure 4.1: Schematic of the Thevenin equivalent circuit model. 45

Figure 4.2: Experimental setup. a) Battery tester Maccor 4200. b) Connected and tested cell in
the thermal chamber. c) CSZ MicroClimate thermal chamber. d) Computer software controlling
the Maccor 4200. 47

Figure 4.3: Current profiles used to validate the proposed model. a) UDDS. b) CCDC..... 48

Figure 4.4: Experimentally established SOC-OCV curve of the LFP cells.....	50
Figure 4.5: Effect of SOH, SOC, and temperature on R_0	51
Figure 4.6: Effect of SOH, SOC, and temperature on R_1	51
Figure 4.7: Effect of SOH, SOC, and temperature on C_1	52
Figure 4.8: Model validation results at 72.9% SOH. a) Using UDDS profile at 40°C. b) Using UDDS profile at 10°C. c) Using CCDC profile at 40°C. d) Using CCDC profile at 10°C.	54
Figure 4.9: Model validation results at 85.5% SOH. a) Using UDDS profile at 40°C. b) Using UDDS profile at 10°C. c) Using CCDC profile at 40°C. d) Using CCDC profile at 10°C.	55
Figure 5.1: Current battery management system (BMS) design and functions.	60
Figure 5.2: Potential design and functions of the cloud-based smart BMS.....	63
Figure 6.1: Experimental setup: experimental setup and MACCOR 4200 battery cycler (left); and tested 20Ah battery pouch cells (right).	70
Figure 6.2: Schematic of the Thevenin equivalent circuit model.	71
Figure 6.3: Experimentally established SOC-OCV curve of the LFP cells.....	72
Figure 6.4: ECM parameters obtained from the HPPC tests: R_0 (top left), R_1 (top right), and C_1 (bottom).....	73
Figure 6.5: Cell voltage model validation plot using UDDS cycle.	74
Figure 6.6: Schematic of the cell replacement simulation framework.	77
Figure 6.7: Total number of cycles, on average, of the battery packs with different replacement rates, for 80% SOH threshold (left), and 70% SOH threshold (right).	80
Figure 7.1: SOH estimation results using neural network algorithm.....	97
Figure 7.2: SOH estimation results using CART algorithm.	98
Figure 7.3: SOH estimation results using LightGBM algorithm.	99
Figure 7.4: SOH estimation results using XGBoost algorithm.	100
Figure 7.5: SOH estimation results using CatBoost algorithm.....	101
Figure 7.6: SOH estimation results using random forest algorithm.	102

List of Tables

Table 3.1: Cell specifications for each chemistry	33
Table 3.2: Model parameters obtained from HPPC data fitting in MATLAB for the LFP cell. ..	38
Table 3.3: Model parameters obtained from HPPC data fitting in MATLAB for the NMC cell.	38
Table 3.4: Model parameters obtained from HPPC data fitting in MATLAB for the LMO cell.	39
Table 3.5: Model parameters obtained from HPPC data fitting in MATLAB for the NCA cell..	39
Table 4.1: Specifications of the lithium-ion cells used in the experiments.	48
Table 4.2: Parameters of the proposed model after fitting.....	53
Table 4.3: Summary of errors for the model validation runs.....	56
Table 4.4: Comparison of errors between validation results using the proposed model and not using the proposed model.	57
Table 5.1: Advantages of cloud-based smart BMS.	62
Table 6.1: Lithium-ion pouch cell specifications.	70
Table 6.2: Capacity and ECM parameters distribution.....	74
Table 6.3: Degradation parameters used in the simulation.....	77
Table 6.4: Cost analysis and comparison between cases of pack replacement and cell replacement.	82
Table 7.1: Setup of the six machine learning algorithms used in the study.....	92
Table 7.2: RMSE of the algorithms tested.....	95
Table 7.3: MAPE of the algorithms tested.....	96

List of Abbreviations

AI	Artificial intelligent
API	Application programming interface
BMS	Battery management system
BTMS	Battery thermal management system
CAN	Controller area network
CART	Classification and regression trees
CatBoost	Categorical boosting
CCDC	Constant charge/discharge current
DaaS	Data as a service
DoD	Depth of discharge
ECM	Equivalent circuit model
EMI	Electromagnetic interference
EOL	End of life
ESS	Energy storage system
EV	Electric vehicle
FUDS	Federal urban dynamic schedule
HPPC	Hybrid pulse power characterization
IC	Incremental capacity
IoT	Internet of things
IR	Internal resistance
LightGBM	Light gradient boosting machine
Li-ion	Lithium ion
MAPE	Mean absolute percentage error
MQTT	Message queuing telemetry transport
ND	Non dynamic
OCP	Open circuit potential
OCV	Open circuit voltage
PCM	Phase change material
RMSE	Root mean squared error

RUL	Remaining useful life
SEI	Solid electrolyte interphase
SOA	Service-oriented architecture
SOC	State of charge
SOF	State of function
SOH	State of health
UDDS	Urban dynamometer driving schedule
UI	User interface
XGBoost	Extreme gradient boosting

Chapter 1 : Introduction

1.1. Motivation

Since the energy demand is projected to increase significantly in the future, the need for renewable energy is at its peak. Due to this increasing demand, the role of energy storage in the power grid is becoming increasingly important [5], [6]. As an enabling technology, it can help integrate more renewable energy sources such as solar and wind, or even clean non-renewable sources like nuclear, into the grid, lowering electricity costs and reducing environmental impact [7], [8], [9]. Lithium-ion (Li-ion) batteries have recently gained a lot of interest as an excellent energy storage system (ESS) due to their high energy and power density, long lifespan, and low self-discharge [10], [11]. Li-ion batteries are used in many real-world applications, such as electric vehicles (EVs), large-scale battery ESSs, and small portable devices like laptops and smartphones [12]. In recent years, over 90% of large-scale ESS capacity was provided by Li-ion batteries annually in the United States [13]. Due to the increasing interest in Li-ion batteries, researchers have been focusing on increasing the energy density and lowering the costs of Li-ion batteries, allowing the battery technology to advance further [14], [15]. Figure 1.1 shows the projected global battery demand from 2020 to 2030.

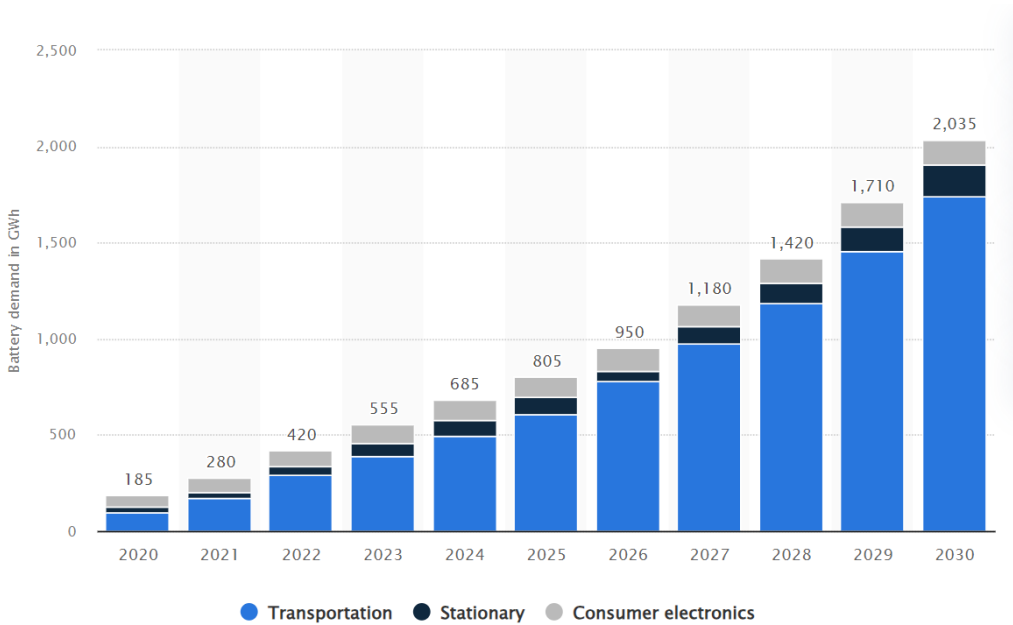


Figure 1.1: Projected global battery demand from 2020 to 2030, by application [16]

In most real-world applications, the battery management system (BMS) is a mandatory component, serving the purpose of monitoring the battery's health and safety. The role of the BMS becomes more significant in applications that have a large number of battery cells such as electric vehicles and battery storage power stations [17], [18]. The BMS is an electronic device that manages a battery system [19]. Originally, the main functions of the BMS were ensuring battery safety and protection by establishing operational voltage, current, and temperature thresholds with warnings if exceeded, as well as cell balancing. Over the years, the BMS has been researched and developed further for improvement in performance, functionalities, and capabilities. Currently, there are more functions in the BMS that help the battery perform more safely and efficiently, including cell monitoring, battery safety and protection, state of charge (SOC) estimation, state of health (SOH) estimation, cell balancing, thermal management, and charge control [2], [20], [21]. Since there are concerns regarding the safety, reliability, and performance of Li-ion batteries, especially in standalone systems, a well-designed BMS is critical. In addition, battery models and algorithms are used in the BMS to predict working voltage, power, and energy capability, estimate SOC and SOH, detect faults, and control battery operation [22], [23]. They have a significant role in ensuring reliable performance and safety, improving the usage efficiency of the batteries, and avoiding malfunctions and catastrophic failures. It is important to have accurate and reliable battery models and algorithms in the BMS.

Despite the recent works in developing better BMS design and battery algorithms, there are still many downsides to the current BMSs. For example, the current infrastructure of the BMS only allows it to utilize simple battery models since it is limited in computing capability and data storage. Therefore, battery models need to be accurate yet simple enough to be implemented in the BMS. The lack of data storage means that online data-driven battery algorithms are improbable, and it also means that battery applications often lose their operational history, so second-life repurposing would be difficult to execute. Another disadvantage of the current BMS design is the lack of flexibility in its usage, as its algorithms are often hard programmed into the BMS, and changing the firmware requires a great amount of effort. The current BMS also does not allow for a plug-and-go style and needs to be programmed specifically for different battery applications.

The first major motivation of this work is the need for a better battery model, specifically the equivalent circuit model (ECM), as the accurate modeling of batteries is crucial for their

effective management and utilization. The ECM is a commonly used model in BMSs for monitoring and controlling Li-ion batteries. Despite its widespread use, there is a need to refine and enhance the ECM to improve its accuracy and reliability. This improvement is critical for optimizing battery performance, ensuring safety, and extending the operational life of Li-ion batteries. The second motivation is to address the significant limitations in the computational capability and data storage of current BMS solutions. These limitations can hinder the development and implementation of advanced battery management algorithms that require significant computational resources and large datasets. A cloud-based BMS offers a promising solution by offloading computation and storage to the cloud. One of the key applications of a cloud-based BMS is the ability to utilize better data storage for advancing battery management technologies, such as cell replacement. The capacity to store and analyze extensive historical data is crucial for developing and implementing effective cell replacement strategies. By ensuring that degraded cells are identified and replaced promptly, the overall efficiency and longevity of the battery system can be greatly enhanced. Another critical application of a cloud-based BMS is the enhancement of computational capability, which is essential for advancing SOH estimation methods. Accurate SOH estimation is vital for maintaining the performance and safety of Li-ion batteries, especially during fast charging cycles and varying operational conditions. Traditional SOH estimation methods are often limited by the computational constraints of conventional BMSs, leading to less accurate and reliable results. By utilizing the superior computational power of the cloud, the proposed BMS can implement advanced machine learning algorithms for real-time SOH estimation. This capability not only improves the reliability of the battery system but also enhances its overall performance and safety. This work will address the gaps discussed, and the main objectives of this thesis are summarized in the section below.

1.2. Research Objectives

The main objective of this research is to improve the performance and life cycle of Li-ion batteries, by enhancing the battery model used in the BMS, building a cloud-based battery management system, investigating a cell replacement strategy for battery packs, and developing an SOH estimation algorithm using machine learning and data-driven techniques. The sub-objectives are as follows:

1. The first sub-objective is to investigate and improve the accuracy and applicability of ECM for Li-ion batteries. This work will evaluate the performance of different ECMs across some common Li-ion battery chemistries, aiming to identify the most suitable ECM for each chemistry, optimizing BMS applications. This work will also develop a novel comprehensive ECM for aging batteries that is more suitable for the online BMS.
2. The second sub-objective is to review the concept and design of a cloud-based BMS to overcome the computational and data storage limitations of traditional BMS solutions. A cloud-based architecture will enable offloading computational tasks and data storage to the cloud, supporting sophisticated and reliable battery management algorithms.
3. The third sub-objective is to leverage the enhanced computational power and data storage capabilities of a cloud-based BMS to advance other applications related to Li-ion battery improvement, such as cell replacement framework and SOH estimation. This work will investigate the feasibility and benefits of cell replacement strategies, which aim to extend battery pack lifespan and improve economic viability. This work will also develop an advanced machine learning approach for online and real-time SOH estimation that has high accuracy and robustness, enhancing the reliability and performance of Li-ion battery systems.

1.3. Thesis Outline

The chapters of the thesis are organized as follows:

- Chapter 2 introduces the background information on Li-ion batteries, including some basic concepts, battery terminologies, degradation mechanisms, and battery faults. Following that, a literature review on the BMS, including functionalities and battery modeling, will be provided. The basic concepts of cloud platform and machine learning will also be introduced.
- Chapter 3 presents an experimental study on the performance of various ECM configurations across four common Li-ion chemistries. It discusses the findings on model accuracy under dynamic and non-dynamic current profiles and identifies the most suitable ECM for each chemistry to optimize BMS applications.

- Chapter 4 then explores how SOH, along with SOC and temperature, affects ECM parameters, focusing on the Thevenin model. It details experimental results and the development of an empirical model to represent these effects, enhancing the accuracy and applicability of the ECM in real-world BMS applications.
- Chapter 5 shows the concept and design of cloud-based BMSs, addressing the computational and data storage limitations of traditional BMS solutions. It evaluates the potential improvements in reliability, accuracy, and safety of Li-ion battery systems achieved through the integration of cloud computing into BMS architecture.
- Chapter 6 examines the use of cloud-based BMS for advancing cell replacement technology in Li-ion battery packs. The study presents the simulation of cell replacement strategies and demonstrates the potential for extending battery pack lifespan and improving economic viability.
- Chapter 7 introduces an advanced machine learning method for online and real-time SOH estimation using machine learning made available by the computational power of a cloud-based BMS. It describes the development and validation of machine learning models that utilize partial charge metrics for accurate and robust SOH estimation, aiming to enhance the reliability and performance of Li-ion battery systems.
- Chapter 8 summarizes the main research contributions of this work as well as offers new directions for future research.

Chapter 2 : Background and Literature Review

2.1. Lithium-Ion Battery

2.1.1. Basic Concept of Battery

A battery is a device that converts stored chemical energy into electrical energy through an electrochemical oxidation-reduction (redox) reaction. For a rechargeable battery, the process is reversed. The redox reaction occurring within batteries involves electrons being transferred from one material to another through an electric circuit [24], [25], [26]. Because batteries convert chemical energy into electric energy through an electrochemical process, they are not subject to the limitations of the Carnot cycle, unlike combustion engines, and thus batteries have higher energy conversion efficiencies [27].

A battery system consists of one or more battery cells, connected in series and/or parallel. The cell consists of three major components: the anode, the cathode, and the electrolyte. The anode is the negative electrode or reducing electrode, which produces electrons and is oxidized during the redox reaction. The anode is usually selected based on some specific requirements, including reducing potential, good conductivity, stability, ease of fabrication, and low cost. Hydrogen, lithium, and zinc are some examples of materials that have been used as the anode [28]. The cathode is the positive electrode or oxidizing electrode, which accepts electrons and is reduced during the redox reaction. A good cathode material should be an efficient oxidizing agent and have a useful working voltage, and some common materials are metallic oxides, oxygen, and halogens [28]. The electrolyte, usually liquid, is the ionic conductor that provides the medium for ions to transfer between the anode and cathode. It should be nonreactive with the electrodes, stagnant with temperature change, safe, and cost-efficient. It should also be ionically conductive but not electronically conductive to prevent internal short-circuiting. There are many shapes and configurations for the cells, including cylindrical, button, and flat, and the components are designed to fit different cell shapes [27].

There are three common classifications for batteries: primary (non-rechargeable), secondary (rechargeable), and flow batteries. Primary batteries are normally discharged once and discarded due to their inability to be effectively recharged, but they have a good shelf life and high

energy density at low discharge rates. They are a convenient, inexpensive, and lightweight solution to many applications such as portable electronic devices, lighting, and cameras. Secondary batteries can be recharged electrically to their original state by directing the current in the opposite direction to that of the discharging process. They are used the same as primary batteries but instead of being discarded, they can be recharged to be used again. Some notable applications for this type of battery are cell phones and laptop computers. Secondary batteries usually possess traits like high power density and high discharge rate. Flow batteries utilize chemical energy outside of the battery in a fluid state. The fluid passes through the battery and reacts to produce electrical energy. An example of this type of battery is fuel cell [27].

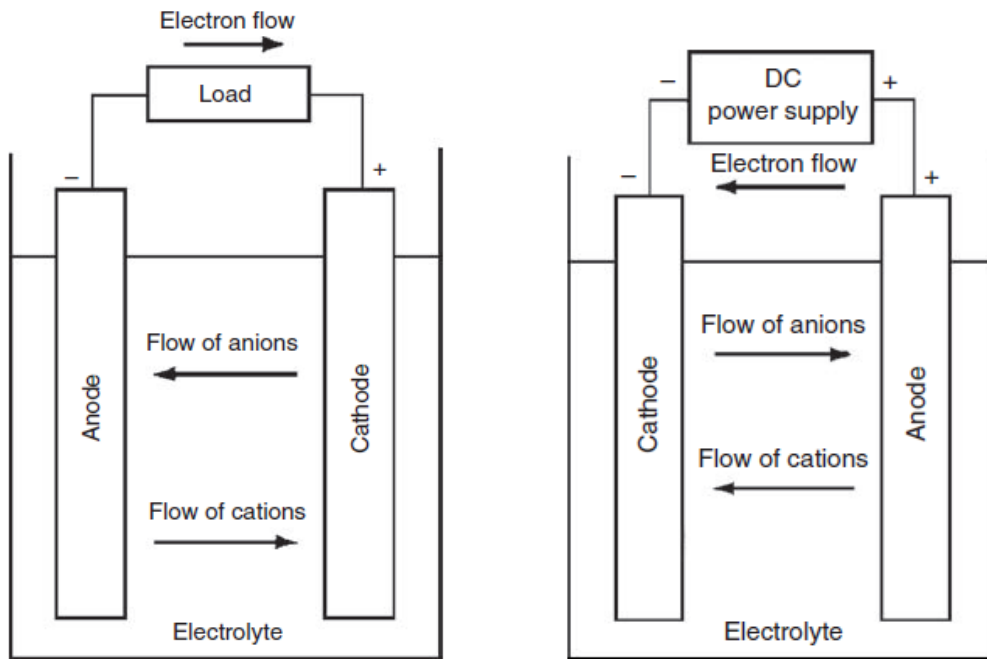


Figure 2.1: Electrochemical operation of a cell during discharge (left) and charge (right) [27].

The operation of a rechargeable cell during the discharge and charge processes is shown in Figure 2.1. During the discharging process, the cell is connected to an external load and the electrons flow from the anode to the cathode through the load. In the electrolyte, the ions flow to their respective destination, completing the electric circuit. During the charging process, the current flow is in reverse, provided by a power supply, and the oxidation and reduction processes occur in the opposite electrode of the discharge - the positive electrode is now the anode and the negative is the cathode.

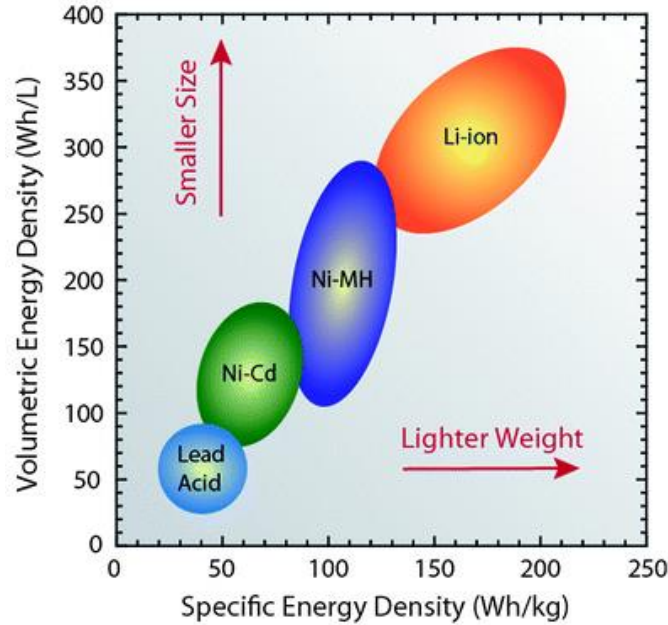


Figure 2.2: Ragone plot for different cell chemistry [29].

Since many battery applications, such as EVs, require high power density and discharge rate, secondary batteries are the most suitable solution. The ability to be recharged also allows for convenience and cost savings, because of the complexity of battery replacement in that application [29]. One of the most important aspects involving the use of batteries in EVs is the range of the vehicle. Users want a longer driving range and better performance, which requires a battery solution that has high energy and power density, low weight, and small volume. Li-ion batteries satisfy many of the EV application requirements [30]. As can be seen in Figure 2.2, they possess higher energy potential while maintaining a smaller size and weight compared to other rechargeable batteries.

Li-ion batteries utilize lithium compounds for both positive and negative electrodes. The Li^+ ions move back and forth between the electrodes as the cell cycles. The negative electrode material is commonly graphite, used for its availability, cycling performance and safety, layered on a copper current collector. The positive electrode has been researched more, with many available materials such as LiCoO_2 (LCO), LiMn_2O_4 (spinel), LiFePO_4 (LFP) and $\text{Li}(\text{NiMnCo})\text{O}_2$ (NMC) [31], [32]. These materials each have different advantages which are appropriate for different applications, such as low cost, high thermal stability, long cycle life, high rate capability and high capacity.

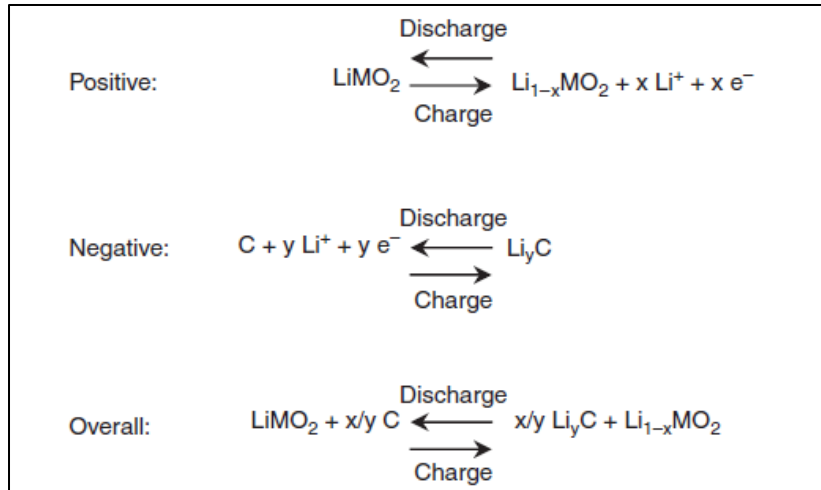


Figure 2.3: Reactions within Li-ion battery cell.

When a Li-ion cell is charged, the active material from the positive electrode is oxidized and the material from the negative electrode is reduced. During this process, lithium ions are deintercalated from the positive to the negative side [29]. The reactions are shown in Figure 2.3, where LiMO_2 represents the metal oxide and C represents the carbonaceous material (graphite). The graphical schematic of a Li-ion cell in operation is shown in Figure 2.4.

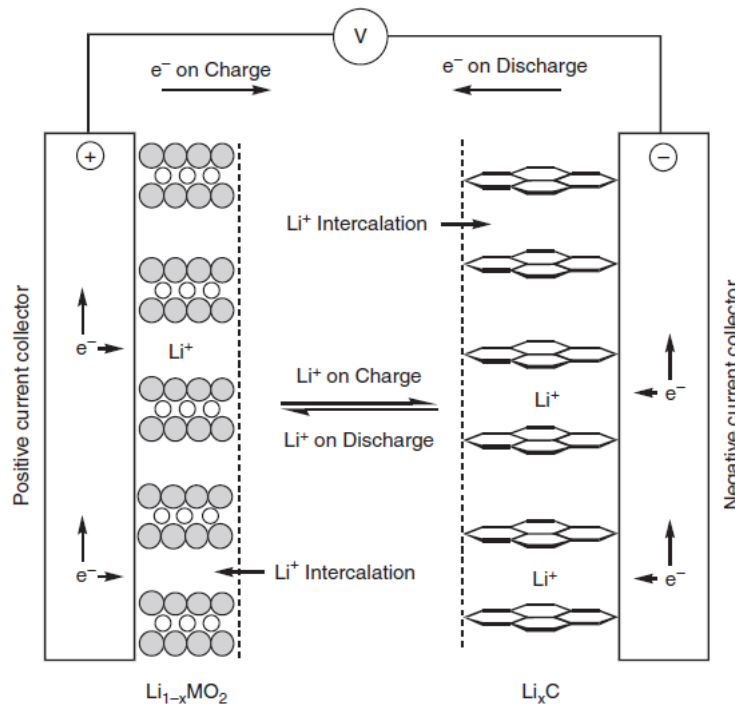


Figure 2.4: Schematic of Li-ion cell in the process of discharge and charge [29].

2.1.2. Battery Terminologies

Some common battery terminologies include voltage, current, capacity, energy, internal resistance, SOC, SOH, and RUL:

- The theoretical voltage of a cell can be calculated from the standard electrode potentials. It is the difference between the voltage potential of the two electrodes. The theoretical voltage is modified by the Nernst equation, which takes into account the non-standard concentration and temperature of the cell during its operation. The actual potential changes with time either because of use or self-discharge by which the activity (concentration) of the electroactive component in the cell is modified. The actual voltage produced will always be lower than the theoretical voltage due to polarisation. It is also affected by the internal resistance losses (IR drop) of the battery which depends on the load current and the internal impedance of the cell. These factors are dependent on electrode kinetics and thus vary with temperature, SOC, and the age of the cell. The actual voltage appearing at the terminal needs to be sufficient for the intended application [27].
- The current of a cell is defined as the rate of flow of electricity or the movement of electrons along a conductor. It occurs when there is a potential difference. For a current to flow, a complete circuit is required, meaning that the flowing charge has to be able to get back to where it starts. The direction of the current is considered to be the direction of the flow of positive charge, which is opposite to the direction where the electrons go.
- The capacity of a cell is determined by the mass of active material contained in the cell, measured in coulombs or ampere-hours. It is essentially the quantity of electricity that can be obtained from the active materials. The cell capacity represents the maximum amount of energy that can be extracted from the battery under certain specified conditions. However, the actual energy storage capabilities of the battery can vary significantly from the nominal-rated capacity, as the battery capacity depends strongly on the age and operational history of the battery, the charging or discharging regimes of the battery, and the temperature [27].
- The energy of the cell considers both voltage and capacity, being the multiplication product of the two quantities. It is the maximum value in watt-hour that can be delivered by a specific electrochemical system. However, energy is not a good metric for cell specification because only a fraction of the theoretical energy of the battery is realized, due

to the need for electrolytes and other nonreactive components such as containers, electrodes, and separators. Better metrics used for batteries to evaluate their performance are specific energy (Wh/kg) and energy density (Wh/L). The specific energy density is the energy that can be derived per unit weight of the cell. The energy density is the energy that can be derived per unit volume of the weight of the cell [27]. For example, the development of pouch cells significantly decreased the weight and volume of the cell, increasing its specific energy and energy density when compared to past cell shapes, thus making it more efficient and viable to use.

- Internal resistance is defined as the resistance to the flow of an electric current within the cell or battery. All batteries have some internal resistance to a certain degree. Batteries have internal resistance because their internal components like electrodes and electrolytes are not completely conductive, and hence, will have some resistance in them. Batteries with high internal resistance often display poor performance in supplying high current pulses, because the current decreases with higher resistance. Batteries with low internal resistance are much better at supplying high current pulses.
- SOC is defined as the available capacity expressed as a percentage of some reference, which can sometimes be the rated capacity of the cell, and sometimes its current (latest) capacity. It is not usually an absolute measure in Coulombs, kWh, or Ah of the energy left in the cell. The fact that it is not an absolute measure combined with an unclear reference point creates some confusion around the SOC estimation. The preferred SOC reference should be the rated capacity of a new cell rather than the current capacity of the cell. This is because the cell capacity gradually reduces as the cell ages [27]. For example, towards the end of the cell's life, its actual capacity, even when the cell is fully charged, will be approaching only 80% of its rated capacity. Therefore, in this case, the cell SOC would only be 80% of its rated capacity [33]. Even though this is the case, some applications still use the cell's current capacity as the reference point, including EVs [34]. This is because the SOC in EVs is normally referred to as the “fuel” gauge. This value gives the users a sense of how much “fuel” is left in their battery. If the battery is indicating a “fuel” level of 80% even when it is fully charged, the users will believe that their battery is not working properly, even though this behavior should be expected from a battery. Using the current capacity rather than the rated capacity is usually a design shortcut to avoid the complexity

of determining and allowing for the age-related capacity adjustments, which are often conveniently ignored.

- SOH is defined as the measurement of the general condition of a battery and its ability to deliver the specified performance compared with a fresh battery. It takes into account factors such as charge acceptance, internal resistance, voltage, and self-discharge. It measures the long-term capability of the cell and gives an indication, not an absolute measurement, of how much of the available "lifetime energy throughput" of the battery has been consumed, and how much is left [27]. In EVs application, it can be analogized to the "odometer" display function which indicates the number of miles traveled since the vehicle was new.
- RUL is generally defined as the duration of a component to reach its failure. For battery, it refers to remaining cycle life, which is defined as after how many cycles, the battery capacity will reach the failure threshold from the current cycle. It represents the period from the observation point to the end of life (EOL). EOL refers to the time and the number of charge-discharge cycles when the battery characteristic parameters reach the replacement threshold.

2.1.3. Battery Degradation

Li-ion batteries are commonly used for ESSs, due to their energy-to-weight ratio and low self-discharge rate [27]. However, in order to make a significant impact on the ESS market, these batteries must satisfy performance requirements and last long enough for customers to be interested [35]. Battery degradation is one of the factors that can affect the ESS performance since it directly affects battery lifetime, performance, and longevity. Degradation can be quantified as runtime on a full charge (estimated in Ah) or as the number of charge/discharge cycles until it degrades irreversibly [36]. For EV application, the EOL point is often defined to be when the battery has degraded to 80% of its original SOC [37].

It was determined that the performance loss of the battery is caused by many different mechanisms [38]. These mechanisms are often difficult to identify and quantify due to the complexity of the reactions and physical changes taking place inside the battery while under operation. The common effects are capacity fade and impedance increase, but the degree of these are distinct depending on the conditions the battery operates at or is stored at and the materials that

make up the battery [35]. While the degree of degradation can vary, its occurrence over time is inevitable. The aging mechanisms can be grouped into two categories, which are calendar aging and cycling aging.

Calendar aging is the degradation of the battery over time when the battery is stored under open circuit potential (OCP) conditions [39]. Essentially, the battery will lose its capacity with time, even if it is not being used. Even though the effect of calendar aging is less than that of cycling aging, some battery applications, such as EVs due to their inactive time, would experience this type of aging the most [30]. The loss of capacity in the cell with time can be reversible and irreversible loss [40]. The reversible capacity loss is the result of the spontaneous re-intercalation of the Li ions from the electrolyte into the unstable cathode when the cell is fully charged [41]. The irreversible capacity loss can be attributed to the side reactions occurring within the cells [42]. These reactions can be caused by the operating conditions of the battery, namely temperature and SOC. With high temperatures, secondary reactions such as corrosion proliferate can occur, causing losses of usable lithium [35]. In research conducted by Grolleau et al. [30], Li-ion cells stored at different temperatures were found to experience different degrees of capacity fade. Cells stored at 30°C experienced less than 10% capacity loss after 450 days of storage, while capacity fade was 20% for cells stored at 45°C. Cells stored at 60°C reached a 20% capacity loss after only 60 days. For the effect of SOC, Ohue et al. showed that cells stored at the same temperature but different SOC have different aging results. The cells stored at higher SOC experienced an increased degradation effect [43]. This is because, at higher SOC, there are significantly more Li ions available at the graphite electrode to partake in potential side reactions there.

Cycling aging refers to aging mechanisms that occur within the cell while it is operating under load. The losses for this type of aging are typically irreversible [44]. They include the loss of capacity in the formation of the solid electrolyte interface (SEI) layer, loss of active materials due to dissolution, structural degradation, electrode delamination, and impedance increase from the formation of the SEI layer that passivates the active particle surface [44]. Aging can occur at both electrodes, but the most prominent loss of capacity has been determined to occur at the anode [26]. The primary source of aging at the anode is the formation of the SEI layer. As the cell is cycled, the graphite is exposed to the electrolyte resulting in the utilization of more lithium to form an SEI over the exposed surface. This leads to the loss of cyclable lithium in the cell as well as an

increase in resistance on the electrode. Many other factors can induce the aging of the battery at the anode, summarized in Figure 2.5. Aging can also occur at the cathode, due to structural factors and SEI formation, similar to the anode [32]. The electrolyte can also be a reason for cycling aging since the materials used in the electrolyte have the capability to undesirably react at low voltage [45]. This can sometimes produce gaseous species in the cell and lead to swelling of the cell, which is a major safety concern [46].

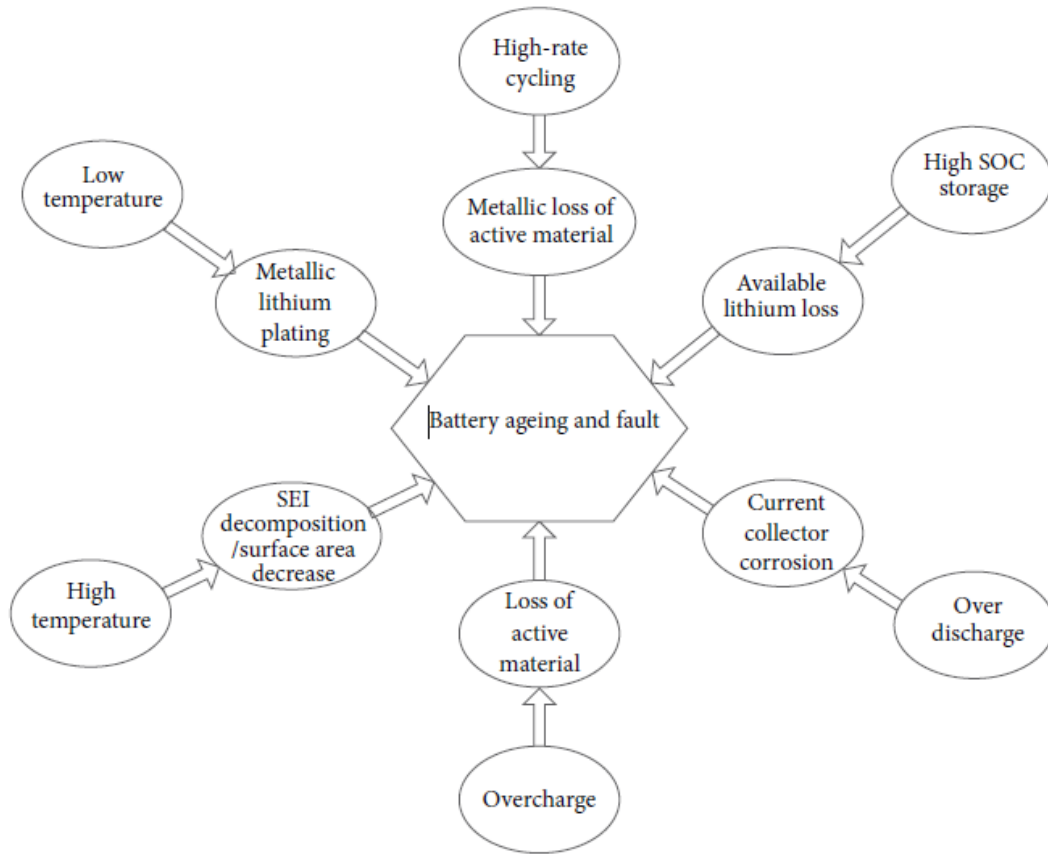


Figure 2.5: Causes for battery aging and their effects.

2.1.4. Battery Faults

A fault is defined as a deviation of at least one property or parameter of the system from the standard conditions. They can affect the control action from the controller, produce measurement errors or change the input/output properties of the system, which leads to degradation and damage of the system [47]. Li-ion battery faults are categorized into internal and external faults. Figure 2.6 shows a summary of various faults in a Li-ion battery system.

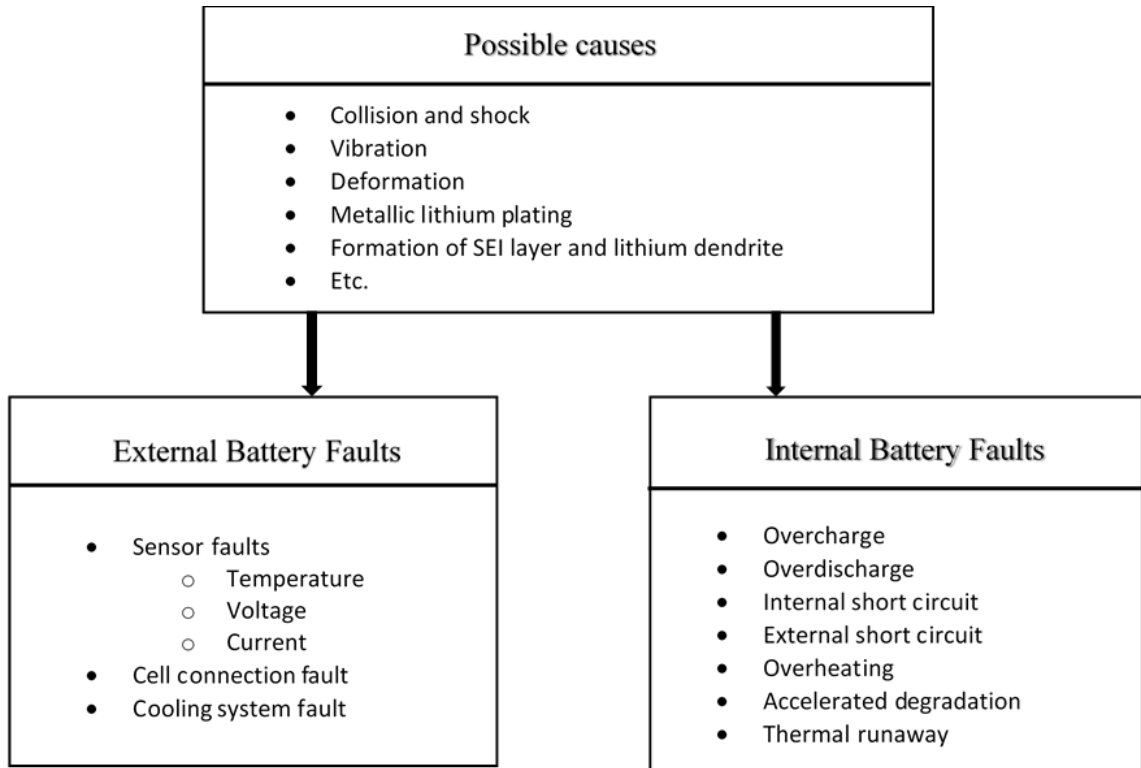


Figure 2.6: Internal and external Li-ion battery faults and their causes.

Internal battery faults are difficult to detect since the operation within a Li-ion cell is still not fully understood [48]. Some examples of internal battery faults are overcharge, overdischarge, internal and external short circuit, overheating, accelerated degradation, and thermal runaway. All these faults affect the battery operation, but accelerated degradation and thermal runaway are the most dangerous since they can significantly affect the Li-ion battery application or directly harm the users [49]. Internal faults are often identified from abnormal responses from the battery operation, which include voltage drop, SOC drop, temperature rise, increase in internal resistance, and physical transformation, such as swelling.

External battery faults can have a significant effect on the other functions of the BMS and cause internal battery faults to occur. There are several types of external faults, which are temperature, voltage, and current sensor faults, cell connection faults, and cooling system faults. The cooling system fault can be considered the most severe fault because it leads to a direct thermal failure, specifically thermal runaway, as the system fails to provide adequate cooling [50].

Most battery faults can eventually lead to thermal runaway. A study by Galushkin et al. [51] concluded that the probability of thermal runaway increases with the number of charge/discharge cycles. The study also found that thermal runaway is related to a variety of exothermic reactions in batteries. The first exothermic reaction to occur is SEI decomposition, and it considerably increases the heat release at the beginning of the thermal runaway. During thermal runaway, the cathode releases oxygen by a phase transition, and the oxygen is consumed by the lithiated anode. A consequence of thermal runaway is a substantial increase in pressure and temperature of the Li-ion cell, which can lead to the destruction of the container and the release of a large amount of flammable and toxic gas. Often in the case of a thermal runaway occurrence, the battery heats up and explodes. Hence, it is the most severe fault that can materialize in a Li-ion battery system.

2.2. Battery Management System

2.2.1. Common Functionalities

The BMS is an important element to keep battery applications safe, reliable, and efficient. It not only controls the operational conditions of the battery to prolong its service life and ensure its safety but also provides accurate estimations of the SOC and SOH for the energy management modules in battery systems. To fulfill these tasks, a BMS has several components and functional requirements to control and monitor the operation of the battery [52].

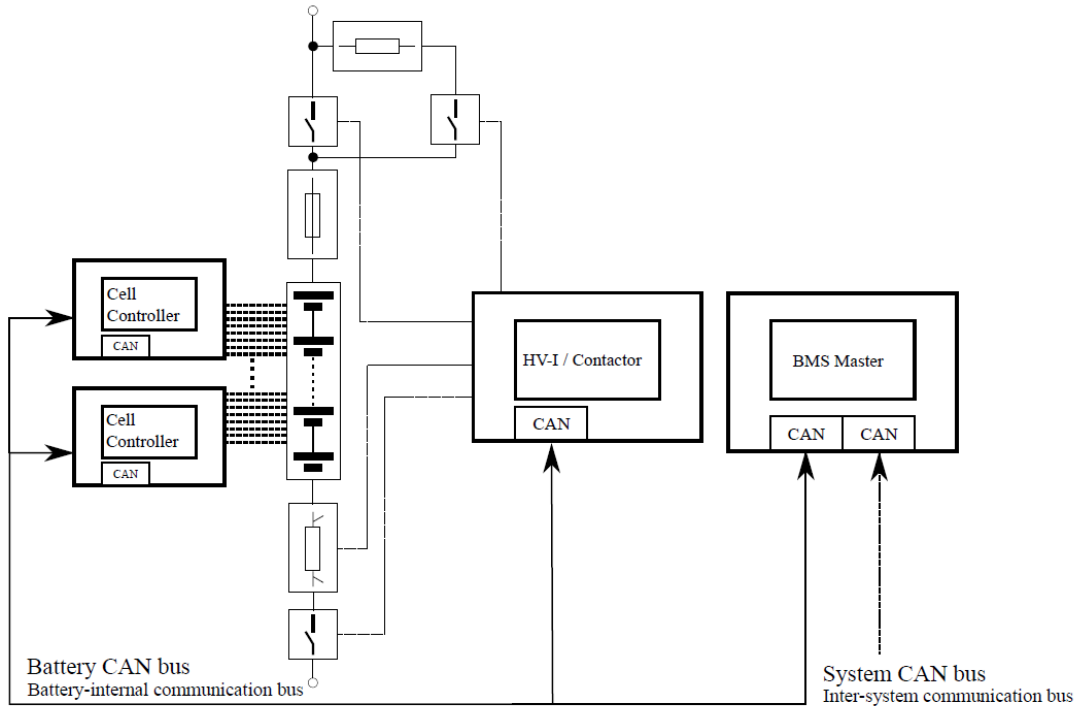


Figure 2.7: Structure of a typical BMS for battery applications [53].

The design of a BMS is complex and requires some considerations about the application's specific needs, the context of the system, and the characteristics of the cells. From these considerations, a list of requirements can be developed. In general, the BMS component and functional requirements include data (temperature, voltage, current) acquisition, data communication between BMS master module and slave modules and between the battery pack and surrounding applications, and other requirements on robustness against electromagnetic interference (EMI), contactors, redundancy of the system in terms of functional safety, galvanic isolation of functional systems, balancing and power consumption, size weight, etc. [53]. The structure of a typical BMS for battery applications is shown in Figure 2.7. The BMS can monitor different parameters in a battery pack (temperature, voltage, current, capacity, SOH, and coolant flow) to determine if any problems arise in the battery and take necessary actions to mitigate the issues. One of the more significant issues is the battery exceeding the operational limits. For example, overcharging can have a very damaging effect on the cells [54].

The main functions of the modern BMS include cell monitoring, cell balancing, battery safety and protection, state estimation, and thermal management, as can be seen in Figure 2.8.

- Cell monitoring: This function involves the acquisition of the current, voltage, and temperature of each cell in the system. The measurements need to reach a certain degree of accuracy, as the data are often used to perform other functions in the BMS. Also, the BMS is responsible for communication. It is the link between batteries and the vehicle and performs communication internally within the battery pack and externally to controllers, other packs, and application systems [55].
- Cell balancing: The imbalance of cell capacity can be caused by inconsistency in capacity and material quality from battery manufacturing, and aging during usage [56]. Cell balancing is to redistribute energy and maintain all cells at similar or the same SOC since battery pack's ability to charge and discharge is limited by the cell with the lowest SOC. There are two cell balancing approaches, active and passive balancing. Active balancing is to transfer excess energy in higher SOC cells into lower SOC cells until they reach the same level. This approach requires expensive hardware and more space in the pack therefore not implemented in EVs. On the other hand, passive balancing dissipates excess energy of higher SOC cells directly into heat to be removed. This is an easier and less expensive approach and widely used in EV applications. The function of cell balancing is necessary because battery capacity and lifetime will be reduced without it [57].
- Battery safety and protection: A main function of the BMS is to ensure the safety of the battery and protect it from operating at conditions that are harmful to both the battery and the users. Hazardous conditions are sometimes caused by the chemical characteristics of the battery. Fault diagnosis is a significant function of the BMS to ensure safe operation. Fault diagnosis algorithms detect the fault, determine its location and type, and perform control to reduce to influence of the fault [58]. Fault diagnosis methods can be categorized into model-based, knowledge-based, and data-driven methods [59]. The BMS also sets safety limits to protect the battery from working beyond the safe operating range of current, voltage, and temperature.
- State estimation: This mainly refers to the estimation of SOC and SOH. An accurate estimation of the battery SOC is necessary because it enables long battery life, prevention from battery failure, efficient operation, and accurate calculations of SOH and cell balancing. SOC estimation methods can be classified into look-up table method, coulomb counting method, model-based estimation methods, data-driven estimation methods, and

hybrid method [10]. Model-based methods require extensive knowledge about the background knowledge and are accurate but time-consuming to develop [56]. Data-driven methods are built upon experimental observations and do not require deep understanding of the theoretical knowledge, but they are constraint to data availability. The data-driven methods are neural network, deep learning, support vector machine, and fuzzy logic. SOH estimation is crucial in selected energy management strategies to prolong battery life and appropriately arrange for the replacement of the battery. There is a need to clearly define SOH since the definition is not definitive. SOH can be estimated by direct measurement methods such as capacity test and ampere counting, indirect analysis methods such as charging curve method and incremental capacity analysis, adaptive algorithms like ECM-based methods, and data-driven methods using empirical models and machine learning [60]. Despite the importance of state estimation, the SOC and SOH cannot be measured directly from the battery terminals. Therefore, algorithms need to be developed to estimate the SOC and SOH of the battery pack and the individual cells based on the measured data of each one.

- Thermal management: The performance of the battery is usually affected by its temperature due to the effect of temperature on degradation and internal resistance. The battery thermal management system (BTMS) can help decrease maximum battery temperature and temperature differences inside the pack [61]. There are three classes of BTMS, active, passive, and hybrid BTMS. Active BTMS are air-based, liquid-based, and thermoelectric whereas passive BTMS are phase change material (PCM)-based and heat pipe-based. Hybrid BTMS use combinations of active and passive approaches such as PCM with air circulation, PCM with liquid circulation, and PCM with heat pipe. Active BTMS require power input which increases cost, design complexity and battery pack weight, and thermal conductivity of air or liquid alone is insufficient to transfer large amount of heat from the pack. Therefore, passive and hybrid BTMS based on PCM are more ideal. PCM possess high latent heat and can regulate temperature by absorbing heat from cells during phase change. They are usually used with metallic fins, foams or meshes, and nanoparticles to enhance thermal conductivity for better heat dissipation [62]. Without proper thermal management, the battery pack is susceptible to thermal runaway propagation as overheat is a direct trigger of thermal runaway.

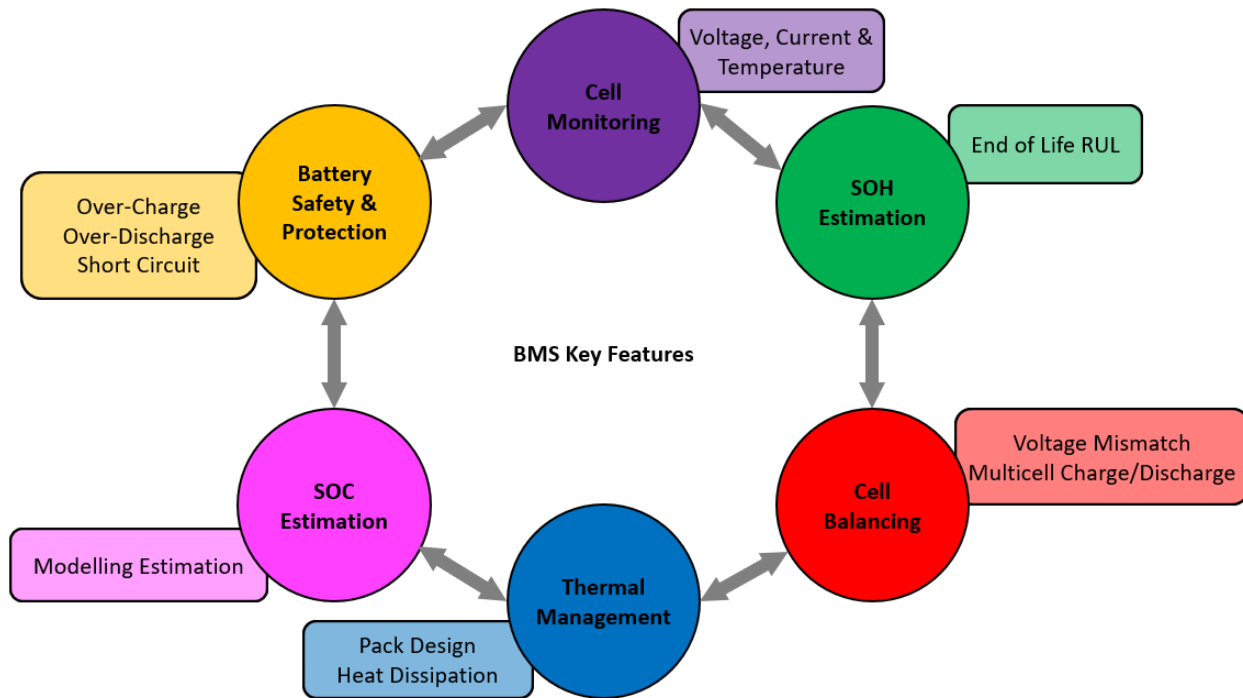


Figure 2.8: Various functions of the BMS.

2.2.2. Battery Modeling

In order to manage and control the battery with a smart system, it is necessary to understand how the battery behaves in various conditions. This prompts the need for mathematical modeling of battery, to predict the system behaviors and provide appropriate control and safety measures. There have been many suggested battery models in the literature, with different levels of detail depending on their intended use [2]. Mathematical models for batteries were essentially the empirical relationships between measured parameters, such as battery voltage, current, overall resistance, temperature, and remaining capacity. With more research being done on battery models, chemistry-based and physics-based models were developed. Some models are a combination of all the above. The three most commonly used types of battery models are electrochemical, empirical, and electrical.

Electrochemical models are based on the physical aspects of the battery and characterize power, current, and voltage [63]. The models use equations developed from the chemical processes that occur within the cell. Some examples of these equations include Fick's law, Ohm's law, the Butler-Volmer and Tafel equations. These models are usually highly accurate because they can describe the behavior of the battery in great detail. However, due to the level of detail of these

models, they are often too complex and computationally inefficient, especially for the use of online applications like EVs. These models often involve a system of coupled time-variant spatial partial differential equations and battery-specific information that is difficult to obtain. The solver may take hours or even days to solve the equations within these models, making them unsuitable for real-time use. These types of battery models are mostly used in research settings, not in battery management systems for vehicles.

Empirical models, also known as mathematical models, use experimental data from cells to predict the behavior of the battery in similar conditions. These models only fit the data without considering the physical or chemical principles that would require large computing requirements. This is more feasible for real-time applications. However, they cannot offer any information on characteristics of the battery which are critical for use in control and optimization algorithms. Also, since they are only based on a limited amount of data in certain conditions, these models cannot predict with high accuracy the battery behavior in other operational conditions [64]. The EV applications are constantly in flux, hence, these models would not satisfy the requirements to be used in EVs. With the rise of the data analysis and machine learning fields nowadays, these models will eventually be developed to potentially have the highest accuracy out of all the types of battery models, when an adequate amount of data is collected.

Electrical models predict the terminal characteristics of the battery, such as current and voltage, through variations of equivalent circuits [65]. An equivalent circuit is a theoretical circuit consisting of electrical components that represent various behaviors of the battery during its operation [66]. Electrical models can efficiently monitor the performance of the battery and other critical battery parameters such as SOC and SOH. They are more intuitive, useful, and easy to implement for engineers. Electrical models are becoming important to compute battery parameters, because of their adaptability for real-time use in battery applications. This ability to be adaptive makes electrical models the most feasible ones to be used in EVs.

2.2.3. Current Drawbacks of BMS

Some limitations of the BMS have hindered the integration of large-scale Li-ion battery systems, thus slowing down the wide adoption of renewable energy in Canada as well as globally [67], [68]. The main reason for these issues is the computational capability and data storage constraints, as the BMS is designed to be locally integrated into the battery system [20]. Battery

algorithms have been researched and developed while considering these constraints, and hence despite significant research efforts to improve these algorithms, many of them are not able to be practically implemented to improve the real-life performance of the BMS [69]. Data mining and machine learning methods, which require large computation and memory, have been implemented in various fields, as the IoT systems and cloud platforms like Amazon Web Services, Google Cloud Platform, and Microsoft Azure have become progressively more advanced, available, and affordable [70], [71], [72]. Machine learning and data-driven methods have been used for battery state estimation, charging management, fault diagnosis, giving promising results, yet being considered impractical due to the current limitations of the BMS.

2.3. Cloud Platform and Machine Learning

2.3.1. Cloud Platform

With the fast development of Internet technologies, the cloud platform has become a multi-service provider that shares information, software, and open resources within the Internet-based environment. Cloud computing was first introduced in 2007 and has since brought significant impacts and changes to numerous fields that were relevant to data science and information technology. Cloud computing is defined as a model that allows the sharing of many computing resources as services to various clients, in which the clients can easily change or adjust their service requirements at a very low cost. Cloud services are provided by delivering both applications and system software in data centers. Tang et al. [73] summarizes seven service components of cloud platform, which are storage as a service, database as a service, information as a service, process as a service, application as a service, platform as a service, and integration as a service. The components of cloud computing include data, information, application semantics, metadata, ontologies, schema, data dictionary, data catalog, and information model.

Before utilizing the cloud platform, integrating existing information, services, and models will be the first step for developers. Some cloud solutions provide a variety of interactions so that the DaaS (Data as a Service) becomes viable. These solutions can help aggregate and manage a large amount of data, making the cloud database easily accessible and usable for the clients [74]. After understanding and defining data, the next step is to create an information model to clouds, defined as the final to-be state of the data architecture for our SOA (service-oriented architecture)

using cloud computing and the jumping-off point for figuring out which data should reside on cloud computing platforms and which should reside on-premise [73].

The process of creating an information model is the procedure to understand the properties and meanings of the data after categorizing the data and to apply the data to desired applications. During this process, all information is defined and relocated to the clouds, which means data is successfully transferred to the applications. Moretti et al. [75] gave an example on data-intensive cloud computing, which describes a cloud implementation having a powerful functional outcome with a friendly easy-to-operation interface. The authors emphasized the significance of defining data and setting up the problem domain. Overall, cloud computing creates a platform that supports heavy application updates, data analysis, and decision making [76], [77], [78]. This qualifies cloud platforms in scalability, elasticity, fault-tolerance, self-manageability, and the ability to run on commodity hardware, which is effective from cloud economies [79].

2.3.2. Machine Learning

Machine learning is an application of artificial intelligence (AI) that provides the ability to learn and improve from experience automatically without human intervention or assistance and adjust actions accordingly (without being explicitly programmed) [80]. Machine learning focuses on the development of computer programs that can access big data and use it to learn for themselves. The process of learning begins with direct experiences, examples, or instructions, in order to look for patterns in data and make better decisions in the future based on previously provided observations.

Machine learning algorithms are often categorized as supervised or unsupervised.

- Supervised machine learning algorithms can apply knowledge learned in the past to new data using labeled examples to predict future events. Through the analysis of a known training dataset, the algorithm produces an inferred function to make predictions about the output values. The method can provide targets for any new input after sufficient training. This type of algorithm can also compare its outputs to the correct intended outputs and determine errors to modify the model accordingly. Types of supervised learning algorithms include active learning, classification, and regression.
- Unsupervised machine learning algorithms are utilized when the information or data used to train is unclassified or unlabeled. Unsupervised algorithms determine how to infer a

function to describe a hidden structure from the unlabeled data. This method does not focus on obtaining the right outputs, but rather on exploring the data and drawing inferences from the datasets to determine the hidden structures from the unlabeled data. Types of unsupervised learning algorithms include clustering, artificial neural network, anomaly detection, and reinforcement learning.

- Semi-supervised machine learning algorithms lie in between supervised and unsupervised learning since they use both labeled and unlabeled data for training, typically a small amount of labeled data and a large amount of unlabeled data. The applications that use this technique can considerably improve learning accuracy. Semi-supervised learning is often selected when the acquired labeled data requires skilled and relevant resources to train and learn from, such as in the medical diagnosis field. Battery algorithms can also benefit from this type of algorithm, as the battery behaviors and data require field-specific expertise to understand and label.

Machine learning enables the analysis of massive quantities of data to draw useful knowledge or solve complex real-world problems. While machine learning algorithms generally produce faster and more accurate results, they may also require additional computing capability and resources to train properly. Combining machine learning with AI and cognitive technologies can make it significantly effective in processing large volumes of information.

Chapter 3 : Investigation of Equivalent Circuit Models Performance in Various Lithium-ion Batteries

This chapter is adapted from the journal article “M.-K. Tran, A. DaCosta, A. Mevawalla, S. Panchal, and M. Fowler, “Comparative Study of Equivalent Circuit Models Performance in Four Common Lithium-Ion Batteries: LFP, NMC, LMO, NCA,” *Batteries*, vol. 7, no. 3, p. 51, 2021”, of which I am the first author. Contribution of authors is detailed in the Statement of Contributions section.

This chapter highlights the work from the author to investigate the difference in results when using equivalent circuit models for different types of chemistries. The purpose of the study is to show that while using equivalent circuit models in the battery management system is adequate, it is not a one-fit-all solution, and therefore, not the most suitable for rigid embedded applications like the battery management system.

3.1. Introduction

Over the past 10 years, the annual energy generation has increased over 73 million megawatts per hour, and renewable energy generation such as solar, wind, and tidal increased over 30 million megawatts per hour in Canada [81]. Energy generated from renewable resources cannot be easily stored like fossil fuels. Therefore, energy storage systems such as batteries are required to store the energy and be able to supply to the grid on demand. The acceleration of climate change has accelerated the development of batteries to reduce carbon footprints and encourage the use of renewable energy [82], [83].

Lithium-ion (Li-ion) batteries are becoming increasingly common due to their advantages as an energy storage system such as long cycle life, low self-discharge rate, small size, light weight, rapid charging capabilities, and wide temperature range [84], [85]. With changes to the materials used in anodes and cathodes such as spherical lithium iron phosphate cathodes [86], and lithium-sulfur [87], Li-ion batteries can have higher power density, higher energy density, and lower costs than competing chemistries, allowing them to be used in applications formerly dominated by other battery types. At the end of 2018, over 90% of large-scale battery storage power capacity was provided by Li-ion batteries in the US [88]. A total of 125 storage systems that held a combined

total of 869 MW was reported at the end of 2018, demonstrating exponential growth and doubling the reported value in 2015, just 3 years prior.

Batteries serve critical roles in the daily lives of their users. Therefore, optimization of battery performance via battery management system (BMS) is called for to further enhance their abilities and longevity. BMS software executes model algorithms, commonly using equivalent circuit models (ECMs), to continuously capture battery dynamics, allowing for the estimation of battery pack information [89]. BMS software can thereby perform the crucial task of maintaining a safe operating area (SOA) for modern electronics equipped with intensive cell arrangements and minimal tolerance for faulty behavior [90]. In the majority of BMS applications, important tasks include (1) determination of battery states (e.g., state of health (SOH), state of charge (SOC), state of function (SOF), etc.), (2) battery cell and battery pack monitoring, (3) energy management during charging and discharging, and (4) thermal management. To provide a specific example, a BMS in a battery application captures measurable information of current, voltage, power, and battery temperature to make comparisons with predicted values from the corresponding model, allowing the BMS to detect battery faults [91]. Among various battery estimation models, equivalent-circuit-based is gaining popularity due to its stability on major commercial battery chemistries such as LFP [92].

ECMs simulate the battery's internal characteristics, which may include three major parts: a static representation of battery chemistry properties such as nominal capacity and open-circuit voltage (OCV), a dynamic representation of the cell's internal operation such as internal resistance and RC time constant, and lastly, a source of potential that drives and completes the simulated circuit [92]. ECMs are constructed based on the physical understanding of the cell configuration and chemistry, and according to the Occam's razor principle which states that only components that correspond to the physical phenomena should be inserted in an equivalent circuit [93]. Therefore, elements of the ECM circuitry are configured to simulate existing battery chemistries. The ECM can help predict a battery's states including SOH, SOC, output power, and transient and dynamic behaviors based on terminal voltage. As mentioned above, ECMs are widely gaining popularity as a cost-efficient and relatively simple model in BMS design. Its suitability is mainly due to the reduced amount of model parameters and the underlying ordinary differential equation

model, allowing quick firmware operation during runtime and the ability to make estimations in advance [94].

ECMs have been studied for the purpose of investigating relationships between model accuracy and complexity, thus demonstrating the overall effectiveness of each type of ECM. He et al. [95] compared seven battery models, including three ECMs of zeroth, first, and second-order, using an LFP cell, to find that the second-order ECM had the best performance, and the first-order ECM was the second best. Hu et al. [65] compared the performance of twelve ECMs, under three sets of training data and temperature range, for NMC and LFP cells. The study found that the first-order ECM was preferable for NMC cells while the first-order ECM with hysteresis was better for LFP cells. Zhang et al. [96] tested two ECMs using an LFP cell, under the Urban Dynamometer Driving Schedule (UDDS) current profile and suggested higher efficiency from a second-order ECM for EV applications.

However, there has not been any comparative study on the performance of different ECMs, relatively, in multiple commonly used Li-ion battery types. This study utilizes four commonly used battery chemistries, including lithium iron phosphate (LFP), lithium nickel manganese cobalt oxide (NMC), lithium manganese oxide (LMO), and lithium nickel cobalt aluminum oxide (NCA). The performance of three widely used ECMs, including first-order ECM, second-order ECM, and first-order ECM with hysteresis, are compared among each other as well as in all four of the battery chemistries. The models are built and characterized using MATLAB and validated experimentally using a UDDS current profile and a non-dynamic current profile. The results are analyzed to evaluate model accuracy and model complexity for different battery chemistries and different applications.

3.2. Background

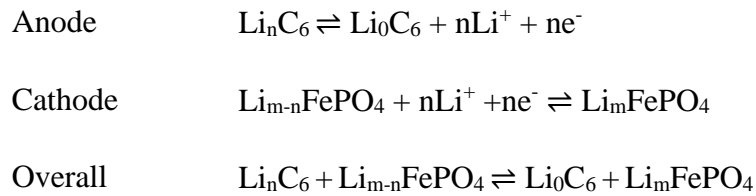
3.2.1. Lithium-ion battery chemistries

Many battery storage devices are made from electrochemical cells [97]. Electrochemical cells convert chemical potential to electrical potential when discharging and vice versa if the cell is charging. This study will focus on lithium-ion batteries and will exclude other popular battery types like lead-acid and nickel-metal hydride.

Li-ion batteries have a structured anode and cathode that houses lithium. The cathode can have three different structures that consist of layered, spinel, or olivine structure. With changes to the cathode materials on Li-ion batteries, the characteristics of energy density and cost effectiveness can be further improved. Among the phosphate-based cathode materials, LFP has the highest capacity though a much lower open circuit voltage [98]. However, when J. B. Goodenough et al. demonstrated the lithium extraction and insertion stability into FePO₄, an olivine structure, LFP solidified its position as the best candidate for phosphate-based cathodes [99].

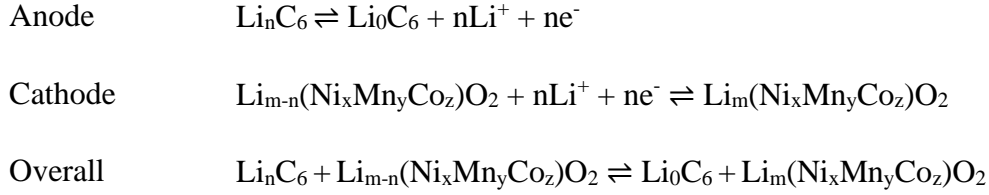
3.2.1.1. Lithium iron phosphate (LFP) battery

When LFP batteries discharge, lithium molecules from the negative electrode detach from layered graphene, becoming lithium ions and electrons. The electrons travel out of the battery as lithium ions move across a separator and both integrate into iron phosphates at the positive electrode. During charge, lithium separates from the iron phosphate, generating lithium ions and electrons. The lithium ions and electrons transfer to the positive electrode and integrate into the graphene structure. The reaction occurs from right to left. The electrochemical reactions are shown below [100].



3.2.1.2. Lithium nickel manganese cobalt oxide (NMC) battery

NMC is a Li-ion battery with a different type of cathode. Unlike LFP, which possesses good capacity and stability, NMC demonstrates improved cycle life, thermal stability, and energy density [101], [102]. Its layered cathode structure demonstrates a single-phase intercalation process as opposed to olivine structures with two phases [100]. The cathode of NMC consists of Li(Ni_xMn_yCo_z)O₂, where the sum of the molar fractions (x, y, z) is equal to 1 [103]. The discharge chemistry of NMC is similar to LFP as they are both Li-ion batteries. It follows the process of lithium oxidation on the anode and reduces at the cathode. The discharge reaction proceeds from left to right whilst the charge reaction proceeds from right to left.

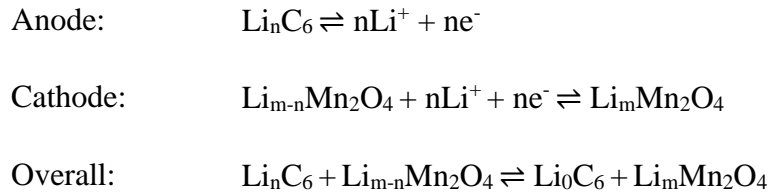


3.2.1.3. Lithium manganese oxide (LMO) battery

LMO batteries were first commercialized in 1975 by the Sanyo company, making it one of the first Li-ion batteries to be used commercially [104]. Newer LMO batteries contain a three-dimensional spinel structure to improve the diffusion of lithium ions [105], allowing it to have high thermal stability, low cost, and environmental affinity [106]. However, LMO batteries suffer from severe capacity fading due to the surface dissolution of manganese in the electrolyte at temperatures above 60°C.

A typical LMO battery provides a working voltage of 3.7 V and a specific capacity of 148 mAh g⁻¹. When compared to the average NMC battery, which has a working voltage of 3.6 V and a specific capacity of 170 mAh g⁻¹, the LMO battery has a slightly higher working voltage but a lower specific capacity.

The discharge chemistry is as follows, with the discharge reaction occurring from left to right and the charge reaction occurring from right to left.

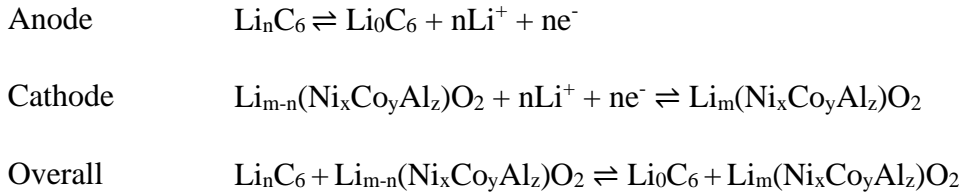


3.2.1.4. Lithium nickel cobalt aluminum oxide (NCA) battery

NCA batteries share many similarities with NMC batteries as they both share the layered cathode structure. However, NCA batteries replace the manganese of the NMC batteries with aluminum. This improves specific energy and lifespan when compared to its NMC counterpart [105]. NCA batteries also have a high gravimetric capacity of 200 mAh.g⁻¹ when compared to the capacities of LMO and LFP batteries at 148 mAh.g⁻¹ and 170 mAh.g⁻¹, respectively. Finally, NCA batteries have are known to have a long lifespan. The main disadvantage of NCA batteries is that

they are not as safe as other battery types. These batteries require special safety monitoring measures for use in applications such as electric vehicles [107].

The discharge chemistry of NCA batteries closely follows that of the other Li-ion batteries listed above. Lithium undergoes oxidation at the anode and reduction at the cathode, with the discharge reaction occurring from left to right and the charge reaction occurring from right to left. The electrochemical reactions can be seen below.



3.2.2. Equivalent circuit models for lithium-ion batteries

ECMs often use resistor-capacitor (RC) pairs to mimic the phenomenological behaviour of a battery's internal behaviour, for example, internal resistance, effective capacitance, and equivalent potential [108]. The commercial RC network model was originally developed by SAFT using the PSpice software platform and was later converted into ADVISOR's MATLAB-compatible platform [109]. It is designed based on the Thevenin model shown in Figure 3.1, which connects several parallel RC networks in series to simulate the dynamic characteristics of the battery.

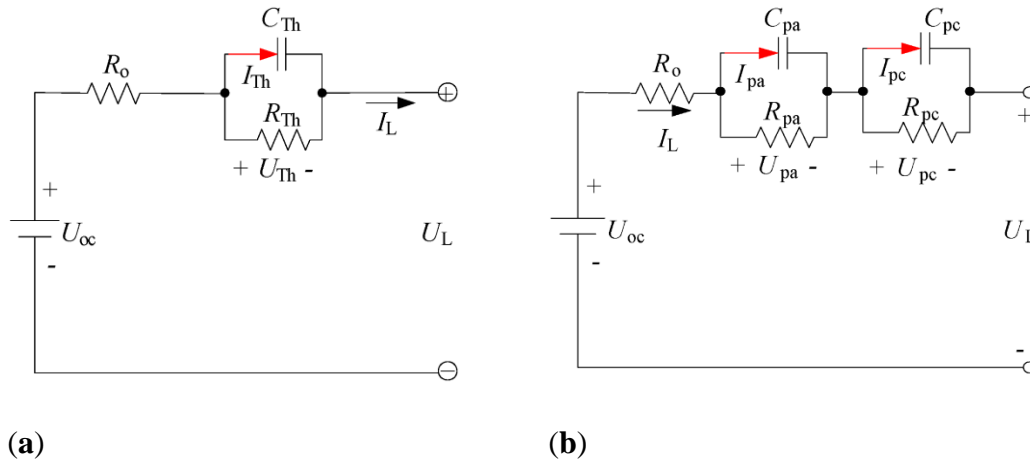


Figure 3.1: Equivalent circuit model diagrams, (a) first-order (1RC), and (b) second-order (2RC).

Figure 3.1 (a) shows a first-order ECM (1RC) which consists of major components including open-circuit voltage (U_{OC}), resistors (R_o , R_{Th}) which are used to represent ohmic resistance and polarization resistance respectively, and capacitance (C_{Th}) that describes battery's transient response during charge and discharge [30]. The second-order ECM (2RC), as represented by Figure 3.1 (b), is defined as a dual polarization (DP) model, which can provide refined representation of polarization characteristics, concentration polarization and electrochemical polarization independently. The 2RC model includes the internal resistance component (R_o) and polarization resistances R_{pa} and R_{pc} that represent a resistance characterizing electrochemical polarization, and a resistance characterizing concentration polarization, respectively. The second-order ECM also includes effective capacitance C_{pa} and C_{pc} which represent the transient response of the battery's charge/discharge process and the polarization characteristic, respectively. Factors including computational time, accuracy, and parameterization are key considerations of a BMS' efficiency [110], [111]. Adding RC networks up to a fifth-order RC model can increase accuracy, but RC networks beyond the second-order model would not achieve an effective balance between computational complexity and accuracy [65].

Hysteresis can be found in modern battery chemistries, which is a phenomenon that affects the cell's OCV during charging or discharging. Hysteresis can even occur in an idle state known as 'zero-current hysteresis', which can cause an OCV response of up to 50 mV or above [112]. Its behavior can depend on factors including charging or discharging relaxation time, battery chemistry, and battery SOC. Prominent hysteresis effects can be found in LFP chemistries, as well as the non-linear regions of SOC for some batteries, between 0–20% and 80–100% [113]. Comparatively, OCV-based estimation algorithms for the estimation models are developed under the combination of a dynamic hysteresis model and an n-RC ECM to further enhance accuracy. For this reason, dedicated circuitry components which represents battery's hysteresis behaviors are added to n-th-order RC model, which are defined as n-th-order RC model with hysteresis [114]. Batteries that exhibit large hysteresis levels would be affected when OCV-based SOC estimation methods are used [115]. The scope of this study will be limited to 1st order ECM with hysteresis.

The equations for the three models discussed in this study are shown below, in discrete form to better suit MATLAB model construction and calculations. The first-order ECM is as follows,

$$V_j = OCV - R_0 I_j - U_{1,j} \quad (3.1)$$

$$U_{1,j+1} = \exp\left(-\frac{\Delta t}{R_1 C_1}\right) U_{1,j} + R_1 [1 - \exp\left(-\frac{\Delta t}{R_1 C_1}\right)] I_j \quad (3.2)$$

the second-order ECM is as follows,

$$V_j = OCV - R_0 I_j - U_{1,j} - U_{2,j} \quad (3.3)$$

$$U_{1,j+1} = \exp\left(-\frac{\Delta t}{R_1 C_1}\right) U_{1,j} + R_1 [1 - \exp\left(-\frac{\Delta t}{R_1 C_1}\right)] I_j \quad (3.4)$$

$$U_{2,j+1} = \exp\left(-\frac{\Delta t}{R_2 C_2}\right) U_{2,j} + R_2 [1 - \exp\left(-\frac{\Delta t}{R_2 C_2}\right)] I_j \quad (3.5)$$

and the first-order ECM with hysteresis (ECMwH) is as follows,

$$V_j = OCV - R_0 I_j - U_{1,j} + H_j \quad (3.6)$$

$$U_{1,j+1} = \exp\left(-\frac{\Delta t}{R_1 C_1}\right) U_{1,j} + R_1 [1 - \exp\left(-\frac{\Delta t}{R_1 C_1}\right)] I_j \quad (3.7)$$

$$H_{j+1} = \exp(-|k I_j \Delta t|) H_j + [1 - \exp(-|k I_j \Delta t|)] h \quad (3.8)$$

where V is the battery terminal voltage, I is the battery current, OCV is the battery open circuit voltage, R_0 is the internal ohmic resistance, U_1 and U_2 are the voltages of the RC networks, $R_1 C_1$ and $R_2 C_2$ are the time constants of the RC networks, H is the hysteresis voltage, k is the hysteresis decaying factor, h is the maximum hysteresis voltage which is positive for charge and negative for discharge, and Δt is the sampling time, with the subscript j being the discrete index. In these equivalent circuit models, V is the output and I is the input, while OCV , R_0 , R_1 , C_1 , R_2 , C_2 , k and h are the model parameters and are functions of the battery SOC.

3.3. Experimental

One cell was tested for each of the four chemistries. The four cells, including LFP, NMC, LMO, and NCA, are presented in Figure 3.2. The specifications of each cell are outlined in Table 3.1. Experimental testing for all four cells was conducted using a MACCOR Model 4200 battery testing system, with each cell inside a fire-resistant chamber at a room temperature of 23°C, as

shown in Figure 3.3. All the tests described below were run at controlled ambient temperature to ensure data consistency.

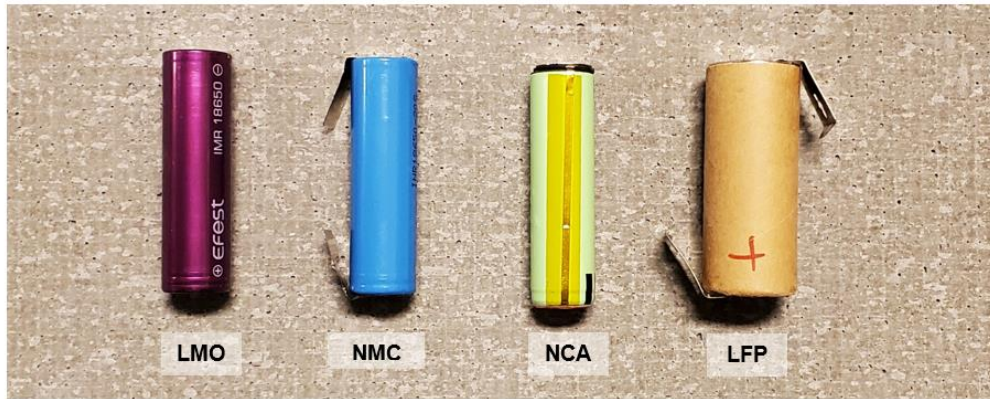
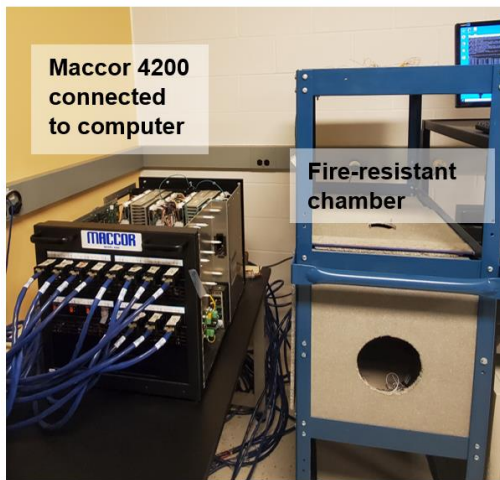


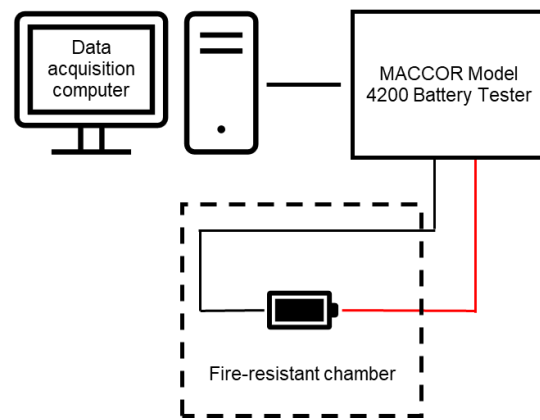
Figure 3.2: Four lithium-ion battery cells with different chemistries tested in the study.

Table 3.1: Cell specifications for each chemistry.

Chemistry	Manufacturer	Cell name	Nominal capacity [mAh]	Nominal voltage [V]	Voltage range [V]
LMO	EFEST	IMR18650V1	2,600	3.70	2.50-4.20
LFP	K2 Energy Solutions	LFP26650P	2,600	3.20	2.00-3.65
NMC	Samsung SDI	INR18650-20S	2,000	3.60	2.50-4.20
NCA	Panasonic	NCR18650B	3,200	3.60	2.50-4.20



(a)



(b)

Figure 3.3: Experimental setup, including (a) battery tester setup, and (b) schematic of setup.

3.3.1. Cell characterization experiments

The characterization of each cell consisted of three stages: (1) capacity testing, (2) SOC-OCV testing, and (3) hybrid pulse power characterization (HPPC) testing. Capacity tests consisted of three complete charge/discharge cycles at 1 C-rate. SOC-OCV tests consisted of a complete charge/discharge cycle at a C-rate of C/25. Lastly, HPPC tests were performed according to the test profile shown in Figure 3.4 (for the NCA cell as a representative for all 4 tested cells). At each SOC level from 0.1 to 0.9 with an interval of 0.1, a one-minute discharge/rest/charge pulse was run. The steps followed in the HPPC test were as follows, beginning at a fully charged state:

- (1) Discharge pulse at 1C for 10 s.
- (2) Rest for 40 s.
- (3) Charge pulse at 0.75C for 10 s.
- (4) Rest for 30 min.
- (5) Discharge at 1C for 6 min (resulting in a 10% drop in SOC).
- (6) Rest for 1 hour.
- (7) Repeat steps (1)-(6) 10 times.

The capacity tests are done to confirm the rated capacity of the cells, to ensure that the 1 C-rate current is accurate. The SOC-OCV tests are conducted to establish the relationship between SOC and OCV. The voltage and current data collected from the HPPC tests are used to fit the ECM parameters aside from OCV, using the '*nlinfit*' function in MATLAB. It should be noted, about the sign convention, that positive current values indicate discharging and negative current values indicate charging.

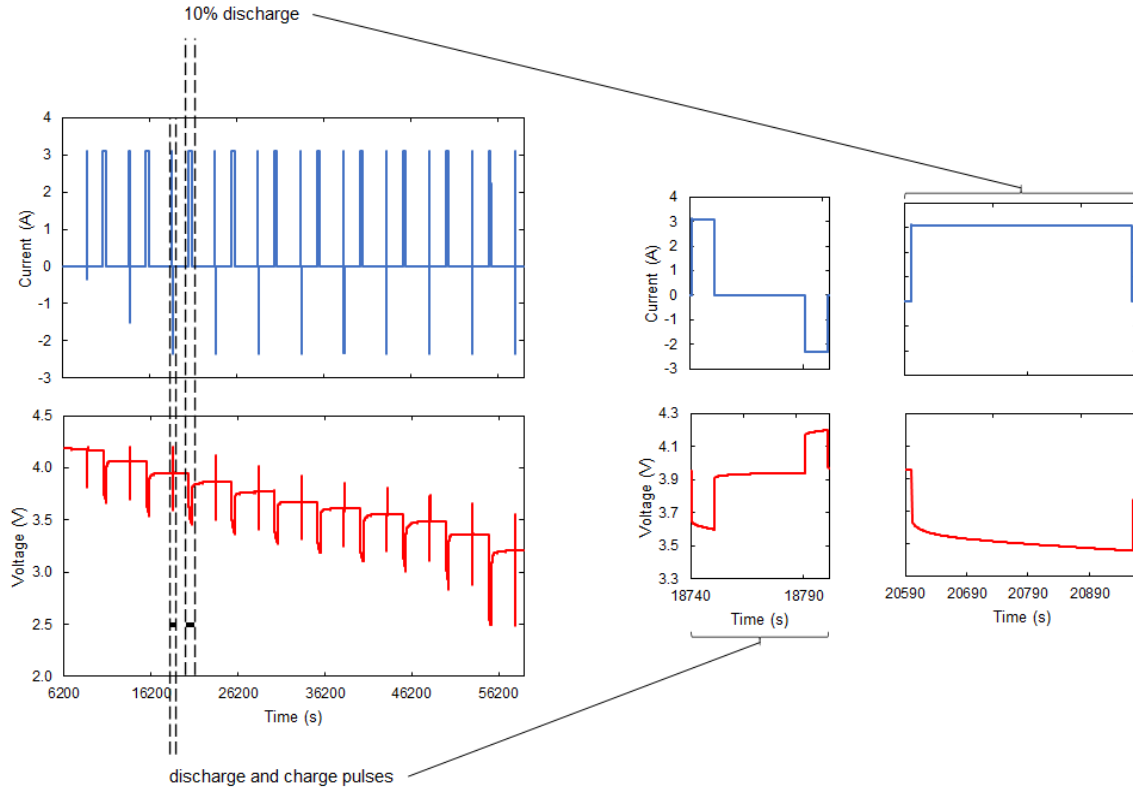


Figure 3.4: HPPC test profile for the NCA cell.

3.3.2. Model validation experiments

To validate the battery models, a dynamic profile and a non-dynamic profile were used, in order to represent different battery applications. A dynamic profile can be described as inconsistent charging and discharging cycles that mimic a real-life application. This is often used in battery testing to obtain real-life simulation data and can validate cell models. For example, UDDS represents general city driving conditions in the United States, established by the United States Environmental Protection Agency (EPA) [116]. The driving conditions can be translated into battery discharge and charge (regenerative braking) patterns. In contrast, a non-dynamic profile consistently performs battery cycles that simulate non-intensive electrical devices such as smartphones and other low-usage devices. Figure 3.5 shows the current profiles for one UDDS drive cycle and a non-dynamic (ND) cycle. The four batteries went through these cycles under the MACCOR, and the experimental voltage and current measurements were collected. The experimental current data was used as the input for the battery models, and the predicted voltage was then calculated as the output using MATLAB. The cycles were run at 11 different initial

battery SOC levels, ranging from 0.3 to 0.8 with an increment of 0.05, as this is the normal operating SOC range for many battery applications. The predicted voltage from the models was then compared to the experimental voltage to evaluate the performance of the models.

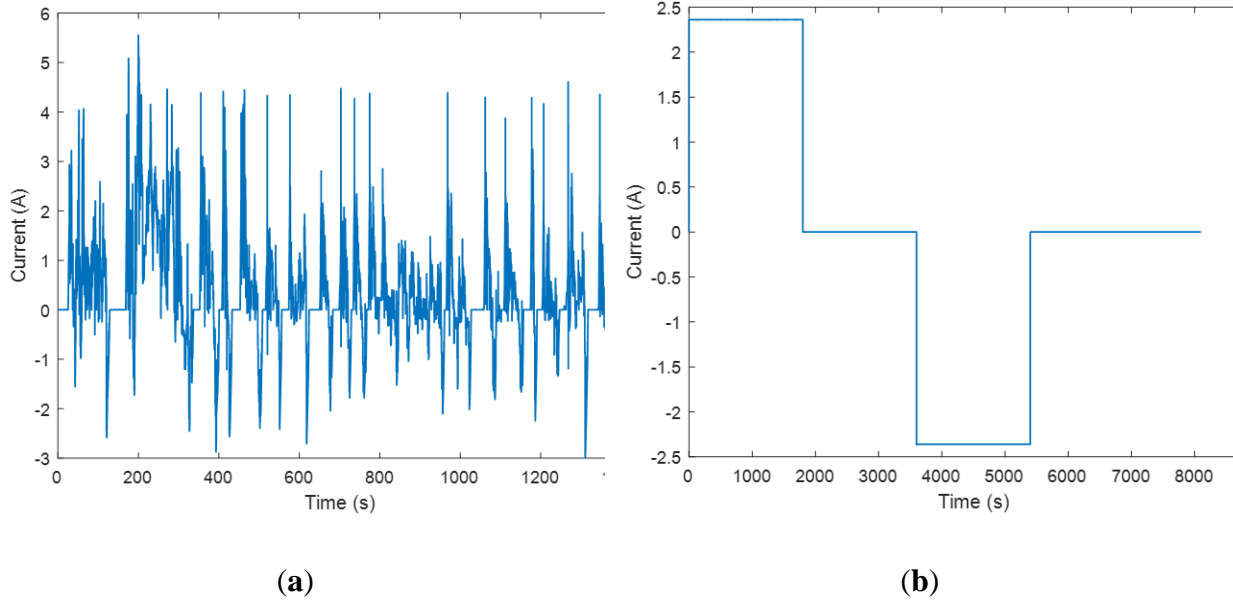


Figure 3.5: Validation current profiles for the four batteries, (a) UDDS cycle, and (b) ND cycle.

3.4. Results

3.4.1. Cell characterization results

The SOC-OCV curves were constructed for each cell chemistry as shown in Figure 6. The lower values of the OCV came from the discharging of the cells whereas the higher OCV values came from charging. The average OCV values are to be used in the three ECMs as a parameter. From Figure 3.6, it is observed that there is more variation between the high and low OCV values in LFP and NCA. It is, hence, expected that the 1RC with hysteresis model will perform better in those cells, compared to NMC and LMO.

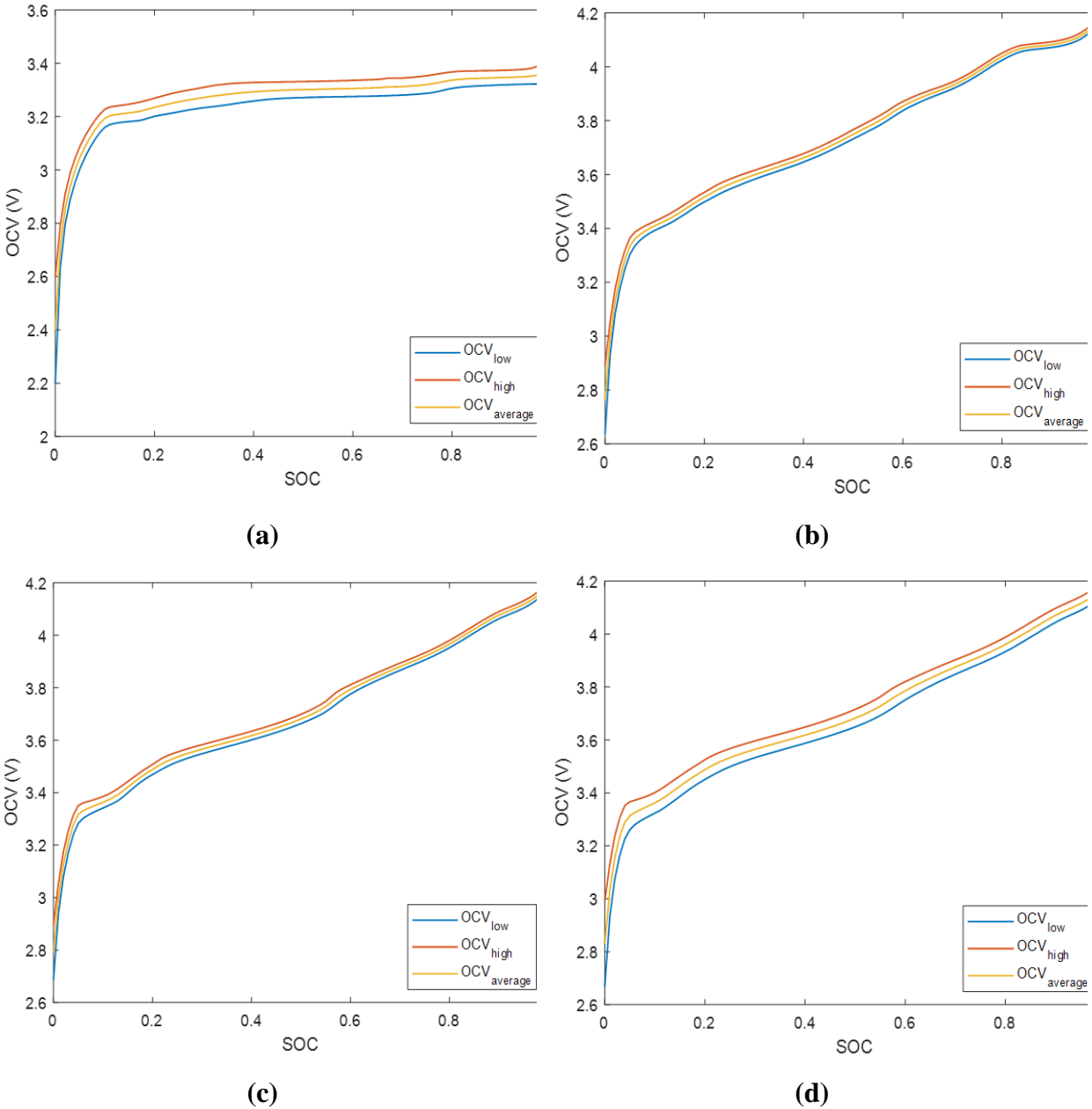


Figure 3.6: SOC-OCV curves for each lithium-ion battery chemistry tested; (a) LFP, (b) NMC, (c) LMO, and (d) NCA.

The data collected from the HPPC runs were fitted with the three ECMs using the *'nlinfit'* function in MATLAB which utilizes the Levenberg-Marquardt nonlinear least squares algorithm to fit data to functions. The MATLAB scripts for the model fitting can be found at <https://github.com/kmtran95/Battery-HPPC-model-fitting>. The voltage and current data from the one-minute pulse, at each SOC level from 0.1 to 0.9, were inputted into MATLAB and fitted with

the *'nlinfit'* function. The results of the fitting can be seen in Tables 3.2, 3.3, 3.4, and 3.5 for LFP, NMC, LMO, and NCA, respectively. The validation experiments would only be conducted under initial SOC levels ranging from 0.3 to 0.8. Thus, only parameter data from 0.3 to 0.8 SOC, obtained from the HPPC runs and interpolated from the result tables, would be utilized for model validation in this study. The parameters would then be used in the ECMs to predict the voltage in the UDDS and ND cycles at different SOC, and validation results are shown in the next sub-section.

Table 3.2: Model parameters obtained from HPPC data fitting in MATLAB for the LFP cell.

SOC	1RC			2RC					1RCwH				
	R0	R1	C1	R0	R1	C1	R2	C2	R0	R1	C1	k	h
	[Ω]	[Ω]	[F]	[Ω]	[Ω]	[F]	[Ω]	[F]	[Ω]	[Ω]	[F]	[]	[V]
0.9	0.0251	0.0280	769.39	0.0228	0.0278	1011.76	0.0047	456.43	0.0241	0.0144	714.37	0.0629	0.0274
0.8	0.0263	0.0351	747.04	0.0237	0.0361	967.72	0.0052	420.79	0.0252	0.0146	700.26	0.0416	0.0309
0.7	0.0271	0.0287	720.09	0.0242	0.0284	962.90	0.0055	355.45	0.0259	0.0148	646.30	0.0673	0.0319
0.6	0.0279	0.0312	687.74	0.0247	0.0311	935.50	0.0061	321.02	0.0266	0.0153	600.76	0.0537	0.0304
0.5	0.0284	0.0317	649.01	0.0248	0.0315	887.06	0.0067	271.69	0.0270	0.0160	558.52	0.0597	0.0300
0.4	0.0296	0.0367	618.50	0.0253	0.0373	863.25	0.0078	238.12	0.0281	0.0166	505.92	0.0353	0.0349
0.3	0.0306	0.0392	567.06	0.0257	0.0402	836.13	0.0094	210.55	0.0288	0.0177	433.25	0.0299	0.0383
0.2	0.0324	0.0487	520.73	0.0268	0.0539	834.83	0.0118	202.02	0.0300	0.0193	353.49	0.0087	0.0341
0.1	0.0344	0.0750	427.09	0.0287	0.1047	754.39	0.0164	214.49	0.0310	0.0234	277.31	0.0003	0.0338

Table 3.3: Model parameters obtained from HPPC data fitting in MATLAB for the NMC cell.

SOC	1RC			2RC					1RCwH				
	R0	R1	C1	R0	R1	C1	R2	C2	R0	R1	C1	k	h
	[Ω]	[Ω]	[F]	[Ω]	[Ω]	[F]	[Ω]	[F]	[Ω]	[Ω]	[F]	[]	[V]
0.9	0.0602	0.0198	1112.36	0.0586	0.0220	2254.18	0.0058	671.31	0.0594	0.0094	903.89	0.0048	0.0107
0.8	0.0612	0.0354	921.69	0.0601	0.0942	2310.05	0.0099	758.97	0.0603	0.0116	754.16	0.0041	0.0132

0.7	0.0610	0.0436	880.62	0.0598	0.1017	1852.54	0.0094	794.67	0.0601	0.0119	781.74	0.0041	0.0127
0.6	0.0615	0.0596	905.44	0.0600	0.1139	1395.74	0.0067	855.04	0.0604	0.0101	886.73	0.0049	0.0169
0.5	0.0613	0.0300	1249.34	0.0599	0.0389	1902.48	0.0045	884.10	0.0605	0.0079	1058.58	0.0057	0.0170
0.4	0.0630	0.0312	1268.09	0.0619	0.0460	2098.65	0.0049	1102.26	0.0623	0.0081	1136.45	0.0048	0.0157
0.3	0.0641	0.0330	1290.36	0.0630	0.0511	2076.67	0.0048	1098.68	0.0633	0.0077	1159.12	0.0045	0.0167
0.2	0.0614	0.0377	1287.61	0.0605	0.0854	2237.54	0.0056	1224.73	0.0607	0.0074	1216.08	0.0043	0.0179
0.1	0.0629	0.0392	1075.17	0.0619	0.1150	2206.02	0.0078	965.10	0.0621	0.0094	954.07	0.0039	0.0170

Table 3.4: Model parameters obtained from HPPC data fitting in MATLAB for the LMO cell.

SOC	1RC			2RC					1RCwH				
	R0	R1	C1	R0	R1	C1	R2	C2	R0	R1	C1	k	h
	[Ω]	[Ω]	[F]	[Ω]	[Ω]	[F]	[Ω]	[F]	[Ω]	[Ω]	[F]	[]	[V]
0.9	0.0428	0.0323	1041.59	0.0417	0.1061	1251.12	0.0078	846.01	0.0419	0.0101	851.06	0.0077	0.0136
0.8	0.0425	0.0404	888.84	0.0410	0.0919	1384.18	0.0062	776.83	0.0417	0.0124	816.91	0.0070	0.0139
0.7	0.0428	0.0515	862.27	0.0417	0.0912	1488.50	0.0079	911.13	0.0420	0.0123	867.86	0.0098	0.0138
0.6	0.0431	0.0661	838.53	0.0411	0.0808	1017.97	0.0044	668.99	0.0423	0.0114	975.99	0.0104	0.0178
0.5	0.0415	0.0307	1318.82	0.0402	0.0362	1744.50	0.0033	981.40	0.0409	0.0077	1301.65	0.0105	0.0177
0.4	0.0417	0.0287	1369.56	0.0405	0.0332	1805.97	0.0031	1074.47	0.0411	0.0076	1370.47	0.0108	0.0164
0.3	0.0424	0.0353	1329.23	0.0413	0.0472	1848.58	0.0036	1258.78	0.0418	0.0076	1366.15	0.0086	0.0173
0.2	0.0439	0.0375	1212.60	0.0426	0.0494	1690.60	0.0040	1036.82	0.0432	0.0082	1195.19	0.0057	0.0190
0.1	0.0553	0.0574	743.89	0.0510	0.0884	1144.14	0.0136	315.48	0.0510	0.0136	615.53	0.0039	0.0218

Table 3.5: Model parameters obtained from HPPC data fitting in MATLAB for the NCA cell.

SOC	1RC			2RC					1RCwH				
	R0	R1	C1	R0	R1	C1	R2	C2	R0	R1	C1	k	h

	[Ω]	[Ω]	[F]	[Ω]	[Ω]	[F]	[Ω]	[F]	[Ω]	[Ω]	[F]	[]	[V]
0.9	0.1086	0.0372	994.96	0.1063	0.0303	726.32	0.0099	636.78	0.1024	0.0338	905.42	0.0019	0.0266
0.8	0.1030	0.0492	928.76	0.1016	0.0302	734.10	0.0102	594.41	0.1016	0.0448	845.17	0.0017	0.0273
0.7	0.1033	0.0534	899.13	0.1020	0.0315	766.53	0.0105	575.44	0.1020	0.0486	818.20	0.0016	0.0272
0.6	0.1034	0.0527	958.57	0.1023	0.0390	929.76	0.0078	613.48	0.1025	0.0480	872.30	0.0027	0.0345
0.5	0.1032	0.0388	1233.95	0.1024	0.0271	1131.40	0.0078	789.73	0.1024	0.0353	1122.90	0.0012	0.0330
0.4	0.1048	0.0403	1237.15	0.1040	0.0275	1161.67	0.0077	791.77	0.1040	0.0367	1125.80	0.0011	0.0306
0.3	0.1050	0.0406	1231.86	0.1042	0.0272	1128.74	0.0077	788.39	0.1042	0.0369	1120.99	0.0011	0.0316
0.2	0.1081	0.0476	1166.00	0.1070	0.0272	982.50	0.0076	746.24	0.1070	0.0433	1061.06	0.0014	0.0373
0.1	0.1344	0.0619	999.38	0.1325	0.0498	747.54	0.0096	639.61	0.1241	0.0588	909.44	0.0016	0.0389

3.4.2. Model validation results

Using the parameters from Tables 3.2, 3.3, 3.4, and 3.5, the battery voltage of each cell can be predicted using the three ECMs, with the measured battery current data being the input of the models. Two types of cycles were used in the validation experiments, a dynamic UDDS and a non-dynamic discharge/rest/charge cycle, representing two different battery application types. In total, there were 132 validation runs, including one for each of the 4 cells, 3 models, and 11 SOC levels. Since there are a large number of runs, only one validation run result is presented as a representative. Figure 3.7 shows the model validation results for the LFP cell using the first-order ECM at 0.6 SOC. As can be seen, the model, for the most part, agrees well with the experimental data. This observation was also seen with the rest of the validation runs. It can be stated that all three models performed relatively well for predicting the battery voltage, indicated by the low errors between the predicted voltage and the experimentally measured voltage. For each run, the root mean square error (RMSE) of the voltage was calculated as a metric for model performance. The performance of each model in different cell chemistries can be evaluated and compared, and further comparative results and analysis are discussed in the next sub-section.

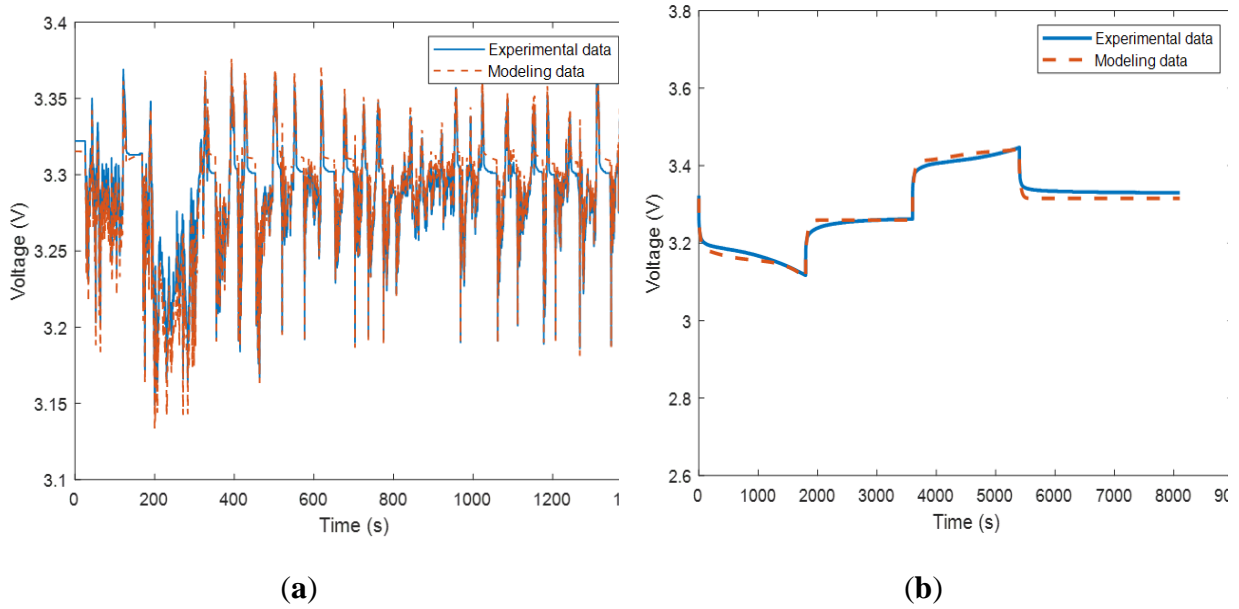


Figure 3.7: Model validation results from the LFP cell using first-order ECM at 0.6 SOC; (a) UDDS cycle, and (b) ND cycle.

3.4.3. Comparative discussion of models and battery chemistries

Figures 3.8 and 3.9 show the comparison between the 3 models for the 4 chemistries in terms of RMSE. The 'Average RMSE', 'Max RMSE', and 'Min RMSE' noted in the figures are the average, maximum, and minimum values of the RMSE for each of the 11 SOC levels that were tested for each model and cell chemistry.

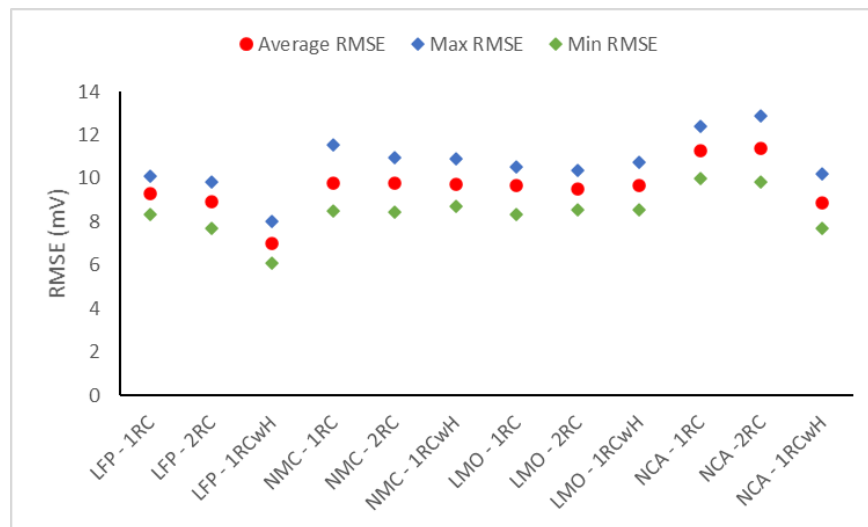


Figure 3.8: Model validation performance of different equivalent circuit models for various lithium-ion cell chemistries under the UDDS cycles.

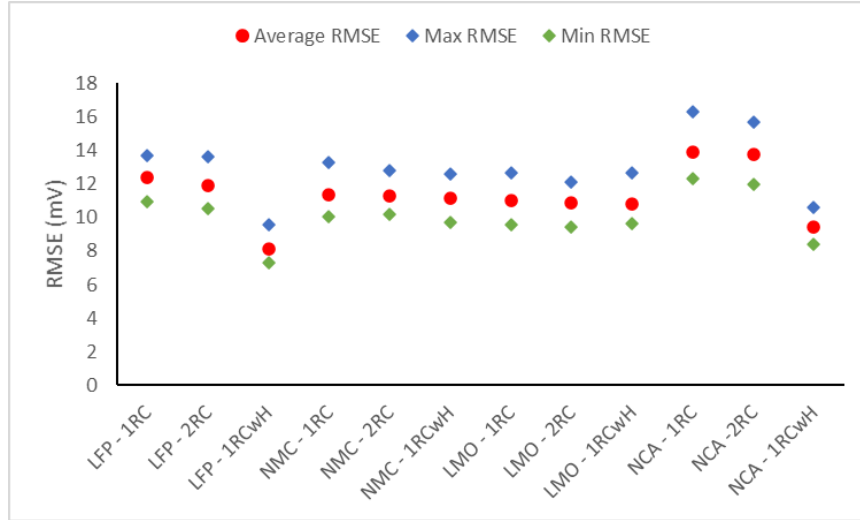


Figure 3.9: Model validation performance of different equivalent circuit models for various lithium-ion cell chemistries under the ND cycles.

As can be seen from the figures, the trends are relatively similar for the two cycles, UDDS and ND. However, the errors from the UDDS cycles are lower than those from the ND cycles, indicating that ECM might perform better in more dynamic applications. In terms of cell chemistry, using ECM without hysteresis, LFP, LMO, and NMC give better model prediction performance than NCA. Using ECM with hysteresis, LFP gives significantly better results than the rest. Also, NCA improves its results from the worst (using ECM without hysteresis) to the second best (using ECM with hysteresis). In terms of model accuracy, the 1RCwH model performed the best in LFP and NCA, which was expected from the SOC-OCV curves observations. For LMO and NMC, all three models have very similar performance, so the simplest model should be sufficient in these cells. In general, the 2RC ECM performs better than the 1RC ECM but not by a significant amount. It should be noted that, in terms of computational complexity, 1RCwH and 2RC have the same number of parameters so it is assumed that they have a similar complexity, while 1RC is the least complex since it has the fewest number of parameters. Therefore, it can be concluded that the 1RCwH model is most suited for LFP and NCA cells due to the high hysteresis effect in those chemistries, and the 1RC model is most suited for LMO and NMC cells because of its lower complexity and comparable performance overall.

3.5. Conclusions

This study investigated and compared the performance of 3 different equivalent circuit models (1RC, 2RC, and 1RC with hysteresis) using 4 Li-ion battery chemistries (LFP, NMC, LMO, and NCA) under dynamic and non-dynamic current profiles. The batteries underwent characterization experiments to obtain model parameters to be used in voltage prediction. The 3 models were then validated experimentally and compared using RMSE to determine the best model for each type of Li-ion battery. The main conclusions from this work are as follows:

1. All 3 ECMs were able to predict battery voltage with low errors.
2. The hysteresis effect is stronger in LFP and NCA compared to NMC and LMO based on the SOC-OCV curves of the batteries.
3. The ECMs are more suitable for dynamic current profiles such as a UDDS cycle compared to non-dynamic profiles like a constant discharge/rest/charge cycle (a difference of approximately 2 mV in RMSE).
4. The ECMs perform the best for the LFP cell, and the worst for the NCA cell, while for NMC and LMO, the results are similar and in between the other two.
5. Overall, the best model for LFP and NCA is 1RC with hysteresis, as the improvement in accuracy is worth the increase in computational complexity. On the other hand, the best model for NMC and LMO is 1RC since it has decent accuracy compared to the other models while having the lowest complexity.

These findings above show that different ECMs are suited for different Li-ion battery chemistries, which should be an important factor to be considered in battery and BMS applications. The results from this study contribute towards a better understanding of battery modeling as well as the future developments of more advanced and accurate battery models to be used in real-world applications.

Chapter 4 : Comprehensive Equivalent Circuit Model

Development for Lithium-ion Battery

This chapter is adapted from the journal article “M.-K. Tran; M. Mathew; S. Janhunen; S. Panchal; K. Raahemifar; R. Fraser; M. Fowler, “A comprehensive equivalent circuit model for lithium-ion batteries, incorporating the effects of state of health, state of charge, and temperature on model parameters,” *J Energy Storage*, vol. 43, p. 103252, 2021”, of which I am the first author. Contribution of authors is detailed in the Statement of Contributions section.

This chapter highlights the work of the author to show that the commonly used equivalent circuit models in practical battery management systems are usually lacking, specifically in terms of parameters changes with battery state of health. This study shows the evidence of the gap, and addresses it with an empirical model, which is a solution that could be improved upon. The proposed model could be used to improve the battery management system performance, but these findings also suggest that the embedded nature of the battery management system might be a significant factor in its limitations.

4.1. Introduction

When modeling the dynamic behavior of a battery, accuracy and complexity are two important factors. The ECM has the potential to satisfy both factors effectively. The model consists of three major components: a component representing the thermodynamic properties of the battery chemistry, such as the open-circuit voltage (OCV) as a function of SOC; another representing the kinetic aspects of the cell internal impedance behavior; and a source or load to complete the circuit for the charge or discharge procedures [117]. ECM parameters typically include an internal ohmic resistance, followed by one or more resistor-capacitor (RC) pairs. The simplest model only takes the internal ohmic resistance into account which does not accurately represent the battery dynamics during operation [118], [119]. Thus, the Thevenin ECM, which has one additional RC pair to combine with the internal ohmic resistance, is widely used since it has a good balance between accuracy and simplicity. The ECM parameters are often estimated using a hybrid pulse power characterization (HPPC) test at different SOC values [120]. Some factors such as temperature and SOC can affect these parameters. For instance, an increase in temperature can lead to higher OCV

in certain Li-ion battery chemistries, and a decrease in SOC can lead to lower charge transfer resistance, which ultimately affects the ECM parameters [22].

The Thevenin ECM is shown in Figure 4.1. The model is used to calculate the battery voltage in response to the current. The OCV is represented by an ideal voltage source, which is correlated with the battery SOC. R_0 accounts for the ohmic resistance of the battery, and the parallel RC network (R_1 and C_1) represents the transient behavior of the battery resulting from the interfacial charge-transfer reactions at the electrode. The product of R_1 and C_1 represents the time constant for the RC pair. The Thevenin ECM is shown in Equations (4.1) and (4.2), expressed in discrete form. The Thevenin ECM is as follows,

$$V_j = OCV - R_0 I_j - U_{1,j} \quad (4.1)$$

$$U_{1,j+1} = \exp\left(-\frac{\Delta t}{R_1 C_1}\right) U_{1,j} + R_1 \left[1 - \exp\left(-\frac{\Delta t}{R_1 C_1}\right)\right] I_j \quad (4.2)$$

where V is the battery terminal voltage, I is the battery current, OCV is the battery open circuit voltage, R_0 is the internal ohmic resistance, U_1 is the voltage of the RC network, R_1 and C_1 are the polarization resistance and capacitance with the product $R_1 C_1$ being the time constant of the RC network, and Δt is the sampling time, with the subscript j being the discrete index. The model parameters OCV, R_0 , R_1 , and C_1 , are known to be functions of SOC and temperature.

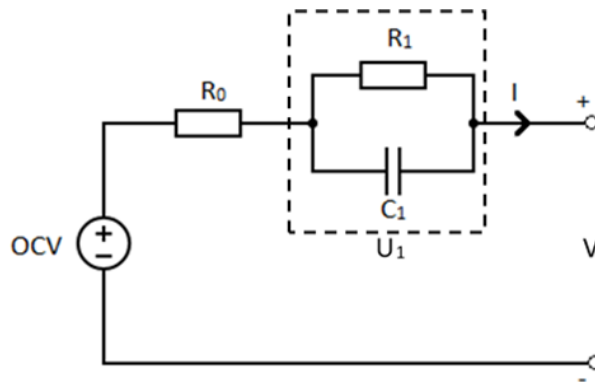


Figure 4.1: Schematic of the Thevenin equivalent circuit model.

Continuous usage of a Li-ion battery can lead to degradation, caused by loss of active materials or solid electrolyte interphase formation, resulting in the decrease of its SOH over time [121], [122], [123]. By understanding and including the possible effects of SOH on ECM

parameters in BMS algorithms, the BMS can improve the performance, reliability, and safety of the battery [124]. There are several methods that enable the online estimation of ECM parameters [125], [126], [127]. However, these methods do not consider either battery degradation or sensor faults, which can affect the accuracy of the estimated values and ultimately the reliability of the BMS. Lai et al. [128] performed a sensitivity analysis of ECM parameters for Li-ion batteries using the one-factor-at-a-time method. The analysis was conducted for different SOC and SOH ranges while excluding temperature analysis. Gomez et al. [129] examined the effect of SOC and temperature on the ECM parameters in the temperature range of 20 to 50°C at various SOC values. A simple model was proposed to integrate these effects into the ECM. The predicted model parameters showed a low variance of 5% when compared to the experimental data, and therefore indicated a good statistical agreement of the proposed model to experimental values. However, the relationship between ECM parameters and all three metrics together (SOH, SOC, and temperature) has not been fully explored in the literature. Also, a form of ECM that includes the effect of battery aging has never been proposed in the literature either. The contribution of this study is the investigation into the effects of SOH, SOC, and temperature on the ECM parameters. Another contribution is the proposal of an empirical model, which integrates these effects into the Thevenin ECM to improve its accuracy and reliability to be used in the BMS for real-world applications. Another important advantage of the proposed model is that it will allow for the simulation of Li-ion batteries at various SOH levels and temperatures, which can be used to develop and test other advanced BMS algorithms or to identify energy storage system design considerations.

4.2. Experimental and Trend Analysis

4.2.1. Experimental

The experiments involved five lithium iron phosphate (LFP) pouch cells at different nominal capacities with specifications shown in Table 4.1. All cells have similar electrical properties except for their capacities, in order to minimize any unwanted variables and ensure the reliability of the experimental results. Cells 1, 2, and 3 were used for characterization and investigation of the effect of SOH, SOC, and temperature on the ECM parameters. Cells 4 and 5 were used to validate the proposed model. The original nominal capacity of these cells was 20 Ah. The lowered capacities were achieved by degrading the battery by cycling the cells over time, where the cells were discharged and charged at C-rates of 2C and 1C, respectively.

The completed experimental setup can be seen in Figure 4.2. The Maccor 4200, shown in Figure 4.2 (a), is the battery tester equipment used in the experiments. The current collectors and voltage sensors from the Maccor were connected to the cells in a thermal chamber, as seen in Figure 4.2 (b). To simulate several different temperatures for the battery testing environments, a CSZ MicroClimate thermal chamber was used as shown in Figure 4.2 (c). Before a test was conducted, the cells rested in the new temperature environment for at least an hour to allow the cell internal temperature to match the environment temperature. The voltage and current data were collected at a frequency of 1 Hz and then stored in a computer that has a software program that controls the Maccor, shown in Figure 4.2 (d).

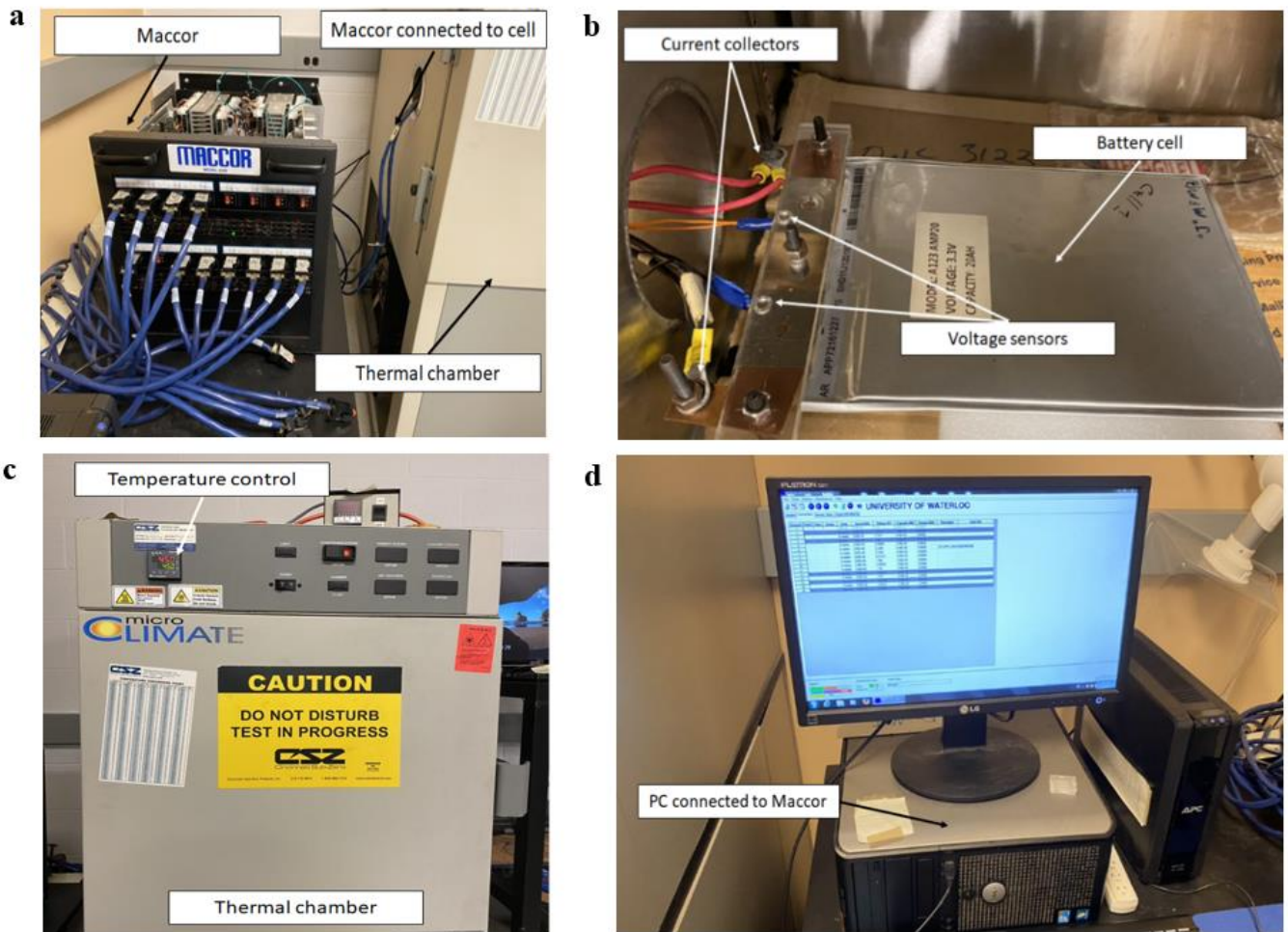


Figure 4.2: Experimental setup. a) Battery tester Maccor 4200. b) Connected and tested cell in the thermal chamber. c) CSZ MicroClimate thermal chamber. d) Computer software controlling the Maccor 4200.

Table 4.1: Specifications of the lithium-ion cells used in the experiments.

Cell Specifications	Cell 1	Cell 2	Cell 3	Cell 4	Cell 5
Capacity (Ah)	18.40	15.70	13.00	14.58	17.10
Cathode Material	LiFePO ₄ (all 5 cells)				
Anode Material	Graphite (all 5 cells)				
Nominal Voltage (V)	3.3 (all 5 cells)				
Cell Weight (g)	496 (all 5 cells)				
Dimensions (mm)	7x160x227 (all 5 cells)				

Characterization tests of cells 1, 2, and 3 included a capacity test, a SOC-OCV test, and multiple HPPC tests at varying temperatures. The capacity test measured cell capacity in Ah through fully discharging and charging the cells at a C-rate of 1C. The SOC-OCV test established the SOC-OCV relationship through a lookup table from the experimental results. The SOC-OCV test was conducted by fully discharging and charging the cells at a C-rate of C/25. The HPPC test was used to determine the ECM parameters of each cell at different temperatures and SOC values. For the HPPC test, at 0.9 SOC, a pulse was run, which consisted of a 10-second discharge at 1C, a 40-second rest period, and a 10-second charge at 0.75C. The cell was then rested for 1 hour and subsequently discharged for 6 minutes at 1C to decrease the SOC level by 0.1. It should be noted that in this study, SOH is defined using battery capacity (total remaining capacity/total initial capacity). These steps were followed by a 1-hour rest period and repeated until the battery reached a SOC of 0.1. The HPPC tests were run for cells 1, 2, and 3, at 5°C, 15°C, 25°C, 35°C, and 45°C, for a SOC range going from 0.9 to 0.1 with an interval of 0.1.

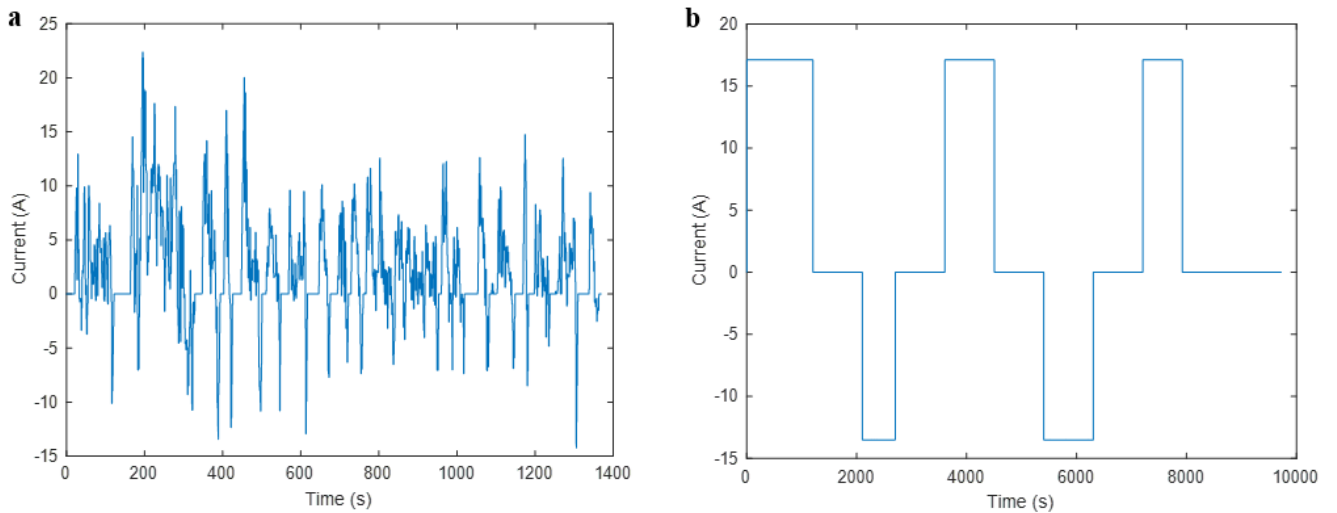


Figure 4.3: Current profiles used to validate the proposed model. a) UDDS. b) CCDC.

To validate the performance of the proposed empirical model, an Urban Dynamic Drive Schedule (UDDS) current profile and a non-dynamic constant charge/discharge cycle (CCDC) current profile were run on cells 4 and 5, at temperatures of 10°C and 40°C. The UDDS drive cycle simulates the dynamic charge and discharge of the battery to recreate the city driving conditions for light-duty vehicles. The CCDC profile was conducted by discharging the battery at 1C and charging the battery at 0.75C several times. The current profiles are shown in Figure 4.3. The battery was first charged to 0.8 SOC, and each of the current profiles was then run to reach 0.3 SOC. Using the proposed model, the parameters of the Thevenin ECM would be calculated based on the SOH, SOC, and temperature of the cells, and used to estimate the voltage to compare to the experimental voltage measurements. The accuracy of the model would then be evaluated and compared to the previous ECM method that does not consider the effect of SOH on the ECM parameters.

4.2.2. Trend Analysis

The OCV-SOC relationship was established experimentally by discharging and charging the cells slowly at a C-rate of C/25 and measuring the voltage through time. The OCV-SOC curve was constructed by averaging the results from all 5 tested cells at the beginning of their lifespan. It is noted that the OCV-SOC does not often change significantly throughout the lifespan of a Li-ion battery, especially within the studied SOC range of 0.3-0.8 [130], and therefore, the initial established OCV-SOC curve was used for all SOH values in this study. Another assumption that was made in this study for the OCV-SOC curve construction is the exclusion of the entropic coefficient, which represents the relationship between the OCV-SOC curve and temperatures. This was done to simplify the model, since the entropic coefficient is often only significant at more extreme SOC levels, and the SOC range studied is 0.3-0.8 where the entropic coefficient values would be close to zero [131]. A look-up table was built, which was needed to estimate the cell OCV which is a parameter in the ECM. The OCV-SOC curve is shown in Figure 4.4.

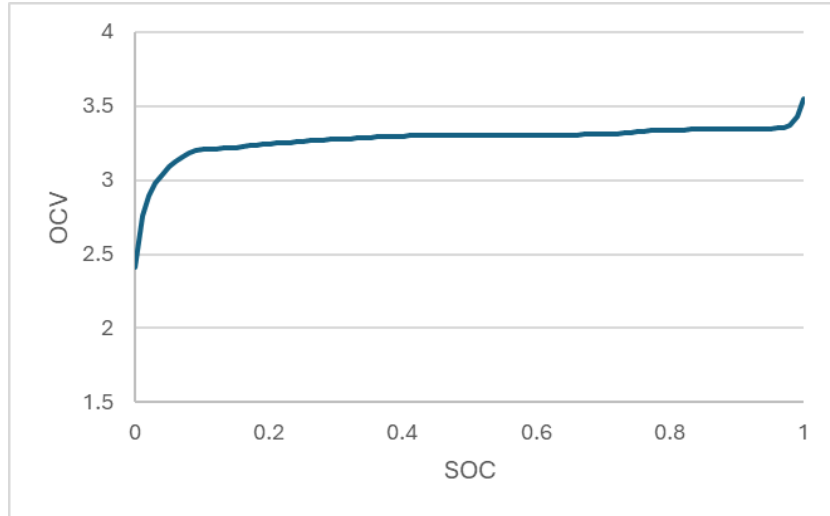


Figure 4.4: Experimentally established SOC-OCV curve of the LFP cells.

The other parameters of the ECM (R_0 , R_1 , and C_1) are known to be functions of SOC and temperature. The model parameters were determined by fitting the experimental results from the HPPC test to the ECM using the “*nlinfit*” built-in function in MATLAB, based on the Levenberg–Marquardt algorithm, which is often used to solve least-squares curve-fitting problems. The model was fitted in MATLAB using data from the 1-minute discharge-rest-charge pulses at different SOC levels ranging from 0.1 to 0.9 with an interval of 0.1 as well as at different temperatures ranging from 5°C to 45°C with an interval of 10°C. Figures 4.5, 4.6, and 4.7, using the obtained fitted parameter values, show the relationship between the ECM parameters (R_0 , R_1 , and C_1) and SOH, SOC, and temperature.

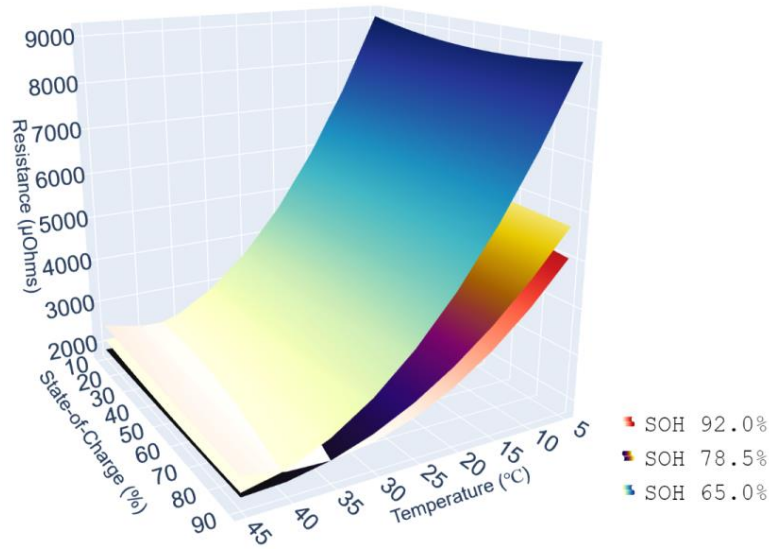


Figure 4.5: Effect of SOH, SOC, and temperature on R_0 .

From Figure 4.5, it can be seen that the ohmic resistance R_0 increases significantly with decreasing temperature at all SOH values. Also, the effect of SOH on R_0 is dependent on temperature, as the interaction effect between SOH and T is shown to be significant. Another observation indicates that R_0 increases as the battery ages, but this increase is only seen significantly at colder temperatures. At warmer temperatures, an increase in resistance is not observed at different SOH values. Finally, R_0 does not seem to vary significantly with SOC.

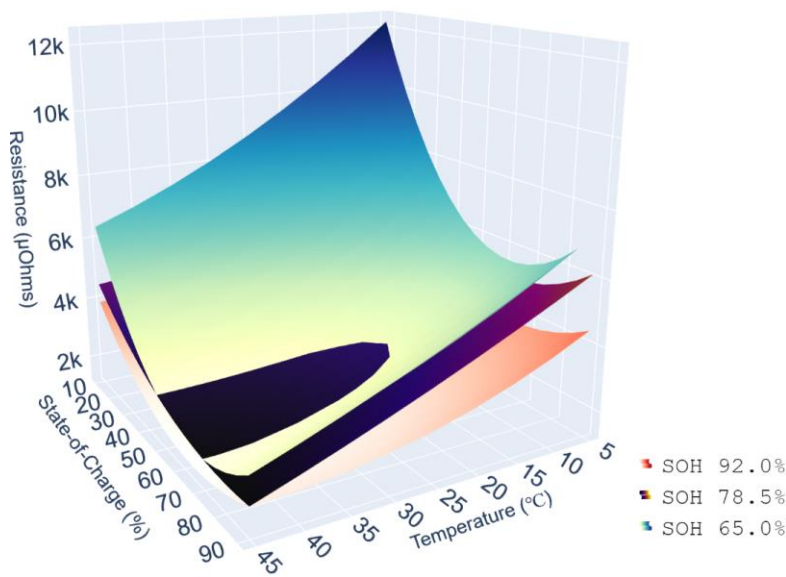


Figure 4.6: Effect of SOH, SOC, and temperature on R_1 .

Figure 4.6 shows that the polarization resistance R_1 increases with SOH, and unlike the ohmic resistance R_0 , the effect is observed at both high and low temperatures. R_1 also increases with decreasing temperature, showing a relatively linear and inversely proportional relationship. Finally, the polarization resistance R_1 varies significantly with SOC, with the resistance increasing when approaching both high and low SOC values. A higher level of variability is observed in the data for this parameter.

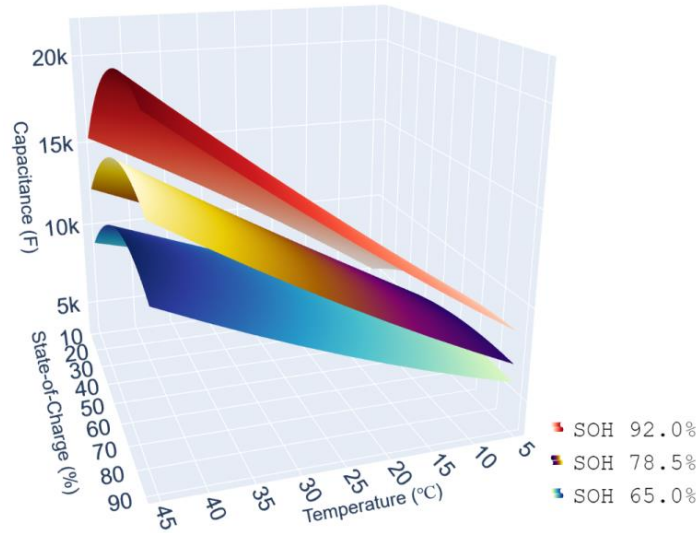


Figure 4.7: Effect of SOH, SOC, and temperature on C_1 .

It can be seen from Figure 4.7 that the polarization capacitance C_1 changes very significantly with SOH at all SOC and temperature values, as the three surfaces are relatively parallel. This shows that C_1 can be a good indicator of degradation, which agrees with the results found in [132]. Overall, C_1 decreases with SOH and increases with temperature. The effects of temperature and SOC on the polarization capacitance do not change with SOH, meaning that the interaction effects between temperature and SOH, and between SOC and SOH are not significant.

Overall, all three ECM parameters R_0 , R_1 , and C_1 are affected by SOH, as well as SOC and temperature. Therefore, it is possible to represent each of these parameters as a function of SOH, SOC, and temperature, which will be discussed in the next section.

4.3. Model Development and Validation

We use an empirical model to represent the relationship between the ECM parameters and the three factors SOH, SOC, and temperature, shown in Figures 4.5-4.7. It should be noted that the

SOC range considered in this study was 0.3 to 0.8 which is a normal operating range for many real-world applications. In this range, the relationship between the three parameters and the three factors can be observed from the figures to be acceptably linear, and no interaction effect between the three factors was prominent. Also, within the studied SOC range, it is observed that the relationships between the ECM parameters (R_0 , R_1 , and C_1) and the three factors SOH, SOC, and temperature are relatively monotonic functions. This explains an observation that, when second-order terms and interaction effects were added in the model development process, it was found that they did not improve the fitting results significantly while demanding more computing capability from adding more parameters to fit. Therefore, the terms in the proposed model are all of first order (linear); this would also allow the model to have low computational complexity, increasing its suitability for practical applications like the BMS. The equation for the empirical model for the ECM parameters is shown as,

$$X = b_0 + b_1SOH + b_2T + b_3SOC \quad (4.3)$$

where X represents any of the ECM parameters R_0 , R_1 , and C_1 .

Table 4.2: Parameters of the proposed model after fitting.

X	b0	b1	b2	b3
R0	10424.73	-48.2181	-114.74	-1.40433
R1	13615.54	-68.0889	-87.527	-37.1084
C1	-11116.7	180.4576	237.4219	40.14711

Using the parameter fitting results to fit Equation (4.3) for each ECM parameter, along with the “*nlinfit*” built-in function in MATLAB, the values for b_0 , b_1 , b_2 , and b_3 in the proposed model were obtained, as shown in Table 4.2. The proposed model parameters of C_1 are inverse in sign compared to the ones of R_0 and R_1 , which agrees with the observations of the trends from Figures 13-15. With this empirical model, we should be able to estimate the values of R_0 , R_1 , and C_1 at any SOC, temperature, and SOH.

In order to validate the proposed model, we conducted 8 validation runs as described in Section 4.2. A dynamic UDDS drive cycle current profile and a non-dynamic CCDC current profile were used for validation. Two SOH values of 72.9% and 85.5%, and two temperature settings of 10°C and 40°C were selected, which were different than the values used for

characterization and fitting the proposed model, to ensure the validation results are unbiased and reliable. The validation results for the 4 runs at SOH of 72.9% are shown in Figure 4.8, and the results for the 4 runs at SOH of 85.5% are shown in Figure 4.9.

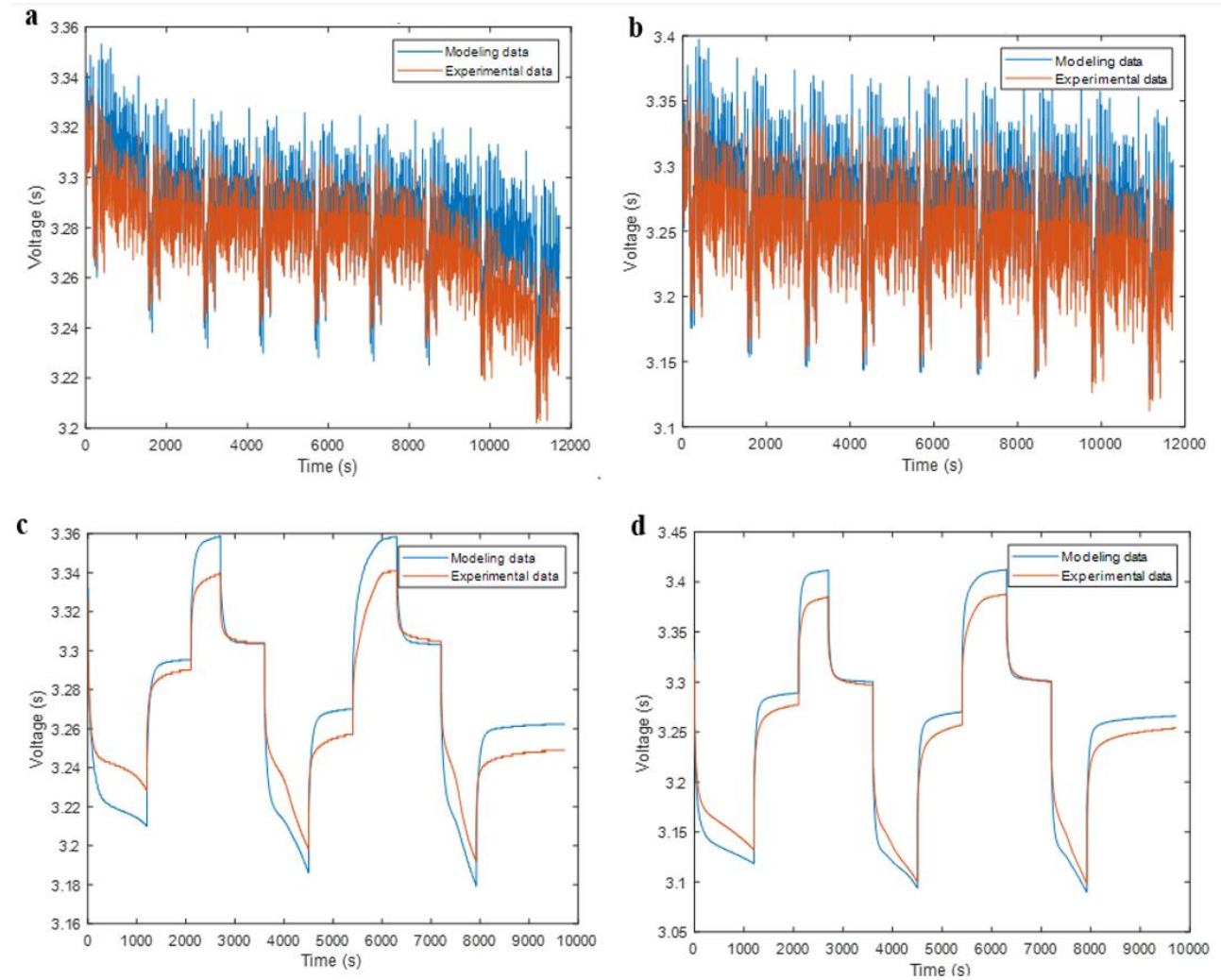


Figure 4.8: Model validation results at 72.9% SOH. a) Using UDDS profile at 40°C. b) Using UDDS profile at 10°C. c) Using CCDC profile at 40°C. d) Using CCDC profile at 10°C.

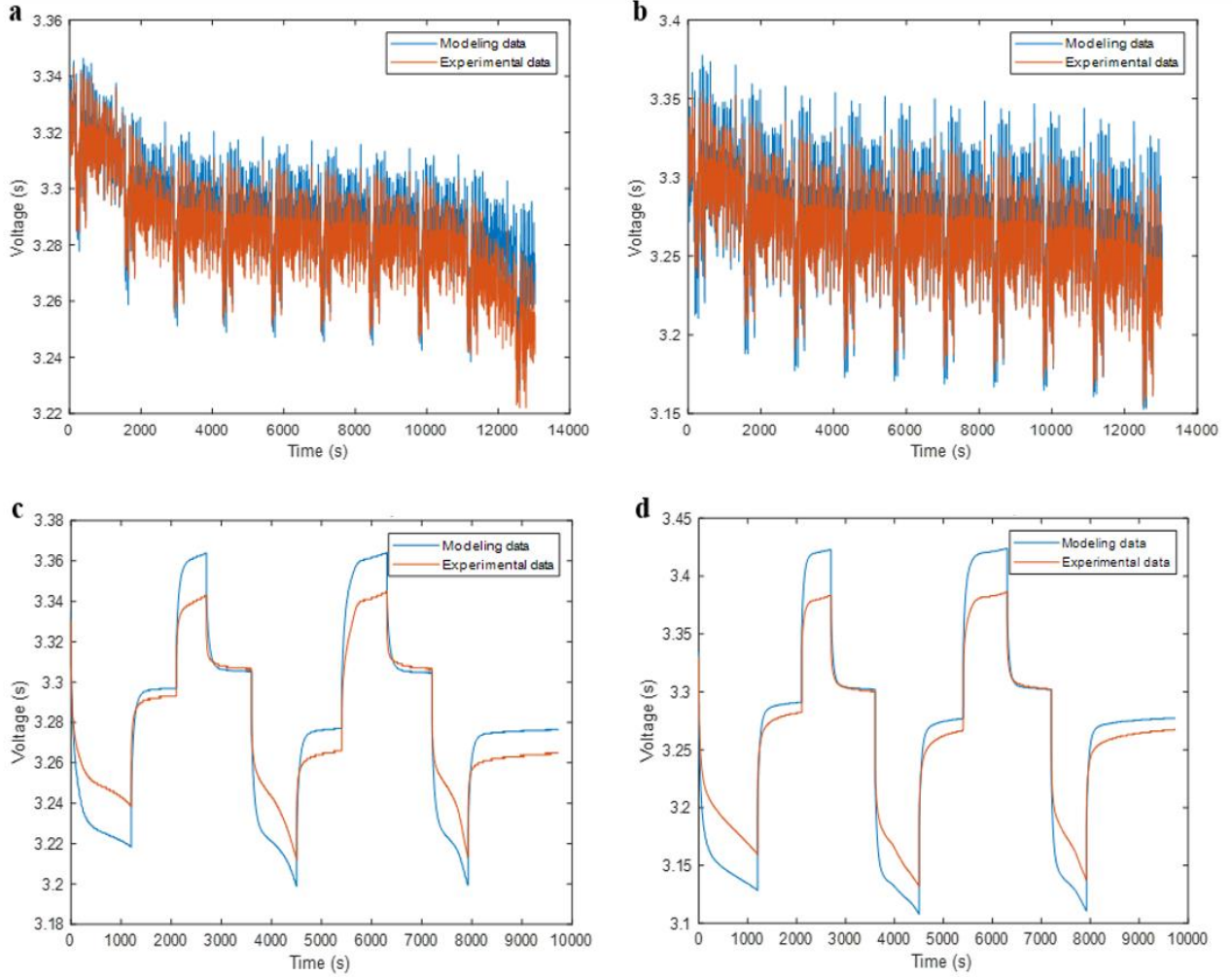


Figure 4.9: Model validation results at 85.5% SOH. a) Using UDDS profile at 40°C. b) Using UDDS profile at 10°C. c) Using CCDC profile at 40°C. d) Using CCDC profile at 10°C.

Figures 4.8 and 4.9 show good agreement between the predicted voltage using the proposed model and the actual voltage obtained from the experiments. To report the error quantitatively, the root-mean-squared error (RMSE) and the mean absolute percentage error (MAPE) can be calculated. Table 4.3 shows the summary of errors for all the validation runs, including RMSE and MAPE. The equations to calculate the RMSE and MAPE for N samples are shown as,

$$RMSE = \sqrt{\frac{\sum_{i=1}^N (V_{mod,i} - V_{exp,i})^2}{N}} \quad (4.4)$$

$$MAPE = \frac{1}{N} \sum_{i=1}^N \left| \frac{V_{mod,i} - V_{exp,i}}{V_{exp,i}} \right| \quad (4.5)$$

where $V_{mod,i}$ and $V_{exp,i}$ are used to represent the predicted and experimental voltage of the validation runs.

Table 4.3: Summary of errors for the model validation runs.

Figure	Run#	Run description	RMSE (mV)	MAPE (%)
8a	1	UDDS – 72.9% SOH – 40°C	11.99	0.32
8b	2	UDDS – 72.9% SOH – 10°C	16.74	0.48
8c	3	CCDC – 72.9% SOH – 40°C	14.78	0.39
8d	4	CCDC – 72.9% SOH – 10°C	18.13	0.49
9a	5	UDDS – 85.5% SOH – 40°C	7.63	0.2
9b	6	UDDS – 85.5% SOH – 10°C	11.14	0.31
9c	7	CCDC – 85.5% SOH – 40°C	8.05	0.20
9d	8	CCDC – 85.5% SOH – 10°C	10.38	0.27

From Figures 4.8 (a), 4.8 (b), 4.9 (a), and 4.9 (b), there was not any significant trend of deviation between each run, an indication to show that the model fitting was sufficient. When examining Figures 4.8 (c), 4.8 (d), 4.9 (c), and 4.9 (d), during the CCDC runs, it is apparent that the modeled voltage is higher during charge and lower during discharge compared to the experimental voltage. This trend is less apparent in the UDDS runs, and the error values are also lower in UDDS runs compared to their corresponding CCDC runs. This observation agrees with the findings in [114] and is due to the lack of representation of hysteresis in the Thevenin ECM, which will be a focus in our future research. Overall, in all cases, a strong agreement was observed between modeled and experimental results at all temperatures and SOHs, as shown by the low RMSE and MAPE values in Table 4.3. The largest deviation between experimental and modeled results was at 10°C and 72.9% SOH using the CCDC current profile, where an RMSE value of 18.13 mV and a MAPE of 0.49% were observed. There are a few other factors that could cause errors aside from the model inaccuracy, including experimental data noise, equipment error, and the capacity of the battery not being modeled as a function of temperature.

Some comparison between the errors found using this proposed model and typical error values found in the literature can be conducted to evaluate the performance of the model. Results from He et al. [95] showed an RMSE of around 13 mV when using a Thevenin ECM for the Federal Urban Dynamic Schedule (FUDS) test, while Hu et al. [65] obtained an RMSE of around

12 mV using the same model. In [114], the Thevenin ECM yielded a MAPE of 0.48%. The difference of the proposed model in this study compared to the Thevenin model used in [1], [65], [95], [114] is that this new model took into account the effect of SOH, whereas the simple model used in previous research works only considered SOC and temperature while keeping the SOH constant. Even with the increase in the number of variables, the error values obtained using the proposed model are comparable to the error values found in the literature, indicating good model accuracy.

Further analysis was conducted to show the improvement of results from using the proposed model. All 8 validation runs shown in Table 4.3 were simulated again but without considering the effect of SOH on the ECM parameters. This was done by using the ECM parameters found at 92% SOH for the 8 validation runs, despite them being at lower SOH levels, to represent the lack of SOH effect consideration. The resulting error values using this approach are compared to the errors when using the proposed model, as shown in Table 4.4. It can be seen that using the proposed model can reduce the errors, both RMSE and MAPE, by approximately half. This reduction in errors shows that the proposed model which considers the effect of SOH on ECM parameters can improve the Thevenin model accuracy significantly.

Table 4.4: Comparison of errors between validation results using the proposed model and not using the proposed model.

Run#	RMSE (mV) using proposed model	RMSE (mV) not using proposed model	MAPE (%) using proposed model	MAPE (%) not using proposed model
1	11.99	21.76	0.30	0.63
2	16.74	30.12	0.48	0.92
3	14.78	29.09	0.39	0.84
4	18.13	38.22	0.49	0.96
5	7.63	14.07	0.20	0.37
6	11.14	23.46	0.31	0.49
7	8.05	15.13	0.20	0.40
8	10.38	25.41	0.27	0.63

The results from these validation experiments suggest that the proposed model can be utilized by researchers in the future to accurately predict the voltage response of the battery at different SOH levels, without having to make the incorrect assumption of constant ECM parameters or having to characterize the battery at different SOHs while it undergoes degradation.

4.4. Conclusions

This study investigated the effect of SOH, SOC, and temperature on the Thevenin ECM parameters experimentally using LFP batteries. An empirical model was also developed and validated to reflect the effect of these factors on the ECM parameters. The main conclusions from this work are as follows:

1. All three ECM parameters were highly dependent on SOH, SOC, and temperature.
2. The ohmic resistance R_0 increased significantly with decreasing temperature at all SOH values. It also increased with decreasing SOH, more so at colder temperatures.
3. The polarization resistance R_1 increased with SOH, and unlike the ohmic resistance R_0 , the effect was observed at both high and low temperatures.
4. The polarization capacitance C_1 decreased with SOH at all SOC and temperature values at a relatively constant rate, which showed that C_1 can be a good indicator of battery degradation.
5. The empirical model developed in this study can be used to accurately predict the voltage profiles of an LFP battery cell at various SOH, SOC, and temperature conditions. The RMSE values and MAPE values when validating the model were low, showing good model accuracy.
6. The proposed model, which considers the effect of SOH on ECM parameters, was shown to improve the accuracy of the Thevenin model significantly. The errors when using the model were approximately half of the errors when the model was not used.

The findings in this study show the significant effect of SOH, or degradation, on the ECM parameters. The proposed empirical model attempting to represent this effect contributes towards a better understanding of battery degradation as well as the future development of more advanced and accurate battery models to be used in real-world applications. For future research, more investigation can be done for other types of battery cell such as cylindrical or prismatic, as well as for other Li-ion battery chemistry such as LMO, NMC, and NCA.

Chapter 5 : Cloud-Based BMS Design and Functionalities

This chapter is adapted from the journal article “M.-K. Tran; S. Panchal; T.D. Khang; K. Panchal; R. Fraser; M. Fowler, “Concept Review of a Cloud-Based Smart Battery Management System for Lithium-Ion Batteries: Feasibility, Logistics, and Functionality,” *Batteries*, vol. 8, p. 19, 2022”, of which I am the first author. Contribution of authors is detailed in the Statement of Contributions section.

This chapter highlights the effort to address the gap in the battery management system performance discussed in the previous chapters, as the battery models used often do not offer adequate accuracy, reliability, and robustness. This study shows a solution to this problem, which is a cloud-based battery management system, and discusses the potential design, architecture, and functionality of the new solution. The study also considers the advantages and disadvantages of the cloud-based system, as well as the challenges faced with its implementation.

5.1. Current Design of the BMS

The BMS for Li-ion battery systems often has different layers for cells, modules, and packs. There is the “master” unit which is the main control and computing device, and there are many “slave” units that are used to monitor the voltage, current, and temperature of individual cells [53], [133], [134]. The “master” and “slave” units are constantly in communication with each other. The “slave” units monitor the cells and modules and collect data through sensors, then send the data to the “master” unit for processing and further control actions. The BMS also communicates with the contactors, in order to assure safety and also to regulate the input and output current for the battery system. The “master” unit can also be in communication with a user interface for applications that require more involved control and monitoring. The current BMS design is offline and local, meaning that it is operating without connection to the internet or any servers. The data is usually stored locally in the “master” unit, or sometimes a separate unit if the data is exchanged asynchronously, and old data is deleted regularly to make room for newer data. The firmware is also hard-programmed into the BMS, which means that the BMS has to be application-specific and cannot be a one-fit-all solution.

The original two main functions of the BMS were monitoring and protecting the battery [135]. The monitoring function refers to the measurement of current, voltage, and temperature of the battery while the protecting function is responsible for bringing the system to a safe state when the measured values fall above or below their safe operational ranges [136]. The current and more modern BMS is relatively more complex and includes functions such as cell monitoring, cell balancing, charge control, state of charge (SOC) and state of health (SOH) estimation, thermal management, fault threshold detection, and battery protection. Figure 5.1 shows the current BMS design and some of its limitations.

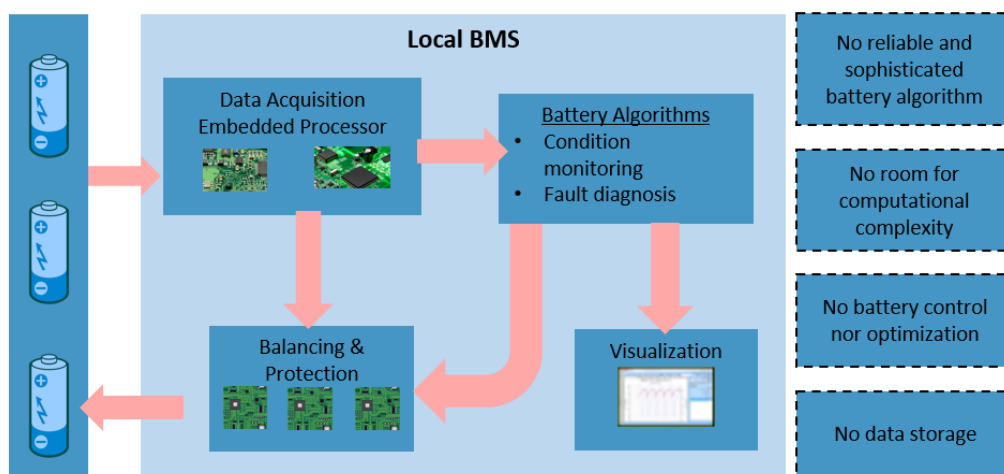


Figure 5.1: Current battery management system (BMS) design and functions.

A major issue with the offline BMS is the unreliability of state estimation algorithms [137]. Various model-based condition monitoring algorithms have been proposed to estimate battery states, including Kalman filter and dual sliding mode observer [138]. Some commonly used battery models in the BMS are electrical models [139], electrochemical models [140], thermal models [141], and coupled models [142]. However, due to the complex internal principles and uncertain working conditions, it is difficult to establish a battery model that can represent the battery's dynamic characteristics accurately [143]. Therefore, more complex data-driven algorithms are required to accurately estimate SOC, SOH, and RUL throughout the entire lifespan of the battery [144], [145]. However, despite the achievable development of these algorithms, they cannot be integrated into the BMS due to its limited computing capability and data storage [146], [147], [148].

Another major issue in the current BMS is the lack of reliable real-time fault diagnosis algorithms [149]. Some battery faults include sensor faults, cell connection defects, internal short-circuiting, external short-circuiting, overheating, and thermal runaway [150]. These faults can cause major performance and safety issues, and hence they need to be identified as early as possible. Various model-based methods currently used in the BMS utilize battery models and algorithms such as sliding mode observer [151], adaptive unscented Kalman filter [152], and structural analysis and sequential residual generator [153] to estimate parameters or residuals to detect battery faults. However, using these methods, many fault features are not reflected in the early stage of system failure. Some data-driven methods using signal processing [154], [155] and machine learning [156], [157] have been proposed to enable early and reliable fault detection but at the expense of high computing effort. Due to the data computing and storage limitations of the BMS, more reliable and accurate real-time fault diagnosis algorithms cannot be implemented.

5.2. Proposed Design of the Cloud-Based BMS

The limitations of the current BMS design have hindered the integration of large-scale Li-ion battery systems, thus slowing down the wide adoption of renewable energy. The main reason for these issues is the computational capability and data storage constraints, as the BMS is currently designed to be locally integrated into the battery system [158]. Battery algorithms have been researched and developed while considering these constraints, and hence despite significant research efforts to improve these algorithms, they are not able to be practically implemented to improve the real-life performance of the BMS due to their higher complexity. The trade-off between accuracy and complexity has always been a problem for BMS developers. However, with the recently proposed design of a cloud-based smart BMS, utilizing the advantages of cloud computing and cloud storage, this problem can potentially be resolved [159], [160], [161].

Data mining and machine learning methods, which require large computation and memory, have been implemented in various fields, as the IoT systems and cloud platforms have become progressively more advanced, available, and affordable [162]. Support-vector machine [163], Gaussian process regression [164], neural networks [165], Markov chain [166], and fuzzy logic [167] are methods that have been used for battery state estimation and fault diagnosis, giving promising results, yet being considered impractical due to the limitations of the BMS. The cloud-based BMS will have high computational power, limitless data storage capability, and great system

reliability. It can perform battery managing functions, like monitoring, diagnostics, prognostics, and optimization, more accurately and reliably. Some advantages of the cloud-based BMS are shown in Table 5.1. The development of the cloud-based smart BMS will potentially enable a new level of smart controls toward the next generation of energy storage technologies, paving the way for mass adoption of renewable energy globally.

Table 5.1: Advantages of cloud-based smart BMS.

BMS components	Advantages
Hardware	Potentially smaller devices leading to lower costs Significantly greater computational capability Virtually unlimited data storage
Software	More efficient operational control and optimization Better and more interactive monitoring and visualization More accurate and reliable prognostics and diagnostics

The cloud-based smart BMS design is outlined in Figure 5.2. The hardware and software requirements for this type of BMS are more demanding than the current BMS design, since it would need some extra components for cloud connection. The new design still has a local BMS consisting of the “slave” units. These “slave” units perform data acquisition by measuring the voltage, current, and temperature of battery cells in the pack using sensors at different sampling rates. There is also a “master” unit in the local BMS, but it would only perform basic safety functions such as cell balancing and fault threshold detection. These functions are better locally since they need to be performed fast in real-time.

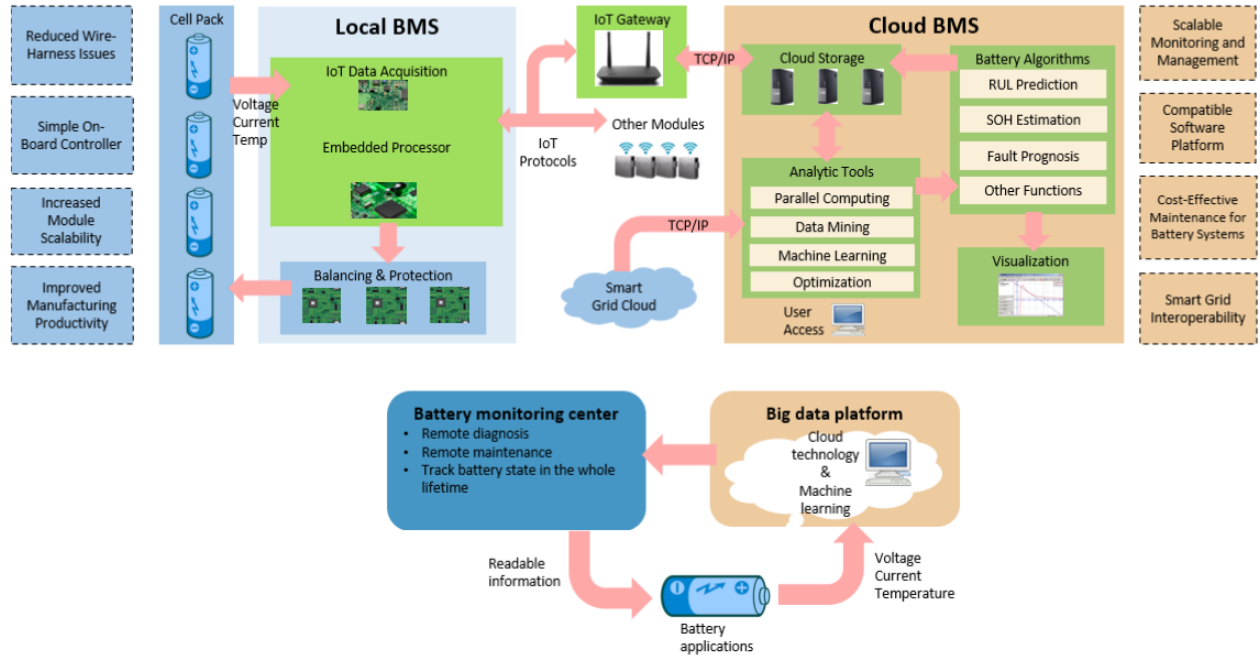


Figure 5.2: Potential design and functions of the cloud-based smart BMS.

As outlined in [160], [161], extra components for cloud connection include an IoT component, a cloud infrastructure, an application programming interface (API), and a user interface (UI). For the IoT component, a fast and stable internet connection like 5G is vital for real-time data transfer between the battery system and the cloud. As well, an IoT device such as Raspberry Pi, which is a small single-board processing unit, can be utilized for data transfer and communication. The measured battery data can be sent to the IoT component by the “slave” units using the Controller Area Network (CAN) protocol, and then forwarded to the cloud by the IoT component under the TCP/IP and Message Queuing Telemetry Transport (MQTT) protocol to ensure security and privacy. The cloud infrastructure usually consists of a data logger and a database. The data logger, which is a part of the IoT device, captures locally a large amount of non-structured or semi-structured data from the battery system and enables a secure gateway and data transfer into the cloud database. The database serves to store all the data to be used in the advanced battery data-analytic algorithms. The API, another component of the cloud-based BMS, acts as a bridge between the cloud database and the battery data analytics tools and algorithms, using popular programming applications such as Matlab and Python. The UI component of the BMS is necessary for the users to inspect and visualize the operation and state of the battery pack in real-time, as well as investigate historical operation data which can help the users schedule

maintenance and repair. This is a significant addition compared to the current BMS design which offers little data visualization. The users can be informed by the UI as soon as any battery system fault is identified through alarms, which helps reduce damaging effects to the batteries, ultimately improving the safety and reliability of the battery system and reducing maintenance costs.

5.3. Functionalities of the Cloud-based BMS

The development of an efficient, reliable, and accurate BMS plays a very significant role in safe and effective battery management and control. The cloud-based smart BMS is a step in the right direction for future battery applications. However, there are still many points to address before it can become practical. For example, there should be a logical split of BMS features and functionalities to utilize both the local processing unit and the cloud platform effectively and efficiently. The functions of a smart BMS, mentioned in previous sections, include data acquisition, cell monitoring, cell balancing, charge control, SOC and SOH estimation, thermal management, fault detection, and fault prognosis. The risks and integration approaches for this type of BMS are other points that should also be brought up in discussion.

The local functions of the BMS should include data acquisition, cell balancing, charge control, thermal management, and fault detection. Some of these functions, however, can be supplemented by the use of the cloud platform. Data acquisition must be performed locally since it is done through physical sensors connected to the battery system. The data cannot be stored locally, therefore, it is transferred to the cloud and stored there to be used to perform other BMS functions. Cell balancing is required as the inconsistency and discrepancy among the cells may negatively affect the pack's capacity, lifespan, and other important performance. Cell balancing for voltage can be done effectively with the local unit, and therefore does not have to utilize the cloud. However, cell balancing for SOC and capacity could benefit from data-driven equalization strategies which would require cloud computing and storage. Charge control prevents the battery system from overcharging and overdischarging and is another function that can be done effectively with the local BMS unit. Thermal management often involves cooling fluids or materials of which flow is controlled and adjusted based on the measured temperature, using control and feedback algorithms. Even though this function can be done locally, the use of the cloud can help improve it for future use, such as selecting a better cooling material or optimizing the control algorithms. Fault detection is another function that should stay in the local BMS units since it needs to be

reliable and done in real-time. The cloud platform depends largely on the internet connection which may not be completely reliable at all times, and hence, it is better and inherently safer to have the fault detection function offline.

The cloud functions of the BMS should include but are not limited to, cell monitoring, RUL prediction, SOH estimation, and fault prognosis. The cell monitoring function can be improved significantly with the help of the cloud platform, as it has better visualization, user interface, and more historical data, instead of a black-box solution like the current offline BMS. The estimation of SOC and SOH has always been a problem for the offline BMS, as it relies on the accuracy of the battery model and the estimation algorithms, which cannot be complex due to the computing limitations. With the cloud platform enabling high computing capability, users can develop and implement more accurate battery models (electrochemical models) and estimation algorithms (machine learning algorithms) for the SOC and SOH of battery systems. Fault prognosis is a supplementary function to the local fault detection function of the BMS. Instead of detecting faults as they occur, fault prognosis would use historical data and machine learning to predict where and when a fault might happen in the battery system, and notify the users to anticipate or prevent the fault. This function is also useful in terms of user behavior warnings as well as warranty tracking. There are other potential BMS functions that are not possible with the current offline BMS, such as lifetime prediction, economic optimization, etc., that can be developed with the implementation of cloud-based smart BMSs. Since this is a relatively new concept, there should be more discussions and research efforts going toward the efficient and effective split of the local and cloud functions for the smart BMS.

There exist some drawbacks associated with the cloud-based solution for the smart BMS. Firstly, a fast and reliable internet connection is a mandatory component of the system. However, this might not be feasible at certain locations or for certain applications, such as mining or remote areas exploration. Also, even for common battery applications, internet outages might affect the performance of the smart BMS. Backup power and internet connection are thus necessary to ensure the smooth operation of the battery systems. Secondly, costs are also an important component of the cloud-based BMS that needs to be investigated more thoroughly. The costs of operating and maintaining the cloud platform depend largely on the amount of data and algorithms used on the cloud. Therefore, researchers need to identify useful battery data and optimal data collection

frequency in order to minimize the costs of the cloud operation without sacrificing the accuracy and reliability of the BMS functions. Finally, since it is a relatively new concept for Li-ion battery systems, it needs to be implemented and tested in a small number of battery applications first, before it can be used widely in other applications. Applications that can benefit greatly from cloud-based smart BMS include EVs and large-scale battery ESSs due to the scale of data collection and the complexity of desired battery algorithms, and in these applications, a cloud solution implementation would also be easier and more sound.

5.4. Conclusions

With the rise of Li-ion batteries, the BMS plays an important role in ensuring safety and optimizing the operation of battery applications. However, the current design of the BMS shows several critical drawbacks. Recent developments in cloud-based smart BMS design will address a major issue of the current BMS, which is the unreliability and inaccuracy of its battery algorithms due to limited computational capability and data storage. It will provide a better solution for condition monitoring, fault prognosis, and optimization of Li-ion battery systems. The flexibility of the cloud system will also allow it to be used with minimal modifications in future ESS solutions such as solid-state Li-ion batteries, lithium-sulfur batteries, or metal-air batteries. By improving the reliability and performance of Li-ion battery systems, the cloud-based smart BMS will contribute to the mass adoption of renewable energy, making energy cheaper, cleaner, and more accessible to the public.

Chapter 6 : Analysis of Cell Replacement in Lithium-Ion Battery Packs

This chapter is adapted from the journal article “M.-K. Tran; C. Cunanan; S. Panchal; R. Fraser; M. Fowler, “Investigation of Individual Cells Replacement Concept in Lithium-Ion Battery Packs with Analysis on Economic Feasibility and Pack Design Requirements,” *Processes*, vol. 9, p. 2263, 2021”, of which I am the first author. Contribution of authors is detailed in the Statement of Contributions section.

Once the cloud-based battery management system is proposed as a future solution, the author introduces a potential application for this new solution. With the data storage of cloud platform, the battery history can be fully observed. This shall lead to the development and improvement of cell replacement strategies in lithium-ion battery packs, as well as the potential use of second-life batteries in stationary energy storage applications. This study highlights the work of the author to investigate the benefits of cell replacement, in terms of costs and battery life span, and also discusses the drawbacks in terms of pack design and implementation.

6.1. Introduction

Renewable energy sources play an important role in providing sustainable and clean energy and mitigating climate change globally. The development of renewable energy harvestings, such as solar and wind, has raised the demand for energy storage systems and transportation methods with reduced CO₂ emissions. Energy storage systems are the key to enable the storage and dispatching of electricity from renewable sources [168]. Lithium-ion (Li-ion) batteries, as an energy storage system, are gaining popularity in recent years, especially in automotive applications and large-scale energy storage facilities, due to their high energy and power density, long cycle life, high fidelity with high temperature tolerance, low self-discharge rate, and rapid charging capabilities [169], [170].

Li-ion battery cells can degrade through cycles of discharge and charge as well as over time even when they are inactive, with dependency on both temperature and state of charge (SOC) [171]. The degradation that occurs through discharge and charge is called cycling aging, while degradation that happens when it is not in use is called calendar aging. The degradation in Li-ion

batteries reduces the amount of energy and power that could be delivered in battery applications. After a certain number of cycles, Li-ion cells will eventually reach their end-of-life (EOL) stage. In some applications, such as electric vehicles, the EOL threshold of a battery is often when its remaining total capacity reaches 80% of its initial total capacity.

As battery packs consist of multiple cells, the potential and performance of the pack would be an overall average reflection to the state of each cell, but not specific to any certain cell [172]. Often in reality, due to the variability in characteristics of the cells, not all cells behave and degrade at the same rate [173]. Factors such as the pack's thermal management, SOC inhomogeneities, and manufacturing configurations are some of the reasons leading to the variation of the capacity fade of individual cells in the same pack [174]. As the battery pack reaches its EOL stage, it would likely contain some cells that are in a healthier state than other cells [175]. This makes replacing the entire pack not completely efficient since some of the cells would still be in usable conditions. The discarding of usable cells would effectively lead to unnecessary costs in Li-ion battery energy storage systems [176], [177]. An alternative strategy would be making the battery pack reconfigurable for individual cell replacement, so that only less healthy cells would be replaced with newer cells, instead of replacing the entire battery pack [178]. This strategy involves monitoring the levels of capacity fade of each individual cell and swapping out the most degraded cells based on a pre-specified capacity fade threshold. As a result, the effect of imbalance and premature aging in the pack could be minimized, and the degraded cells can be eliminated before causing more damage to the pack.

Some studies have been conducted previously to investigate the cell replacement concept. Kampker et al. [179] proposed a battery remanufacturing framework and suggested that the optimal depth of disassembly is up to the cell level, based on the reliability characteristic and the architecture of the cells within the battery applications. Mathew et al. [180] provided further analysis to a Li-ion cell replacement framework, with data collected from simulation to examine the optimal cell replacement interval. Nenadic et al. [181] examined the most viable cell replacement strategies under two scenarios of pack's early-life failure and reuse of Li-ion battery packs in less demanding applications. Some other recent studies have also explored cell-to-cell variation which could further prove the effectiveness of the cell replacement concept. Lu et al. [182] proposed a method to evaluate cell-to-cell variation in Li-ion batteries based on five cloud

indicators during charging. Omariba et al. [183] showed various Li-ion cell balancing methodologies to mitigate cell-to-cell variation and evaluate its relationship with the overall battery performance. As individual cell aging has an undermining effect on the lifespan of a battery pack, Rehman et al. [184] proposed a lifespan-extending algorithm that targets individual Li-ion cells differently to reduce any increase in the capacity mismatch. Zheng et al. [185] extended the investigation of the aging effect to a Li-ion battery pack by analyzing the evolution of battery capacity loss using the electric quantity capacity scatter diagram (ECSD) cell aging mechanism.

The concept of cell replacement in Li-ion battery packs is relatively new, and despite some recent efforts to investigate this concept, the feasibility, in terms of economics and design, of cell replacement has not been well-studied. In this study, a battery voltage model and a battery degradation model are presented to develop a cell replacement simulation framework. The simulation framework is then used to investigate the economic feasibility and design requirements of the cell replacement idea. Specifically, a pack of 40 Li-ion cells is simulated to its EOL stage, and another set of 40 Li-ion cells is used as the replacement for the cells in the original pack. The simulation is conducted repeatedly, using MATLAB, to determine if replacing cells individually would be more beneficial, in terms of battery life and costs, compared to replacing the entire pack that could still consist of healthy cells. The results of the simulation in this study are then analyzed to decide whether the cell replacement concept would be practical, or under what conditions would it be practical to be used in real-world applications.

6.2. Experimental

Lithium iron phosphate (LFP) pouch cells were used in this study. The specifications of the cells are shown in Table 6.1. The nominal capacity of the cells was 20 Ah, and the rated voltage range was 2.00 – 3.65 V. Experimental data was necessary to develop a realistic and robust battery cell model for the simulation. The mean and variance of the parameter values gathered in these experiments were used to generate randomized parameter values in the simulation. Specifically, the data were obtained by performing tests on four different LFP cells. The mean and variation in the parameters experimentally were then used to develop a distribution that was applied to stochastically generate the parameters for the 10 sets of 80 cells in the simulation framework, which will be further explained in Section 6.3.

Table 6.1: Lithium-ion pouch cell specifications.

Specifications	Value
Nominal Capacity	20.0 Ah
Nominal Voltage	3.3 V
Voltage Limits	2.0 - 3.65 V
Cell Weight	496 g
Dimensions	7.25 mm x 160 mm x 227 mm
Operating Temperature	-30 - 55 °C

The experiments were all conducted using a MACCOR 4200 battery cycler. The experimental setup is shown in Figure 6.1. The two types of experimental procedures that were conducted to obtain the data were a hybrid pulse power characterization (HPPC) test and the determination of the open-circuit voltage (OCV) to produce the SOC-OCV curve. The HPPC test is often used to determine the dynamic power capability over a useable voltage range of a given cell or battery [186]. In this study, the HPPC tests are used to determine the ohmic resistance and the polarization resistance and capacitance of the cells as a function of the SOC. The determination of the SOC-OCV curve is useful to estimate the OCV as a function of the SOC which can be used in further equations in the equivalent circuit model (ECM).



Figure 6.1: Experimental setup: experimental setup and MACCOR 4200 battery cycler (left); and tested 20Ah battery pouch cells (right).

Firstly, the HPPC test was used to determine the parameters for the ECM (R_0 , R_1 , C_1) at each SOC from 20% to 90%. To start, the cell was charged or discharged to the desired starting SOC of either 20% or 90%. The HPPC test was then carried out, for both charging and discharging, at 10% intervals between 20% and 90% SOC. The HPPC pulse consisted of a 1C discharge for 10 seconds, a 40-second rest period, and a 0.75C charge for 10 seconds. To move between the 10% SOC intervals, a constant-current discharge or charge of 1C of 6 minutes and a subsequent rest for 1 hour was performed. Secondly, the OCV curves were determined for the four cells across the SOC range of 0% to 100%, and the final curve was taken as the average of the four curves. For this test, the cells, at full charge, were subjected to a C/25 discharge current until they were completely drained, followed by an hour of rest, and then a C/25 charge until they were fully charged. The overall OCV curves were determined by taking the average of the charge and the discharge curves.

6.3. Modeling and Simulation

6.3.1. Cell voltage model

6.3.1.1. Model development

The battery cell voltage model used to represent the cells in this study is the Thevenin ECM, shown in Figure 6.2. This model provides a good balance between computational efficiency and accuracy. The Thevenin ECM consists of four main parameters, which are V_{oc} , R_0 , R_1 , and C_1 . V_{oc} represents the OCV of the battery; R_0 represents the internal resistance of the cell; and R_1 and C_1 represent the transient behavior of the cell as an RC pair with one being a resistor and the other being a capacitor. R_1 and C_1 are in parallel with each other, but in series with the voltage source and the R_0 element.

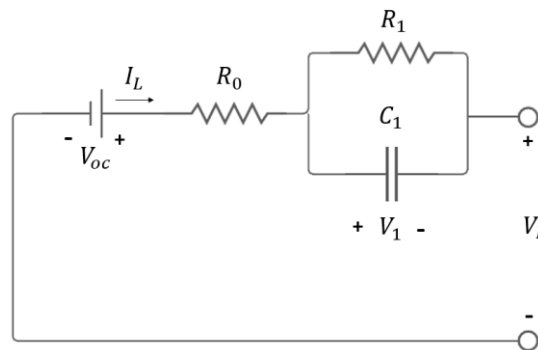


Figure 6.2: Schematic of the Thevenin equivalent circuit model.

The equations for the Thevenin ECM are shown below,

$$\frac{d(V_1)}{dt} = \frac{V_1}{R_1 C_1} + \frac{I_L}{C_1} \quad (6.1)$$

$$V_L = V_{oc} - V_1 - I_L R_0 \quad (6.2)$$

Using the OCV test and the HPPC test, the values of the four parameters (V_{oc} , R_0 , R_1 , and C_1) can be obtained at different SOC levels. The current I_L is an input variable to the model. The terminal voltage V_L can then be determined by solving Equations (6.1) and (6.2).

6.3.1.2. Model validation and results

The overall OCV curve was determined by averaging the four individual cell curves obtained from the OCV tests. The resulting final curve is shown in Figure 6.3. Following the HPPC procedure by Hu et al. [65], the other three ECM parameters (R_0 , R_1 , and C_1) were determined at the SOC levels between 20% and 90%. The results are plotted in Figure 6.4. For the overall trends, it can be seen that as SOC increases, the R_0 value decreases, the R_1 value stays the same, and the C_1 value increases. However, since the values of the ECM parameters were close enough along the SOC range to be used in the cycling simulation, they will be assumed as lookup tables – and not a continuous function of the SOC – when they are generated.

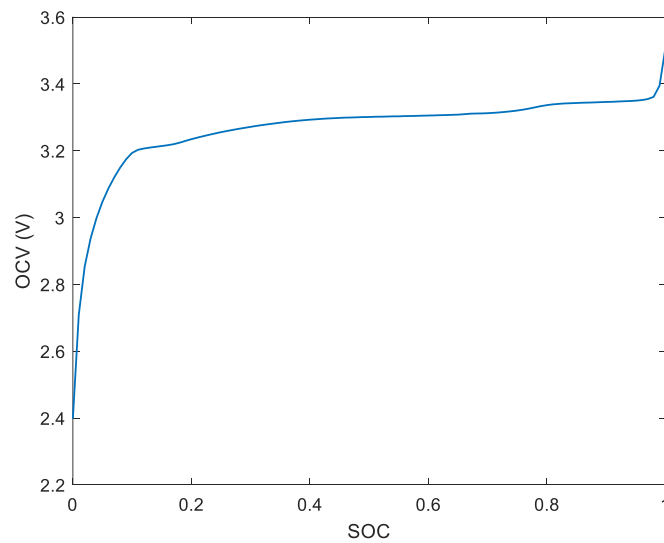


Figure 6.3: Experimentally established SOC-OCV curve of the LFP cells.

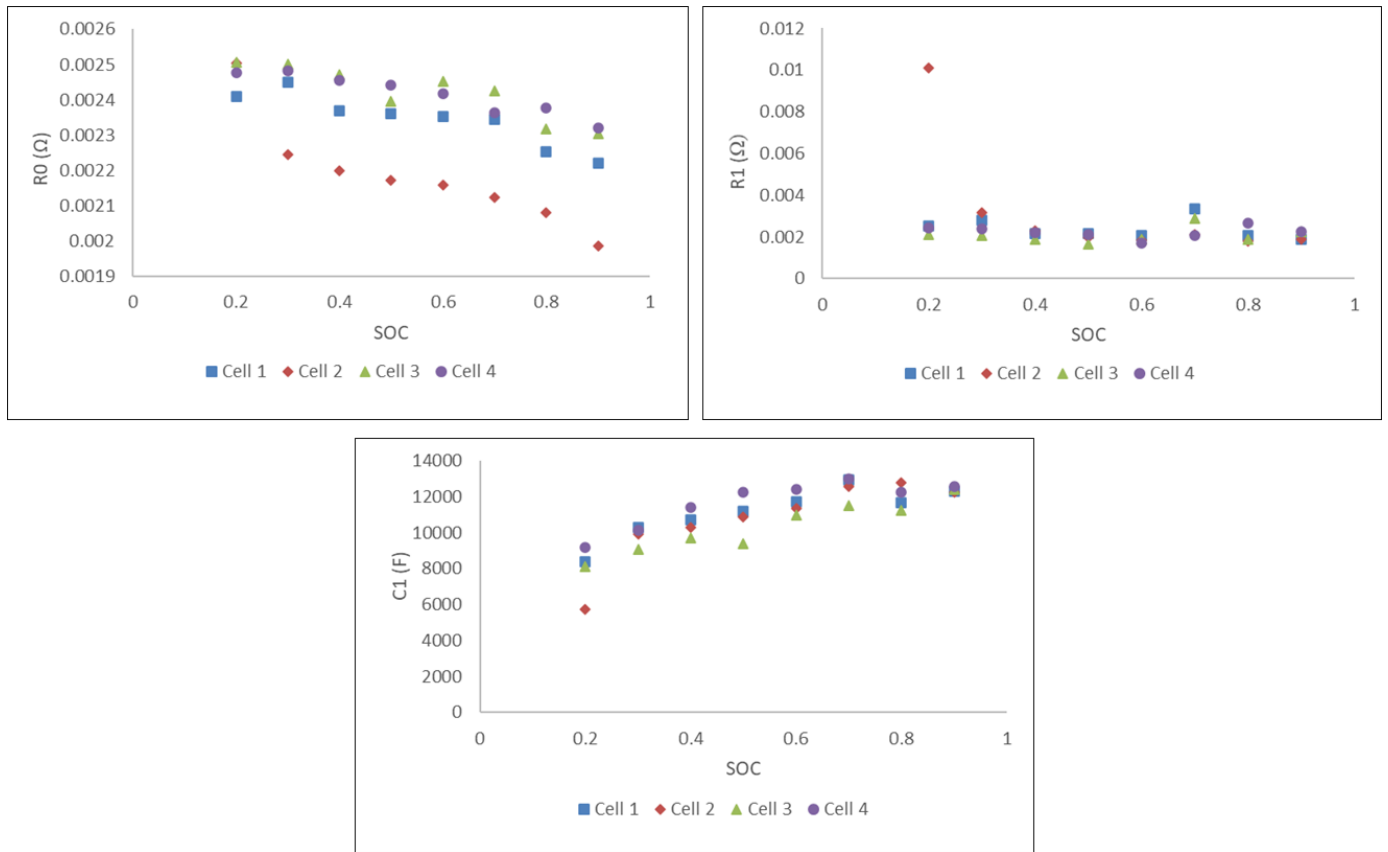


Figure 6.4: ECM parameters obtained from the HPPC tests: R_0 (top left), R_1 (top right), and C_1 (bottom).

To validate that the cell voltage model is viable, the Urban Dynamometer Driving Schedule (UDDS) was used. The UDDS cycle is commonly used to replicate the driving conditions within a city. The current profile from the UDDS was tested experimentally on the battery, and the corresponding experimental voltage values were measured. Then, the voltage values predicted from the ECM with the current profile input and the newly obtained parameters were compared to the measured values, as seen in Figure 6.5. It is shown that the model was well-fitted to the experimental data, with an average absolute percent error of around 0.6%.

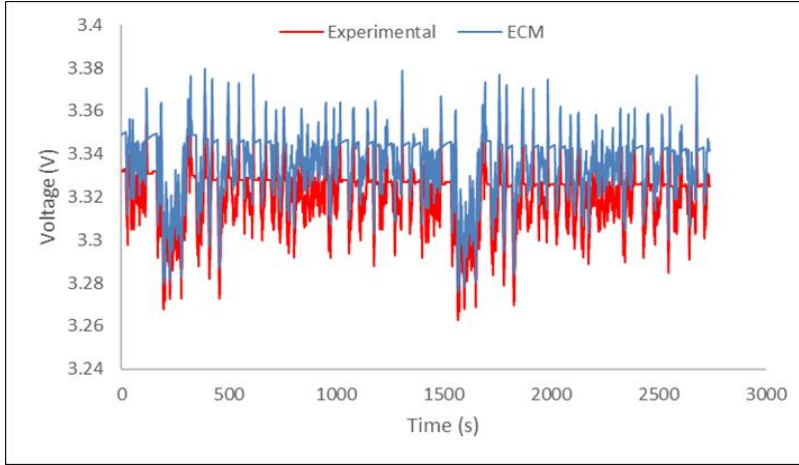


Figure 6.5: Cell voltage model validation plot using UDDS cycle.

For the equations used in the simulation framework, shown in later sections, the mean and the standard deviation values were utilized to establish the distribution of the parameters. These would be the X_{mean} and the $Stdev$ in Equation (6.6). The mean of the parameters values between the four cells was taken at 50% SOC. The standard deviation of the capacity and the R0 parameter was around 2-5%, while the R1 and C1 parameters had a standard deviation of 10-12% between the four cells. The results are displayed in Table 6.2, and these values were subsequently used in the simulation in Section 3.4, specifically in Equation (6.6).

Table 6.2: Capacity and ECM parameters distribution.

Parameter	Mean	Standard Deviation	Units
Capacity	19.1750	0.4787	<i>Ah</i>
R0	0.0023	0.00012	Ω
R1	0.0019	0.00023	Ω
C1	10921	1188.1	<i>F</i>

6.3.2. Cell degradation model

There are several methods to quantify and simulate battery cell degradation [187], [188]. The battery degradation model used in this analysis is based on the empirical model proposed by Schmalsteig et al. [188]. This battery degradation model was used and validated in our previous work [180]. This model was chosen because it is empirical which would require less computational

time, and because it has fitting parameters that could vary stochastically, which allows for more realistic cell variation. This degradation model takes into consideration the effects of the depth of discharge (DoD) and the average voltage (V_{avg}) of the cell throughout the current profile. It was simplified to depend only on cycling aging and neglect calendar aging, for the purpose of this study. The degradation model is coupled with the voltage model to predict the degradation profile of the cells.

The degradation model used in the simulation framework involves Equations (6.3), (6.4), and (6.5). CAP_{cyc} represents the ratio between the current total cell capacity and the initial total cell capacity, which indicates capacity fade. This value decreases as cycling progresses. Res_{cyc} represents the ratio between the current cell resistance to the initial cell resistance. This value increases as cycling progresses. The $\beta_{cap/res}$ represents β_{cap} or β_{res} , which are the parameters for capacity fade and resistance increase in Equations (6.3) and (6.4). Both are calculated using the same equation but with different values of a , b , c , and d , which are shown in Section 3.4.

$$CAP_{cyc} = 1 - \beta_{cap} \sqrt{Q_{processed}} \quad (6.3)$$

$$Res_{cyc} = 1 + \beta_{res} Q_{processed} \quad (6.4)$$

$$\beta_{cap/res} = a(V_{avg} - b)^2 + c + d * DoD \quad (6.5)$$

6.3.3. Pack voltage model

The pack voltage model is used to combine the individual cell voltage models in series to obtain the overall performance of the battery pack, by simplifying n Thevenin ECMs in series into a single Thevenin ECM with n RC circuits. This model is used to produce the pack voltage, OCV, and SOC corresponding to the current profile and determine the pack capacity. The information obtained can be used to evaluate the overall performance of the pack as it degrades. The pack voltage model is also used to update the cell-level ECM parameters to make sure that all cells will be realistically subjected to the same current profile as they are connected in series. However, the variation in individual cell degradation rates can lead to variance in some cycling characteristics like DoD and SOC.

6.3.4. Cell replacement simulation framework

The simulation in this study was performed using object-oriented programming in MATLAB. It utilized the three different models described in previous sections: the cell voltage model, the cell degradation model, and the pack voltage model. Figure 6.6 outlines the overall simulation framework.

The simulation initially generated 10 sets of 80 individual LFP cells, which were all stochastically vary in their capacity, ECM parameters, and degradation parameters. The ECM parameters (R_0 , R_1 , C_1) and the capacity were generated for each cell using Equation (6.6),

$$Y = X_{mean} + X_{mean} * (Rand) * (Stdev) \quad (6.6)$$

where Y represents the parameter values generated for an individual cell. X_{mean} is the average of the given parameter across the four cells from the experiment. $Rand$ is a normally distributed random number between -1 and 1. $Stdev$ is the standard deviation of the given parameter across the four cells from the experiment.

The degradation parameters for each cell in the simulation are generated using the formula below,

$$Y = Z + Z * (Var) * (Rand) \quad (6.7)$$

where Y represents the values of the generated parameter, while Z is the degradation parameter values given in Table 6.3 which were taken from our previous work [180]. Var is the variability of the model which is 3% in this study. However, for the parameter b , the Var value is further divided by 2. $Rand$ is a normally distributed random number between -1 and 1.

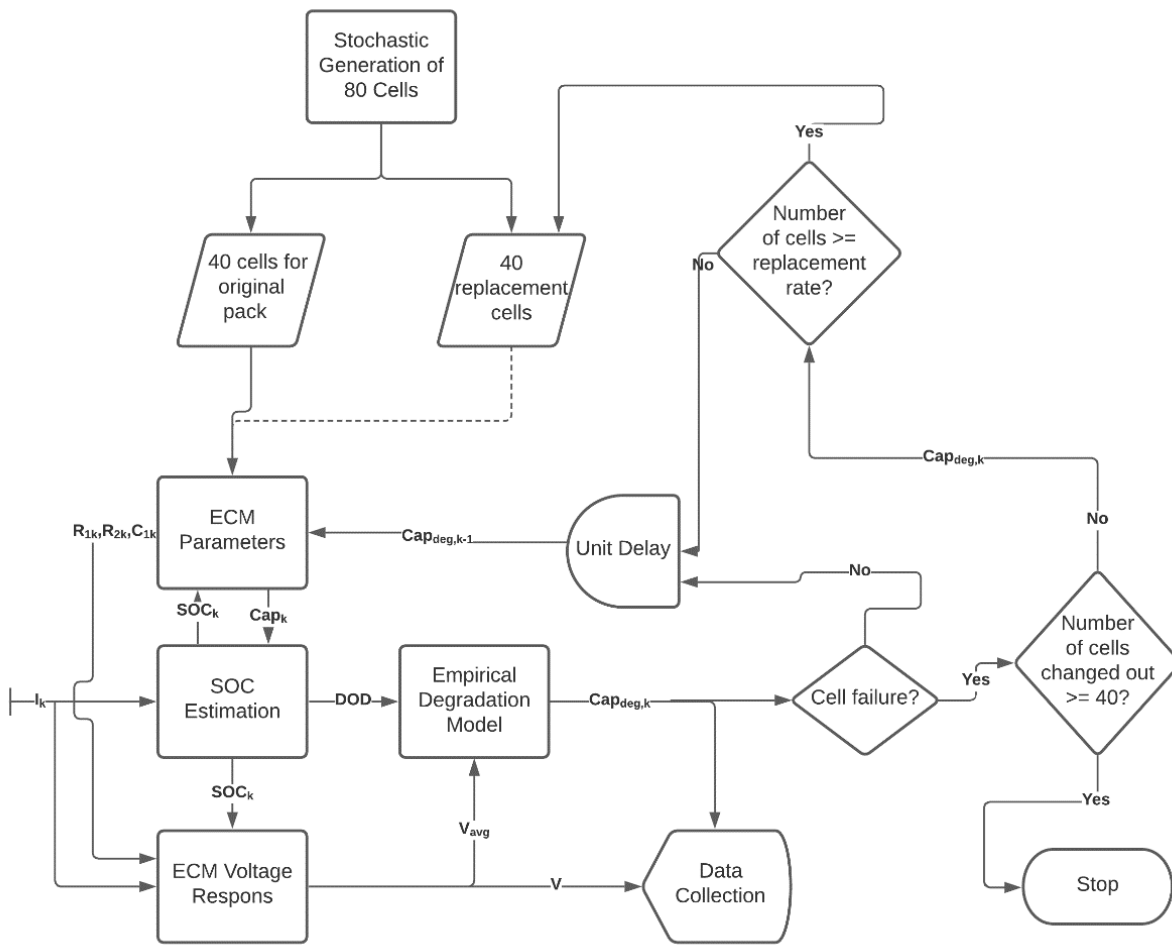


Figure 6.6: Schematic of the cell replacement simulation framework.

Table 6.3: Degradation parameters used in the simulation.

Parameter	Capacity Fade	Resistance Rise	Units
a	0.00142	$2.780 \cdot 10^{-5}$	$\sqrt{Ah} * V^{-1}$
b	3.274	3.199	V
c	0.00119	$-2.237 \cdot 10^{-5}$	\sqrt{Ah}^{-1}
d	$-9.219 \cdot 10^{-4}$	$7.361 \cdot 10^{-5}$	\sqrt{Ah}^{-1}

The stochastic variation techniques described above provided a reasonable estimation of how a real-world pack would degrade over time. For each of the 10 sets of cells, the 80 cells were

indexed, and the first 40 cells were used, in series, in the initial battery pack. The 40-cell packs (2.64 kWh) represent standard battery packs used in various real-world applications. The other 40 cells would be used when the cells in the initial pack needed replacement.

The battery packs simulated were subjected to discharge and charge cycles of 1C between 20% and 80% average SOC. The simulation started at 80% for each cell. One cycle refers to one complete discharge and charge of a cell. The determination of the current amount needed to achieve 1C was based on the total capacity of the pack. The SOC of each cell was determined using Equation (6.8), which is based on the coulomb counting method, where I is the battery current, SOC_0 is the initial SOC, and C_n is the maximum battery capacity.

$$SOC = SOC_0 + \frac{1}{C_n} \int \frac{I}{3600} dt \quad (6.8)$$

The voltage was determined using the ECM model for each cycle. The voltage and the SOC values were then used in the degradation model to calculate the capacity fade. The capacity of each cell was checked each cycle to ensure that the cells were below the cell failure limit.

A maintenance event is defined as the time at which at least one cell replacement occurs. The replacement rate is defined by the number of cells that have gone below the cell failure limit and would be replaced during a maintenance event. The cell failure limit for the main case study is 82% state of health (SOH) or CAP_{cyc} . For example, if the replacement rate was 4, then 4 individual cells would have to fall below 82% SOH before a replacement (maintenance event) would occur. The replacement would immediately swap the 4 old cells with 4 fresh cells from the remaining 40 fresh cells that were not initially put into the pack. This would result in 10 maintenance events in the simulation as there are 40 other cells. The replacement would also rely on the indices of the cells, occurring in order from cell 41 to cell 80. The 4 fresh cells for the first maintenance event in this example would be the cells indexed from 41 to 44. The replacement rates tested in this study were for every 1, 2, 4, 5, 8, 10, and 20 cells. The values of replacement rates were selected as there were 40 additional cells, and in order to utilize all the additional cells, the rates need to be divisors of 40. As well, there was a simulation for simply an ordinary pack replacement (no cell replacement), which acts as a reference point for comparison between cell replacement and no cell replacement. In the pack replacement case, the initial pack would be

replaced with a new pack, consisting of the remaining 40 cells, with completely new packaging as there would be no cell replacement when the pack's SOH has fallen below 80%.

The cell failure limit was chosen to be higher than the pack failure limit of 80%, as it was necessary for the cell failure limit to be above the pack failure limit to ensure that most cells did not degrade past 80%. However, if the cell failure limit was set too high, then there would be cells that are replaced while still being relatively healthy. Therefore, in the main case study, it was determined to be 82%. An additional test was performed with a cell failure limit of 72% and a pack failure limit of 70%.

The capacity of each cell was recorded for each cycle. The pack capacity was calculated based on the capacity of the weakest cell. The SOH of the pack is the ratio between the weakest cell capacity and the nominal cell capacity, given by the equation below,

$$SOH_{pack} = \frac{\min(Cap_{cell1}, Cap_{cell2}, \dots, Cap_{cellN})}{Nominal\ Cell\ Capacity} * 100 \quad (6.9)$$

6.4. Results and Discussion

6.4.1. Cell replacement concept simulation and results

The simulation across the 10 data sets of 80 cells showed that the total number of cycles in the lifespan of a battery pack generally increases when the replacement rate increases. It should be noted that when the replacement rate increases, the number of maintenance events decreases because the greater number of cells replaced at each maintenance event would result in fewer maintenance events. Figure 6.7 shows the results of the cell replacement simulation with different replacement rates, for the battery pack's SOH thresholds of 80% (cell's SOH threshold of 82%) and 70% (cell's SOH threshold of 72%). The total number of cycles was calculated as the average of the 10 sets of 80 cells that were simulated, with each set yielding a battery pack of 40 cells as well as 40 additional replacement cells.

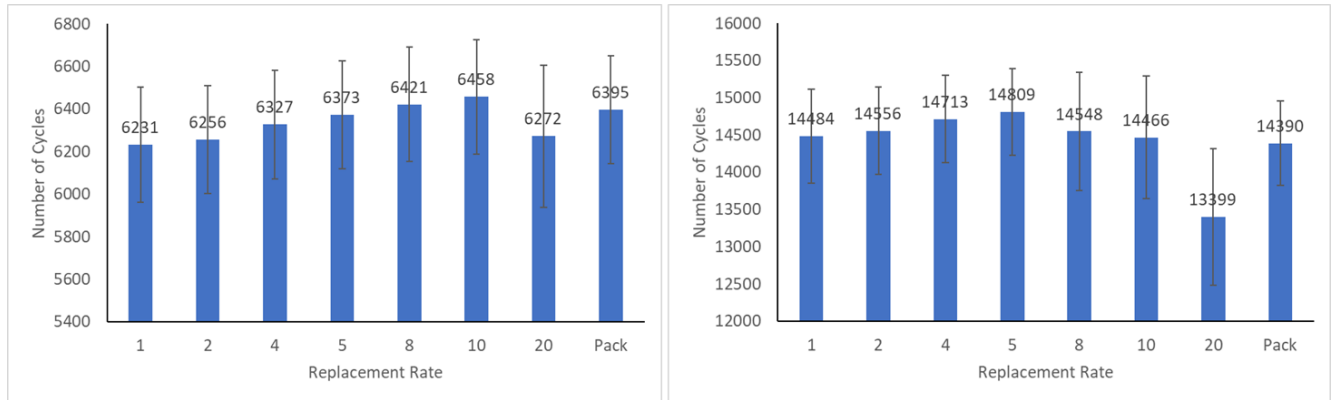


Figure 6.7: Total number of cycles, on average, of the battery packs with different replacement rates, for 80% SOH threshold (left), and 70% SOH threshold (right).

From Figure 6.7, for the pack SOH threshold of 80%, it is observed that a replacement rate of 10 (replacing 10 cells at every maintenance event) allowed for the greatest number of cycles, which was 6,458 cycles. An ordinary pack replacement, which is the common practice currently, gave a total number of 6,395 cycles, which is 63 cycles lower than the case with the replacement rate of 10. However, the replacement rate of 10 would require 4 maintenance events, meaning an additional 3 visits to the vehicle shop or dealership compared to the pack replacement method. The pack replacement approach also showed to have better results than most other cell replacement cases except for cases with replacement rates of 8 and 10. The lowest number of cycles was given by the replacement at every 20 failed cells, which was 6,272 cycles. This is likely because the SOH of the pack fell below 80% before its 20 individual cells broke down below 82%.

Figure 6.7 also indicates that lowering the threshold from 80% SOH to 70% SOH with a cell failure limit of 72% led to an increase, by over double in all cases, of the total number of cycles. The average total number of cycles for the optimal replacement rate was 14,809 cycles, for the replacement rate of 5. This is 8,351 cycles more than the case of the 80% SOH threshold. The pack replacement approach, in this case, resulted in an average of 14,390 cycles, which was 419 fewer cycles than the best cell replacement case, or around 3% lower instead of only 1% like in the 80% SOH threshold case. The pack replacement method also then gave worse results than most other cell replacement cases except for the case with the replacement rates of 20. This indicated that lowering the pack SOH threshold could provide a significantly greater battery life if lower battery capacity was acceptable to the application, which is the case for many stationary battery

applications. It is noted that if continuous cell replacement is performed, then there will be cases where a lot of replacements occur at times close to each other, especially for low replacement rates such as 1, 2, or 4. This might prove inconvenient in the real-world setting when several replacements might occur on the same day or week.

6.4.2. Battery pack design requirements for cell replacement concept

For the cell replacement concept to be feasible in the real-world setting, there are two main design criteria to be considered. The two criteria include good individual cell monitoring and identification and easy accessibility to the cells that need replacement. The first criterium is achieved when a battery management system (BMS) is installed such that one can monitor each cell's SOH. This design consideration is indispensable in the future for the BMS, not only because of cell replacement but also due to cell aging, balancing, and safety [189]. It also allows for the second criteria to be met since, without individual cell identification, cell replacement cannot be conducted effectively. The second design criterium is achieved if cells can easily be removed and installed physically in the pack. This can be difficult at the moment as many battery packs nowadays use fusion to connect cells together [190]. Fusion is the act of using molten metals similar in composition to the current-carrying parts to create an electrical pathway for the cells to be placed in series or parallel. This is seen as the most advanced and reliable approach because it creates less interfacial resistance problems which can often occur in the other methods of connecting cells, such as through simple physical contact of the current-carrying parts. This design consideration is required for the cell replacement concept to be practical, as it would not be economical to spend a significant amount of time and labor to replace individual cells in the battery pack. This criterium can be achieved if one can find a way to make compression – physical contact – a viable option for internal cell connections or find a way to easily replace cells that are fused within a battery pack.

6.4.3. Economic feasibility of cell replacement concept

The economic benefit and feasibility of the cell replacement concept were assessed by estimating the price of the cases using cell replacement versus pack replacement. The costs were then related to the cycling performance of the packs in both the 70% and 80% SOH threshold cases. This was used to make conclusions on when cell replacement would become beneficial.

Firstly, the cost of each cell was set to \$28, which was the original price of the LFP cells. This was then multiplied by the number of cells and the cells-to-pack cost proportion to obtain the total cost of the original pack as well as the proportion of the cost between the material and the pack. The cells-to-pack cost proportion was set to 48% as Wentker et al. [191] suggested. However, a 50% price increase was added to the manufacturing costs of the packs for the cell replacement cases, because it would require a different and robust design and result in greater costs. To obtain the total cost of the pack replacement case, the original pack cost was doubled as one would simply replace the original battery pack with another similar pack with the same price. For the cell replacement cases, only the costs of the cells were considered because a brand-new pack is not necessary with the pack systems that are already in place being reused. Lastly, the labour costs were set to be \$100 per maintenance event. The number of maintenance events was selected according to the optimal number of cycles for both the 70% and 80% SOH threshold cases, which were 8 and 4, respectively. A summary of cost analysis and comparison between cases of pack replacement and cell replacement is shown in Table 6.4.

Table 6.4: Cost analysis and comparison between cases of pack replacement and cell replacement.

	Pack replacement	Cell Replacement
Cell cost (USD/cell)	\$28.00	\$28.00
Total number of cells in one pack	40	40
Cells-to-pack cost proportion	48%	NA
Cell cost for original pack (40 cells)	\$1,120.00	\$1,120.00
Initial pack manufacturing cost	\$1,213.33	\$1,820.00
Total cost of original pack	\$2,333.33	\$2,940.00
Total cost of replacement	\$2,333.33	\$1,120.00
Total labour cost of replacement (for 80% SOH threshold)	\$100.00	\$400.00
Total labour cost of replacement (for 70% SOH threshold)	\$100.00	\$800.00
Total cost (for 80% SOH threshold)	\$4,766.67	\$4,460.00
Total cost (for 70% SOH threshold)	\$4,766.67	\$4,860.00

The results show that the total pack replacement costs were estimated to be around \$4,766.67 while the total cell replacement costs were \$4,860.00 and \$4,460.00 for the 70% and 80% SOH threshold cases, respectively. This indicates that the cell replacement costs were cheaper for the 80% SOH threshold case, but not for the 70% SOH threshold one due to the increased number of maintenance events that led to higher total costs. For the 80% SOH threshold case, the total cost of cell replacement was about 6% (or \$306.67) lower than that of pack replacement, while being able to improve the total number of battery pack cycles by 1% (or 63 cycles). For the 70% SOH threshold case, even though the cell replacement's total cost was about 2% (or \$93.33) higher than the pack replacement's total cost, the cell replacement method was able to increase the total number of pack cycles by 3% (or 419 cycles). In both cases, the cell replacement approach can be seen as a better option than the pack replacement approach. Overall, it can be concluded that if the design requirements for the cell replacement concept are fulfilled as discussed in Section 4.2, this concept will be feasible and beneficial economically.

6.5. Conclusions

This study investigated the concept of cell replacement for Li-ion battery packs using MATLAB simulation based on experimental data from 20-Ah LFP pouch cells. A battery voltage model and a battery degradation model were used to set up the simulation framework. The simulation stochastically generated 10 sets of runs, with each set consisting of 80 LFP cells where 40 cells were put in a battery pack and the other 40 cells were utilized as additional cells for replacement. The investigated pack failure SOH thresholds were 70% and 80%, while the cell failure SOH thresholds were 72% and 82%, respectively. The main conclusions from this work are as follows:

1. The cell voltage model was validated and can be used to generate cells stochastically.
2. The cell replacement approach can increase the total number of battery cycles by 63 cycles (or a 1% increase), on average, in the 80% SOH threshold case. This approach can also increase the total number of cycles by 419 cycles (or a 3% increase), on average, in the 70% SOH threshold case.
3. Lowering the pack SOH threshold from 80% to 70% would significantly increase the total number of cycles if the battery application could accept the lower battery capacity.

4. The cell replacement concept is only feasible if two main design criteria can be satisfied, including individual cell monitoring and identification and accessibility to cells that require replacement. However, these design requirements can be difficult to achieve without significant costs.
5. If the design requirements can be met, the cell replacement method will be more economically beneficial than the current pack replacement approach, as it allows the reusing of many different components of the battery pack.

The findings in this study show that the cell replacement concept can be viable and more economically beneficial than the current approach of replacing the entire pack, given that the design requirements are fulfilled. Future research work will focus on other evaluation criteria to highlight the advantages of the cell replacement concept such as supply chain benefits, maintenance ease, waste reduction, etc., as well as other chemistries of Li-ion batteries, the use of better battery models, and the approach to satisfy the design requirements discussed in this study.

Chapter 7 : Online Lithium-ion Battery State of Health Estimation Using Machine Learning

This chapter is adapted from the manuscript “Real-time state of health estimation for lithium-ion battery during fast charge using partial charge metrics and machine learning approaches”, by M.-K. Tran, T.D. Khang, T.P.M. Linh, S. Panchal, M. Fowler, which was submitted to the Journal of Energy Storage. Contribution of authors is detailed in the Statement of Contributions section.

This chapter highlights another extension of potential applications from the cloud-based battery management system solution. Accurate and robust battery state of health estimation usually requires a significant amount of data and computing power, whereas online and real-time state of health estimation is often fast but lacking in accuracy and robustness. Cloud-based battery management system is expected to solve this problem and offer better solutions than existing approaches in current online and real-time applications. This study shows the development of a new approach, that utilizes machine learning and big data to achieve better accuracy and robustness for online state of health estimation of lithium-ion batteries.

7.1. Introduction

The demand for rechargeable, high-performance batteries has surged in recent years. Among all battery types, lithium-ion (Li-ion) batteries have garnered the most interest. Li-ion batteries are pivotal for the future of electric vehicles and energy storage systems, due to their numerous advantages, including high energy density, high power density, long cycle life, low self-discharge rate, compact size, light weight, fast charging capabilities, and wide operational temperature range [1], [2]. However, in order to use Li-ion battery systems effectively and safely, a battery management system (BMS) is needed. The BMS, with its many essential functions including state estimation, charge control, and fault diagnostics, ensures the safety and performance of the Li-ion battery systems during operation [52]. One key function of the BMS for Li-ion batteries is to track the remaining capacity of the battery throughout its lifespan, since aging and improper use can diminish battery capacity, leading to potential battery failure, damage, or even explosion [17], [135]. Therefore, it is essential to monitor the real-time health status of Li-

ion battery systems and convey this information to users. Tracking the remaining battery capacity allows for precise predictions of the available energy and power and assists with developing effective battery management strategies and maintenance plans [58], [68]. The portion of the original capacity that remains usable is commonly known as the state of health (SOH). There has been some research on SOH estimation for Li-ion batteries, and the common approaches can be divided into three main categories which are electrical model-based, aging model-based, and feature correlation-based methods [192], [193].

Electrical model-based methods involve constructing a model that captures the electrical behavior of the battery, with model parameters updated over time to minimize the difference between estimated and measured outputs like the terminal voltage [65]. This iterative process allows the use of continuously updating model parameters in calculating the battery SOH directly or indirectly. However, these methods are often computationally intensive and potentially slow in real-time applications. Also, the accuracy of the models heavily depends on the precise identification and updating of parameters, which can be sensitive to measurement errors and noise. Aging model-based methods use empirical models based on historical operational data to predict the battery SOH [188]. These models are parameterized from extensive aging tests, providing SOH estimates based on the battery usage history. However, these methods are based on empirical data, which may not account for all possible aging mechanisms and stress factors, potentially leading to inaccuracies in SOH estimation. Also, aging models are often pre-parameterized and may not adapt well to changes in operating conditions or new battery technologies, limiting their flexibility and long-term accuracy. Feature correlation-based methods focus on finding a relationship between measurable battery features and the SOH through laboratory experiments or existing datasets [164]. These features might include measurable metrics like voltage and current profiles, or derived metrics like internal resistance and incremental capacity. Once these correlations are established, they can be applied in practice to estimate SOH by obtaining the relevant features during battery operation. Some studies have shown that correlations between impedance spectroscopy data and SOH allow reliable and non-invasive estimation. Using incremental capacity analysis, some researchers were also able to estimate battery SOH.

Among the existing battery models used in the BMS, the equivalent circuit model (ECM) is the most prominent due to its fast execution time, simplicity, and accuracy. ECM parameters

typically include an internal ohmic resistance, followed by one or more resistor-capacitor (RC) pairs. The simplest model only takes the internal ohmic resistance into account which does not accurately represent the battery dynamics during operation. Thus, the Thevenin ECM, which has one additional RC pair to combine with the internal ohmic resistance, is widely used since it has a good balance between accuracy and simplicity. The parameters of the ECM, namely the open-circuit voltage (OCV) and internal resistance, are often affected by the state of charge (SOC), temperature, and SOH of the battery, and these effects have been characterized in literature [2]. These relationships, with the involvement of machine learning, can be utilized in an SOH estimation technique that uses the concept of partial charge, a feature correlation-based approach, which is more suitable for online and real-time applications.

There have been several studies that focused on the concept of partial charge in SOH estimation. Fan et al. [194] presented a method for predicting the remaining capacity of Li-ion batteries using partial charge curves and health feature fusion through canonical correlation analysis, followed by Gaussian process regression for aging model establishment. Six datasets from NASA and the University of Oxford were used for validation of the method. Cao et al. [195] devised a capacity estimation method for Li-ion batteries in electric vehicles, addressing the challenge of insufficient data due to partial charging. By fitting partial charge voltage curves with polynomial functions and using the resulting parameters as health indicators, a deep learning model was then used to estimate battery capacity, requiring less voltage data and offering flexibility across various charging phases. A similar study from Yao et al. [196] introduced a deep transfer learning method for estimating Li-ion battery capacity, addressing challenges in obtaining cycling data during charging/discharging processes. By utilizing capacity increment features of partial charging/discharging segments and employing a deep transfer convolutional neural network with fine-tuning, the proposed method achieved high accuracy with values of root mean square error (RMSE) and mean absolute percentage error (MAPE) of only 0.0220 and 0.0247, respectively. Lyu et al. [197] developed a data-fusion-model method for estimating Li-ion battery capacity using partial charge curves. It involved extracting battery aging features, employing dual Gaussian process regressions to establish a data-driven battery aging state-space representation, and utilizing Particle Filter and Gaussian Process Particle Filter for capacity estimation. Tian et al. [198] proposed a flexible method for estimating both the maximum and remaining capacities of batteries using short pieces of charging data to obtain SOC and SOH simultaneously. Validation

on battery degradation data, using eight 0.74 Ah batteries charged at a C-rate of 1C, demonstrated good capacity estimation, with an RMSE lower than 12.68 mAh. Xue et al. [199] presented a deep learning method for online capacity estimation of Li-ion batteries, utilizing a predictive model called deep convolutional time memory network, which fuses convolutional neural network and long short-term memory units. By directly feeding partial charge voltage and current data into the model without complex pre-processing, the proposed algorithm achieved capacity estimation with absolute errors of less than 0.021 Ah and 0.11 Ah for two types of batteries. He et al. [200] developed a novel incremental capacity (IC) feature-based method for estimating the SOH of Li-ion batteries using partial charge data. By calibrating a linear model between specific features of interest and SOH based on full-range charging data and then extracting corresponding features from IC curves obtained with partial charge data, the proposed method achieved SOH estimation accuracy within 5%. Schmitt et al. [201] introduced a method to analyze degradation modes and estimate remaining cell capacity by reconstructing OCV curves from partial charging curves of Li-ion batteries with silicon-graphite and NMC-811 electrodes. The study demonstrated that accurate OCV reconstruction and degradation mode estimation are achievable from partial charge curves within a specific SOC window. Their capacity estimation accuracy was within 2% between 10% and 80% SOC, with a maximum current rate of C/15 recommended for accurate degradation mode estimation.

The discussed methods above in existing literature have gaps that need to be addressed. This study will introduce an approach that can be used with fast charging as opposed to low-current charging, and it should be adaptable to various types of Li-ion batteries as machine learning methods will be used with extracted partial charging metrics to estimate the SOH. This approach also does not require any historical data memorized by the BMS, and it can estimate the SOH for any given charge cycle during the lifespan of the battery. Multiple machine learning methods will be considered before selecting the best option. The proposed approach is based on the ECM, and therefore, it is not empirical and can be explained by existing physical concepts. The approach also aims at improving the accuracy of SOH estimation and making sure that it is implementable in the BMS in online applications.

7.2. Methodology

7.2.1. Dataset description

The dataset utilized for learning, validation, and testing in this study came from a study by Severson et al. [67]. The dataset consists of data from 124 commercial Li-ion battery cells subjected to fast-charging conditions until failure. These batteries are lithium-ion phosphate (LFP)/graphite cells, specifically, the APR18650M1A battery manufactured by A123 Systems. Each cell possesses a nominal capacity of 1.1Ah and a nominal voltage of 3.3V. The cells were cycled within horizontal cylindrical fixtures on a 48-channel Arbin LBT potentiostat, situated in a forced convection temperature chamber consistently maintained at 30°C.

Each cell in the dataset was charged using either a one-step or two-step fast-charging policy, denoted as “C1(Q1)-C2.” Here, C1 and C2 refer to the first and second constant-current steps, respectively, and Q1 indicates the SOC percentage at which the current transitions from C1 to C2. The second current step concludes at 80% SOC, followed by charging at 1C in constant-current constant-voltage mode. The charging process adheres to upper and lower cutoff voltages of 3.6 V and 2.0 V, respectively. All cells were discharged at a rate of 4C.

Temperature measurements were conducted by affixing a Type T thermocouple to the exposed cell can, using thermal epoxy (OMEGATHERM 201) and Kapton tape, after removing a small section of the plastic insulation. The reliability of temperature measurements may vary due to inconsistent thermal contact and occasional loss of contact during cycling.

7.2.2. Development of SOH estimation approach

The ECM is often used to represent the relationship between battery voltage and current. The OCV is a parameter in the model, represented by an ideal voltage source, and is correlated with SOC. The resistance and capacitance parameters represent some other physical behaviors of the battery such as charge transfer and polarization. The first-order ECM is as follows,

$$V_i = OCV_i - R_{0,i}I_i - U_{1,i} \quad (7.1)$$

$$U_{1,i} = \exp\left(-\frac{\Delta t}{R_{1,i}C_{1,i}}\right)U_{1,i-1} + R_{1,i}\left(1 - \exp\left(-\frac{\Delta t}{R_{1,i}C_{1,i}}\right)\right)I_{i-1} \quad (7.2)$$

where V is the battery voltage, I is the battery current, OCV is the open circuit voltage, R_0 is the internal ohmic resistance, R_1C_1 is the transient charge transfer time constant, U_1 is the voltage of the R_1C_1 portion, and Δt is the sampling time. In this model, OCV , R_0 , R_1 , and C_1 are the parameters, and they are known to be functions of SOC, temperature, and SOH.

One way to calculate the capacity is with SOC, as shown below,

$$Q = \frac{\int_{t_1}^{t_2} I(t) dt}{SOC_{t_2} - SOC_{t_1}} \quad (7.3)$$

where the battery is charged at a current I for time t_1 to t_2 , and the SOC goes from SOC_{t_1} to SOC_{t_2} . If it is assumed that the BMS uses discrete calculation at a rate of 1Hz, and the current remains relatively constant, which is often the case during constant-current charging at lower SOC, we can rewrite Equation (7.3) to

$$Q = \frac{I\Delta t}{SOC_{t_2} - SOC_{t_1}} \quad (7.4)$$

Since OCV and SOC have an established relationship, Equation (7.4) becomes

$$Q = \frac{I\Delta t}{f(OCV_{t_2}) - f(OCV_{t_1})} \quad (7.5)$$

where f represents SOC as a function of OCV . From Equation (7.1), OCV can be represented as

$$OCV_i = V_i + R_{0,i}I_i + U_{1,i} \quad (7.6)$$

The parameters OCV , R_0 , R_1 , and C_1 are all functions of SOC, temperature, and SOH. However, SOC is already represented by current and time, and SOH is represented by Q , so in order to not overfit the model, only temperature needs to be added as a variable. Therefore, Equation (7.5) can be rewritten as follows,

$$Q = F\left(\frac{I\Delta t}{V_{t_2} - V_{t_1}}, I, T\right) \quad (7.7)$$

where I and T are the average current and temperature during charge from V_{t_1} to V_{t_2} . The range of voltage from V_{t_1} to V_{t_2} needs to be sufficiently large enough to account for noise, but small enough for I and T to remain relatively constant. It is recommended to be between 0.1V and 0.2V on cell

level, based on some initial investigation. Specifically, for the dataset used in this study, the voltage range is 3.1V to 3.3V ($V_{t1} = 3.1V$ and $V_{t2} = 3.3V$). Equation (7.7) shows that the battery capacity can be estimated as a function of the three metrics, which are all obtainable by measurements or calculations by the BMS. The function F can be difficult to obtain mathematically, but with the use of machine learning, this function can be represented given enough data for an algorithm to learn. Using machine learning, the three metrics shall be the inputs while the output is battery capacity (one set of data points per charging cycle per battery). In order to improve the accuracy of the capacity estimation, parameter weighing factors are also considered when setting up the machine learning algorithms. The three metrics are not of the same significance, and $\frac{I\Delta t}{V_{t2}-V_{t1}}$ has the closest relationship to capacity, so it was given the highest weighing factor. This approach, as can be seen, does not require any historical data like others in existing literature, making it suitable for even the simplest BMS application.

Multiple machine learning algorithms are considered for this study and will be described further in Section 7.3. For validation of results, the error metrics used are RMSE and MAPE, which are calculated as follows,

$$RMSE = \sqrt{\frac{1}{N} \sum_{i=1}^N (y_{pred,i} - y_{exp,i})^2} \quad (7.8)$$

$$MAPE = \frac{1}{N} \sum_{i=1}^N \left| \frac{y_{pred,i} - y_{exp,i}}{y_{exp,i}} \right| \quad (7.9)$$

7.3. Proposed machine learning algorithms

In this study, six commonly used machine learning algorithms were selected for SOH estimation, using the methodology and dataset outlined above. They were built using the scikit-learn library with some other algorithm-specific libraries. Table 7.1 shows the setup for each algorithm in Python, and the following subsections briefly introduce each of the algorithms. There are 124 cells in the dataset. Data from 115 cells were used for training and evaluation, while 9 cells were used for testing. For training and evaluation, four folds were used for training and one fold was used for validation.

Table 7.1: Setup of the six machine learning algorithms used in the study.

Algorithm	Python Library	Parameters	Training/Evaluation Method
Neural Network	PyTorch scikit-learn	<p>Loss Function: loss_fn = nn.MSELoss() (Mean Squared Error)</p> <p>Learning Rate: 3e-4</p> <p>Epochs: 100</p> <p>Batch Size: 128</p> <p>Input Layer: 9 neurons</p> <p>Hidden Layer 1: 128 neurons, ReLU activation</p> <p>Hidden Layer 2: 256 neurons, ReLU activation</p> <p>Hidden Layer 3: 128 neurons, ReLU activation</p> <p>Hidden Layer 4: 64 neurons, ReLU activation</p> <p>Output Layer: 1 neuron</p>	<p>K-fold Cross-Validation: with k = 5, using 4 folds for training and 1 fold for evaluation</p> <p>Input Data Normalization: using StandardScaler (Mean = 0, Variance = 1 across all dimensions)</p>
Classification and Regression Trees (CART)	scikit-learn	<p>Objective: 'squared_error'</p> <p>Max Depth: 3</p>	<p>K-fold Cross-Validation: with k = 5, using 4 folds for training and 1 fold for evaluation</p>
Light Gradient Boosting Machine (LightGBM)	scikit-learn lightgbm	<p>Objective: 'regression'</p> <p>Metric: 'mse' (Mean Squared Error)</p> <p>Number of Leaves: 31</p> <p>Learning Rate: 0.05</p> <p>Verbose: -1</p> <p>Number of Estimators: 100</p>	<p>K-fold Cross-Validation: with k = 5, using 4 folds for training and 1 fold for evaluation</p>

Extreme Gradient Boosting (XGBoost)	scikit-learn xgboost	Objective: 'reg:squarederror' (use squared error for regression) Learning Rate: 0.05 Max Depth: 3 Number of Estimators: 100	K-fold Cross-Validation: with k = 5, using 4 folds for training and 1 fold for evaluation
Categorical Boosting (CatBoost)	scikit-learn catboost	Learning Rate: 0.05 Depth: 3 Number of Estimators: 100	K-fold Cross-Validation: with k = 5, using 4 folds for training and 1 fold for evaluation
Random Forest	scikit-learn	Objective: 'squared_error' (use squared error for regression) Max Depth: 3 Number of Estimators: 100 Max Leaf Nodes: 31	K-fold Cross-Validation: with k = 5, using 4 folds for training and 1 fold for evaluation

7.3.1. Neural network

Neural networks consist of layers of interconnected neurons that perform weighted sums of their inputs and apply activation functions to produce outputs [202]. The learning process involves adjusting the weights through backpropagation, which minimizes the loss function by calculating gradients and updating the weights accordingly. Neural networks are highly flexible and capable of modeling complex and non-linear relationships, making them suitable for various tasks. However, they require large datasets and significant computational resources for training, are prone to overfitting, and can be difficult to interpret.

7.3.2. Classification and regression trees (CART)

CART is a decision tree learning technique that builds binary trees for classification and regression tasks, improving upon older decision tree algorithms like ID3 and C4.5 [203]. The algorithm recursively splits the data into subsets based on the feature that results in the highest information gained for classification or the largest reduction in variance for regression. Each node in the tree represents a decision based on a feature, and each leaf node represents a predicted

outcome. CART is easy to understand and interpret, requires little data preprocessing, and can handle both numerical and categorical data. However, it is prone to overfitting if not properly pruned, can be unstable with small changes in data, and may be biased towards features with many levels.

7.3.3. Light gradient boosting machine (LightGBM)

LightGBM is a gradient boosting framework that utilizes tree-based learning algorithms designed for efficiency and scalability [204]. It constructs decision trees sequentially, with each tree correcting the errors of its predecessor, using a histogram-based algorithm to find the best splits. This method is highly efficient and scalable, making it suitable for large datasets, and supports parallel and GPU learning, which accelerates training. However, it is sensitive to hyperparameter tuning, requires careful handling of categorical features, and can be challenging to interpret.

7.3.4. Extreme gradient boosting (XGBoost)

XGBoost is an optimized gradient boosting library designed for high efficiency, flexibility, and portability [205]. It uses a gradient boosting framework that builds additive models in a forward-stage approach, leveraging second-order gradients to approximate the loss function for better optimization. XGBoost is known for its high performance and efficiency, robust handling of missing data, and regularization capabilities that reduce overfitting. Despite these advantages, XGBoost is complex, can be computationally expensive for large datasets, and demands substantial memory for large-scale applications.

7.3.5. Categorical boosting (CatBoost)

CatBoost is a gradient boosting library that builds decision trees sequentially, like other gradient boosting methods, but includes innovative techniques for handling categorical features directly and reducing overfitting [206]. CatBoost excels in handling categorical features without extensive preprocessing and is robust against overfitting due to ordered boosting and other regularization techniques. However, it requires careful hyperparameter tuning and may be slower compared to LightGBM.

7.3.6. Random forest

Random forest is an ensemble learning method that constructs multiple decision trees during training and aggregates their predictions [207]. For classification, it outputs the mode of the classes, and for regression, it averages the predictions of the individual trees. The algorithm randomly selects subsets of the training data and features to build each tree independently. It can reduce overfitting by averaging multiple trees and handle large datasets with higher dimensionality. However, it can be computationally intensive, memory-consuming, and less interpretable than single decision trees.

7.4. Results and analysis

Using the three metrics introduced in Section 7.2 and six machine learning algorithms discussed in Section 7.3, data from 115 cells in the dataset were used to train and validate the algorithms. Separately, 9 cells randomly selected from the dataset, not used in the training and validation, were used for testing to evaluate the performance of these algorithms. Figures 7.1 to 7.6 show the results of all the test cells for each of the algorithm used. As can be seen, LightGBM and neural network performed the best for the proposed SOH indication metrics.

To further quantify the performance of the approach and algorithms, RMSE and MAPE were calculated for each cell and algorithm. Tables 7.1 and 7.2 show the error results.

Table 7.2: RMSE of the algorithms tested.

Cell	Neural network	CART	LightGBM	XGBoost	CatBoost	Random forest
4	0.0126	0.0534	0.0164	0.0319	0.0392	0.0483
14	0.0092	0.0331	0.0097	0.0111	0.0185	0.0325
16	0.0100	0.0302	0.0163	0.0152	0.0178	0.0296
18	0.0095	0.0403	0.0132	0.0172	0.0229	0.0397
29	0.0076	0.0228	0.0170	0.0200	0.0208	0.0222
32	0.0071	0.0353	0.0107	0.0155	0.0175	0.0339
36	0.0088	0.0373	0.0128	0.0163	0.0204	0.0354
82	0.0113	0.0237	0.0124	0.0115	0.0108	0.0224
96	0.0098	0.0254	0.0124	0.0178	0.0182	0.0251
Average	0.0095	0.0335	0.0134	0.0174	0.0207	0.0321

Table 7.3: MAPE of the algorithms tested.

Cell	Neural network	CART	LightGBM	XGBoost	CatBoost	Random forest
4	0.93%	4.15%	1.31%	2.26%	2.67%	3.74%
14	0.66%	2.05%	0.71%	0.86%	1.24%	2.03%
16	0.69%	2.08%	1.30%	1.23%	1.47%	2.08%
18	0.71%	3.15%	1.04%	1.40%	1.93%	3.12%
29	0.51%	1.79%	1.42%	1.69%	1.78%	1.76%
32	0.49%	3.02%	0.79%	1.29%	1.41%	2.91%
36	0.66%	3.15%	1.06%	1.42%	1.67%	3.00%
82	0.85%	1.73%	0.97%	0.85%	0.76%	1.65%
96	0.73%	2.10%	1.00%	1.51%	1.51%	2.07%
Average	0.69%	2.58%	1.07%	1.39%	1.61%	2.48%

Looking at the errors, it can be seen that the neural network model delivered the best results. This can be attributed to the neural network's ability to capture and model complex, non-linear relationships inherent in the battery health data, because of its deep architecture and multiple layers of neurons. Additionally, the backpropagation algorithm allows for effective adjustment of weights, leading to a highly accurate model capable of generalizing well to new data. LightGBM performed the second best, due to its efficient and scalable learning algorithm, which can effectively handle large datasets and complex feature interactions.

On the contrary, CART did not perform well, returning the worst results among the methods tested. This is likely due to its tendency to overfit the training data, as CART builds a single tree that can become too complex without adequate pruning. Moreover, CART is less robust to variations in the data, and its binary splits can lead to high variance, making it less effective at capturing the intricate patterns in battery health data. The lack of an ensemble approach, which other methods like gradient boosting methods use to improve generalization, further limited CART's performance. Also, the random forest algorithm, while generally reducing overfitting by averaging multiple trees, returned the second-worst performance, likely due to the complex patterns in the data. The individual trees in the forest might have lacked the depth to capture subtle interactions in the battery data, leading to less accurate predictions compared to methods like neural networks and gradient boosting techniques.

Neural network

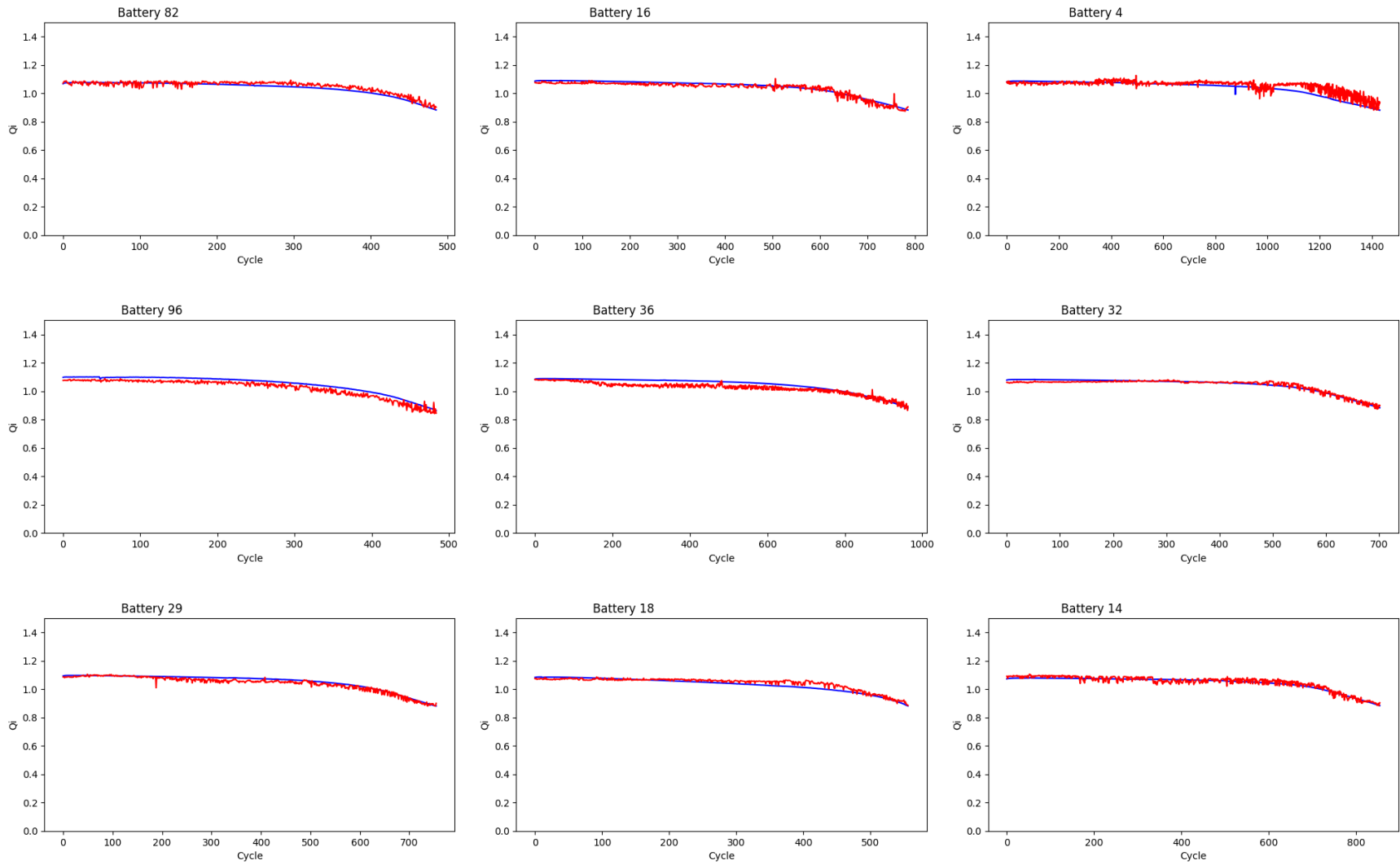


Figure 7.1: SOH estimation results using neural network algorithm.

CART Regression

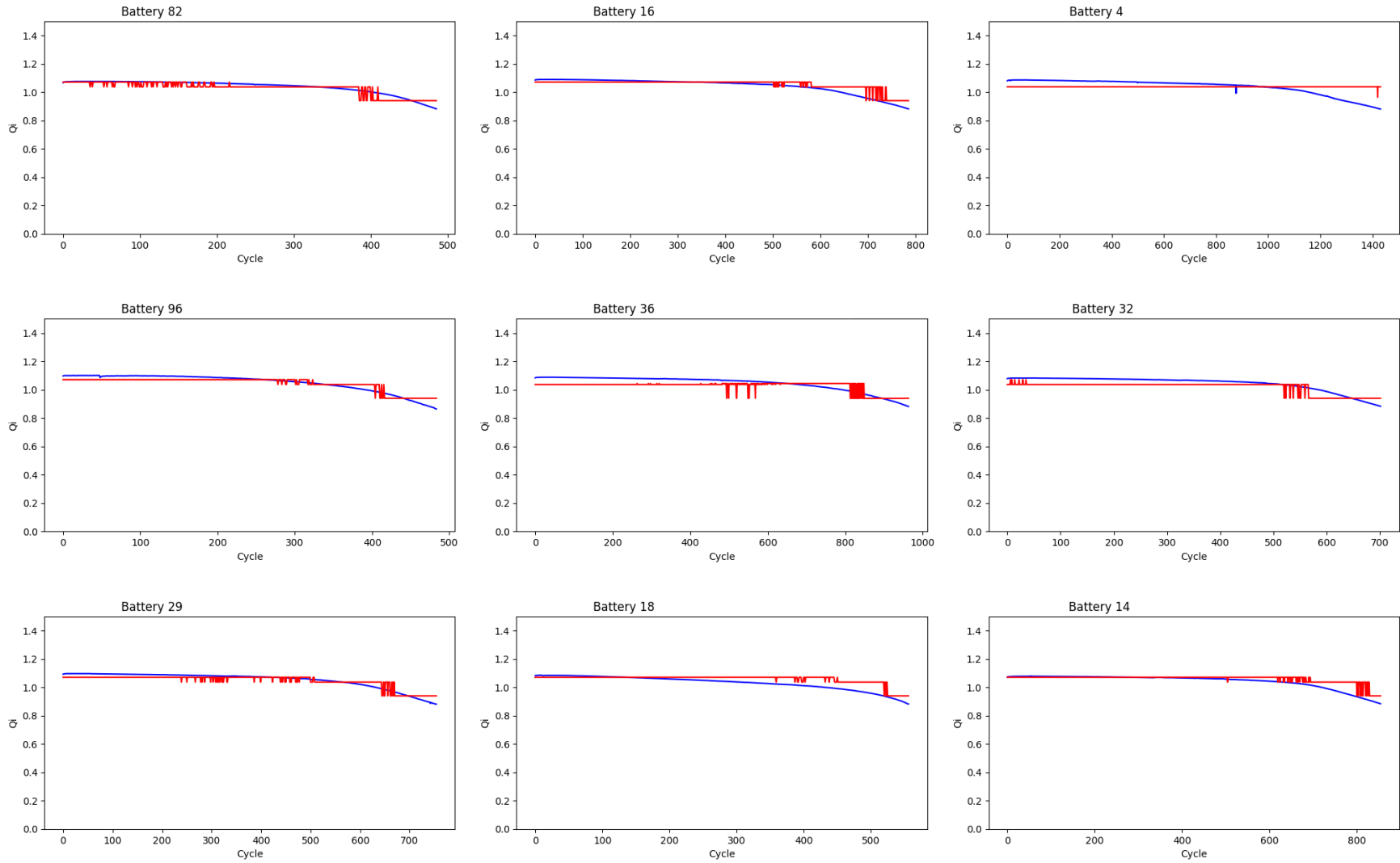


Figure 7.2: SOH estimation results using CART algorithm.

LightGBM

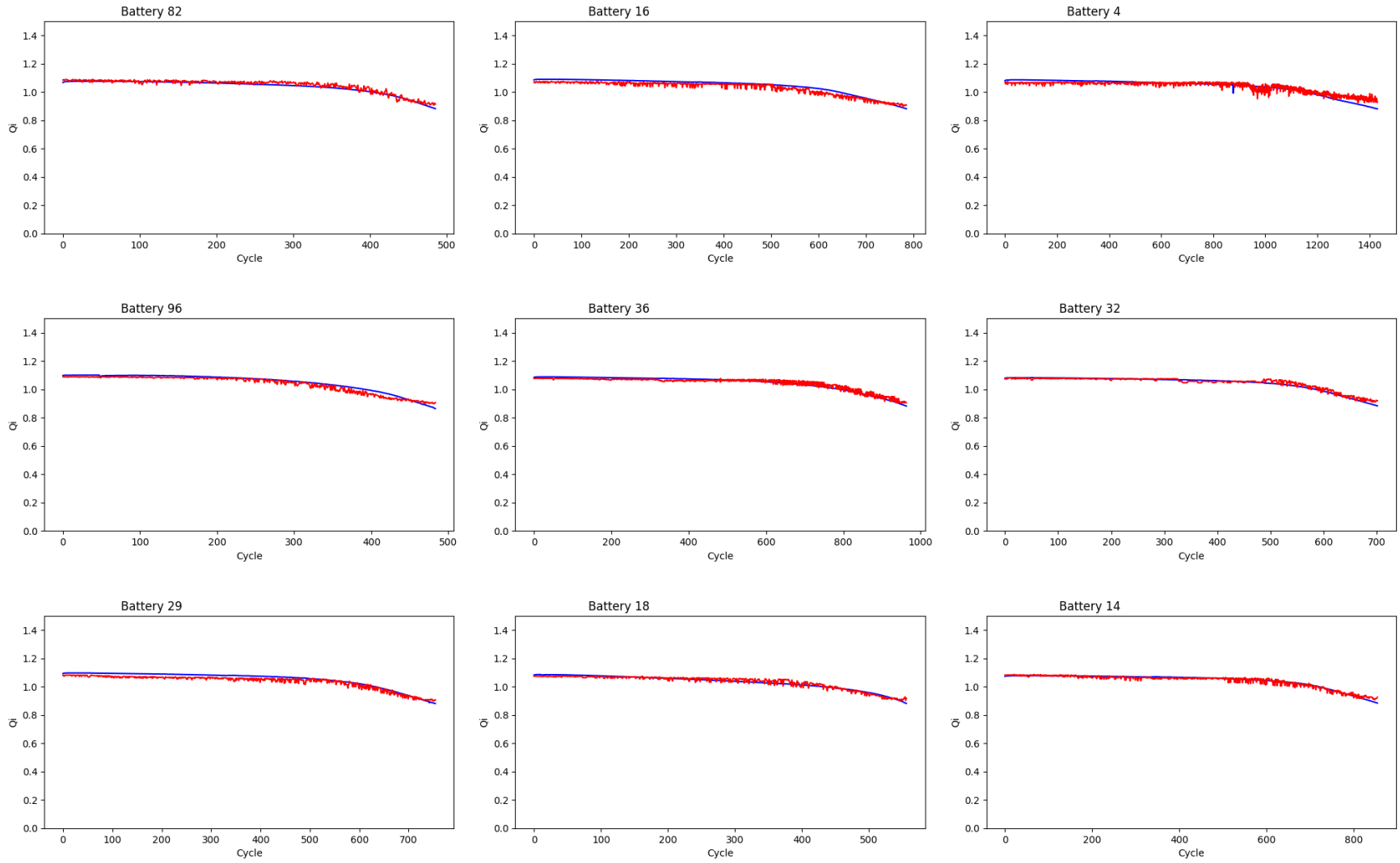


Figure 7.3: SOH estimation results using LightGBM algorithm.

XGBoost Regression

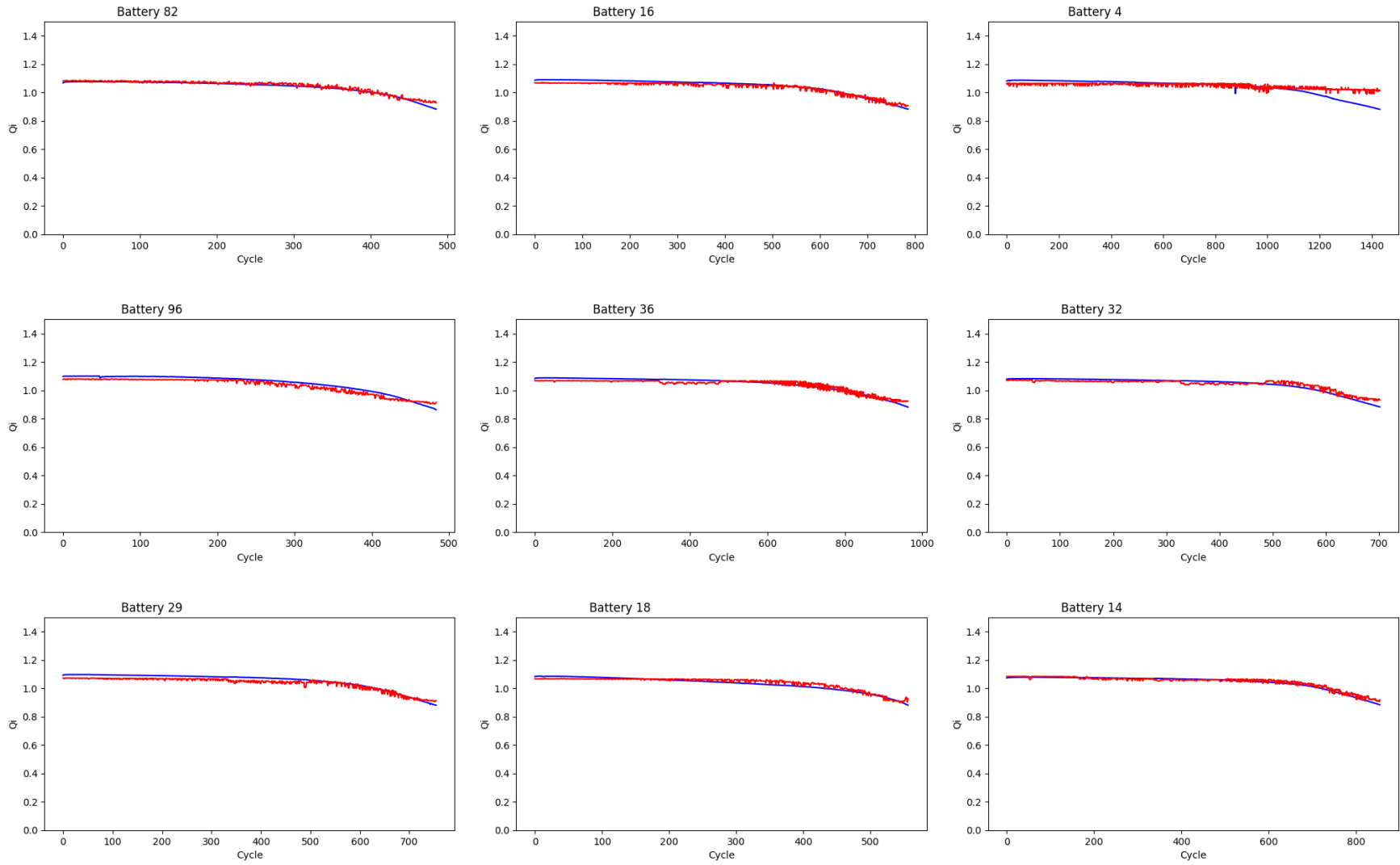


Figure 7.4: SOH estimation results using XGBoost algorithm.

CatBoostRegressor

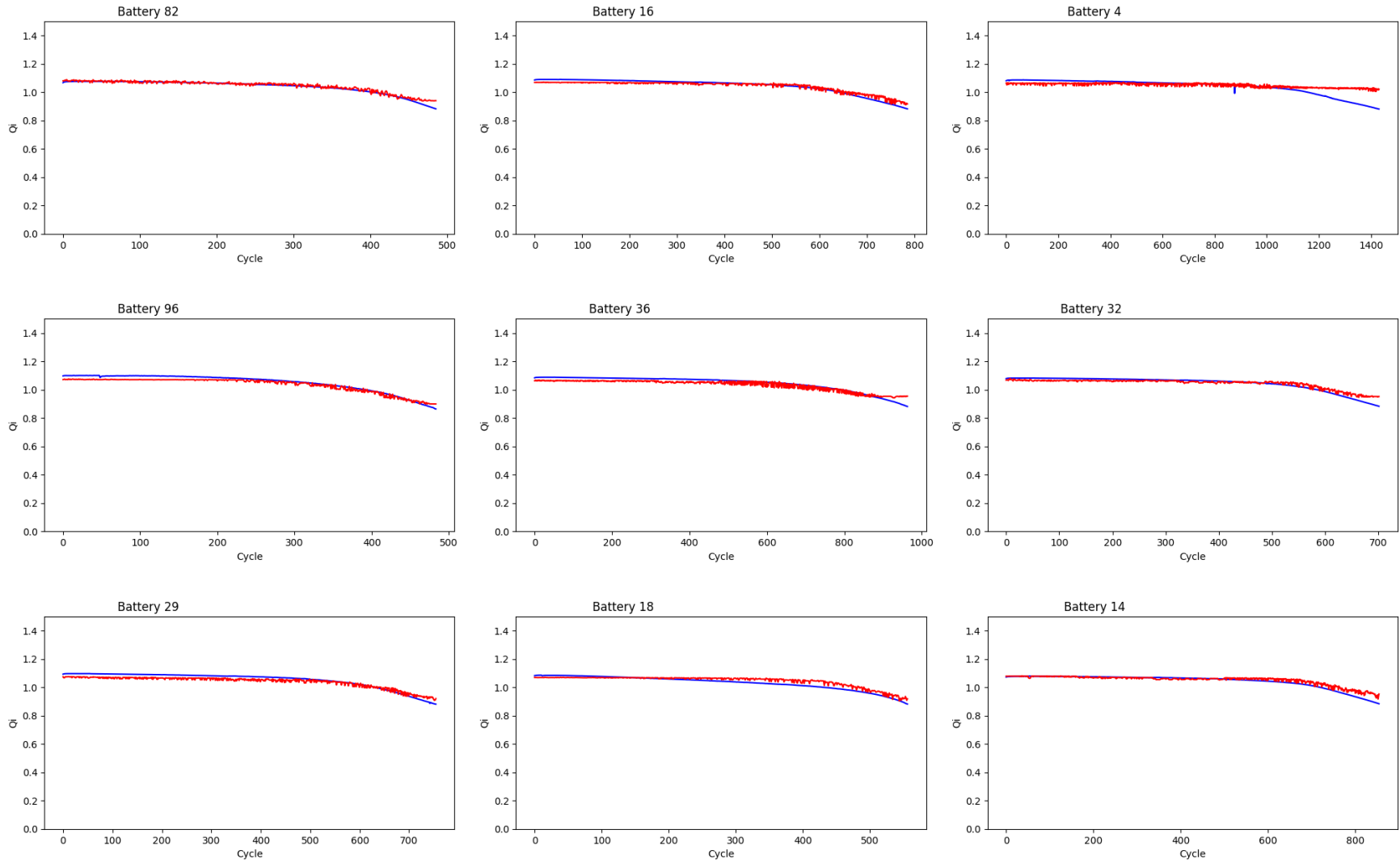


Figure 7.5: SOH estimation results using CatBoost algorithm.

Random Forest Regression

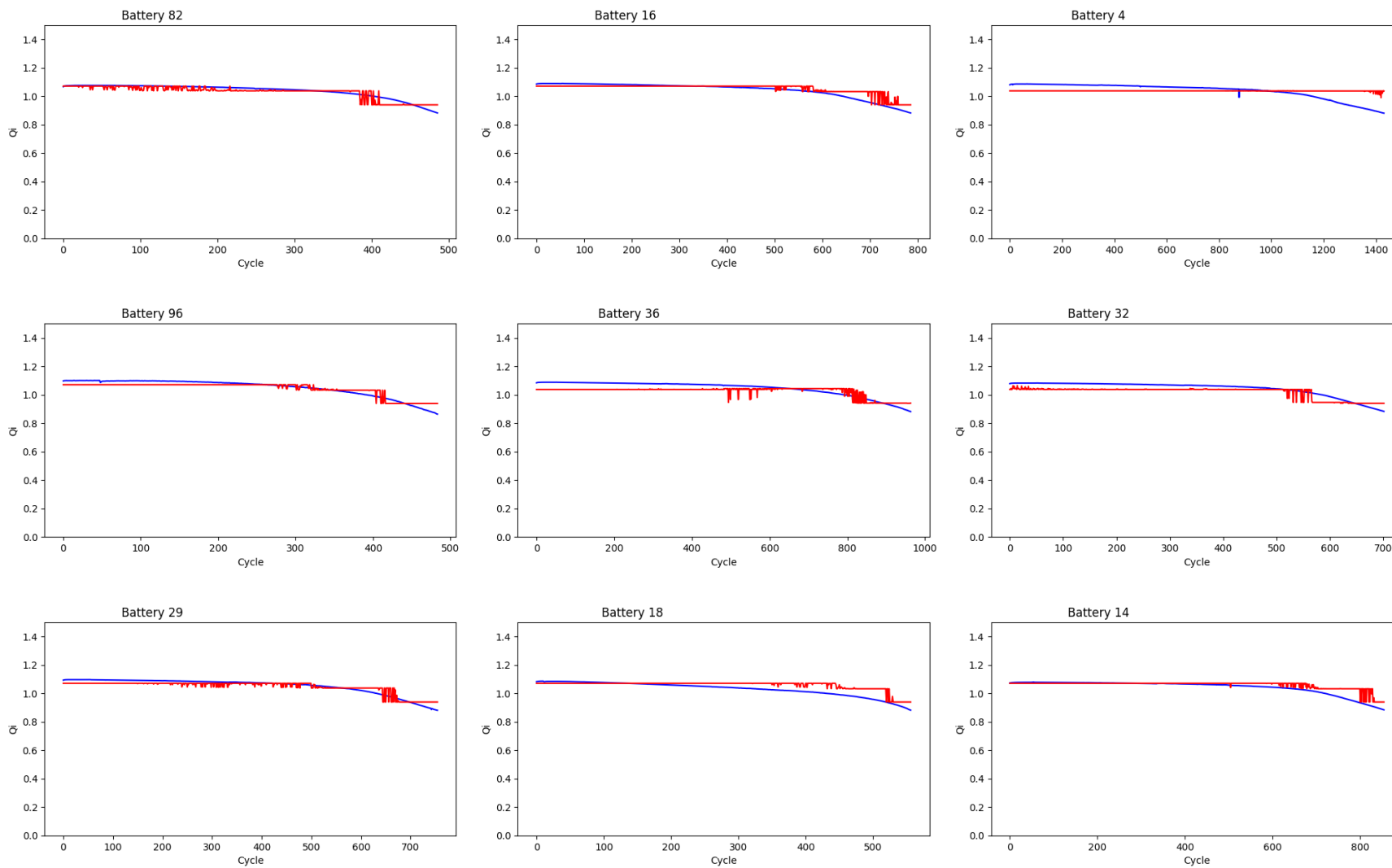


Figure 7.6: SOH estimation results using random forest algorithm.

Therefore, the neural network algorithm should be selected as the model to be used with the proposed SOH estimation approach. The results from the neural network algorithm consist of an average RSME of 9.50mAh and an average MAPE of 0.69%. Compared to other existing online SOH estimation methods used in the BMS from the recent review study by Bulow et al. [208], the proposed method in this study outperformed most others. Overall, the proposed approach has great accuracy while having high robustness and low complexity to be easily implemented in an embedded BMS for online and real-time battery applications.

7.5. Conclusions

This study proposed a novel approach for online and real-time SOH estimation of Li-ion batteries during fast charging cycles. The method utilized partial charge metrics combined with machine learning algorithms. The dataset used in this study consisted of 124 cells, of which, 115 cells were used to train and validate, and 9 were used to test and evaluate the performance of the approaches. During each charging cycle, three metrics were extracted as inputs and the battery capacity was the measured output, which were used as training and validation data for machine learning. Using the 9 cells for testing, it was found that the neural network algorithm returned the best SOH estimation results, with an RMSE of 9.50mAh and a MAPE of 0.69%, which indicated better performance than most existing SOH estimation approaches in literature. Overall, the proposed approach offers excellent accuracy, high robustness, and low complexity, making it ideal for implementation in the BMS for online and real-time applications.

Chapter 8 : Conclusions and Recommendations

8.1. Conclusions and Contributions

The focus of this work has been on investigating and improving battery modeling, cloud-based BMS architecture, cell replacement strategies, and SOH estimation for Li-ion batteries. The following sections summarize the five main research contributions from this thesis, corresponding to each chapter.

8.1.1. Contribution to Battery Modeling 1

This work investigated and compared the performance of three different ECMs using four Li-ion battery chemistries, LFP, NMC, LMO, and NCA, under dynamic and non-dynamic current profiles. Batteries underwent characterization experiments to obtain model parameters for voltage prediction, and the models were validated experimentally and compared using RMSE to determine the best model for each battery type. The main conclusions are that all three ECMs predicted battery voltage with low errors, and the hysteresis effect was stronger in LFP and NCA compared to NMC and LMO. Additionally, the ECMs performed better under dynamic current profiles, such as a UDDS cycle, compared to non-dynamic profiles. The ECMs performed best for the LFP cell and worst for the NCA cell, with NMC and LMO showing similar intermediate results. The best model for LFP and NCA was 1RC with hysteresis, while for NMC and LMO, the best model was 1RC due to its balance of accuracy and computational simplicity. These findings highlight the importance of selecting suitable ECMs based on battery chemistry, contributing to better battery modeling and BMS applications.

8.1.2. Contribution to Battery Modeling 2

This work then examined the effects of SOH, SOC, and temperature on the Thevenin ECM parameters using LFP batteries. An empirical model was developed and validated to reflect these factors. The main conclusions are that the ECM parameters were highly dependent on SOH, SOC, and temperature. The ohmic resistance increased with decreasing temperature and SOH, particularly at colder temperatures. The polarization resistance increased with SOH at both high and low temperatures. The polarization capacitance decreased with SOH across all SOC and temperature values. The empirical model accurately predicted voltage profiles under various

conditions with low RMSE and MAPE values, and the proposed model, accounting for SOH effects, significantly improved the accuracy of the Thevenin model. These findings underscore the impact of SOH on ECM parameters and the value of the proposed empirical model for advanced battery modeling and real-world applications.

8.1.3. Contribution to Cloud-Based BMS

This work also explored the potential of cloud-based smart BMS design to address limitations in traditional BMS, such as computational capability and data storage constraints. The key benefits of the cloud-based approach include improved condition monitoring, fault prognosis, and optimization of Li-ion battery systems. The flexibility of the cloud system allows it to be used with minimal modifications in future energy storage solutions, including solid-state Li-ion, lithium-sulfur, and metal-air batteries. By enhancing the reliability and performance of Li-ion battery systems, this contribution supports more efficient and widespread use of Li-ion battery systems, promoting cleaner and more accessible energy solutions.

8.1.4. Contribution to Analysis of Cell Replacement Strategies

This work investigated cell replacement for Li-ion battery packs using MATLAB simulations based on experimental data from 20-Ah LFP pouch cells. The main findings are that the validated cell voltage model can stochastically generate cells, and the cell replacement approach increased the total number of battery cycles by 63 cycles at the 80% SOH threshold and by 419 cycles at the 70% SOH threshold. Lowering the pack SOH threshold from 80% to 70% significantly increased the total number of cycles, provided the application could accept the lower capacity. The feasibility of cell replacement hinges on individual cell monitoring and accessibility, which may incur significant costs. These results demonstrate the economic potential of cell replacement over entire pack replacement, given certain design requirements are met, and suggest avenues for future research on optimizing this strategy.

8.1.5. Contribution to State of Health Estimation

Finally, this work proposed a novel method for online and real-time SOH estimation of Li-ion batteries during fast charging cycles, utilizing partial charge metrics and machine learning algorithms. The neural network algorithm provided the best SOH estimation results with an RMSE of 9.50 mAh and a MAPE of 0.69%, outperforming many existing approaches. The proposed

approach offers excellent accuracy, robustness, and low complexity, making it suitable for implementation in BMS for real-time applications. These findings contribute to the development of more accurate and efficient SOH estimation methods, enhancing the reliability and performance of BMS in real-world applications.

8.2. Recommendations and Future Work

Based on the findings and contributions of this thesis, several recommendations for future research are proposed to further advance the fields of battery modeling, smart BMS development, and BMS functions and algorithms improvement.

- Future research should investigate the integration of the ECM with data-driven battery models. By leveraging the computational power and data storage capabilities of cloud-based BMS, ECM parameters can be updated frequently using real-time data. This hybrid approach can enhance the accuracy and robustness of battery models by continuously learning from operational data and adapting to changing conditions. The real-time data can help in dynamically adjusting the model parameters, leading to more accurate voltage, SOC, and SOH estimations. Additionally, machine learning algorithms can be employed to detect patterns and anomalies in the data, providing insights that ECMs in traditional BMS might miss.
- It is also essential to analyze the economic and environmental impacts of deploying cloud-based BMS on a large scale. Future studies should evaluate the cost-benefit ratio, potential savings from improved battery management, and the environmental footprint associated with increased data transfer and storage. Additionally, optimizing the data transfer rate and determining the ideal amount of data to be stored on the cloud will help balance performance and sustainability. This analysis should include a comprehensive assessment of the lifecycle costs, including infrastructure investments, operational costs, and potential savings from extended battery life and reduced maintenance. The environmental impact should consider the energy consumption of data centers, the carbon footprint of data transmission, and the benefits of improved battery utilization and reduced waste.
- Further research is needed to refine the mechanical and electrical design aspects that enable the cell replacement strategies in battery packs. Innovative solutions, such as using springs for battery terminals and employing compression for the pack busbar, should be explored

to replace the current approach of welding cells in place within the pack. These advancements could significantly reduce the complexity and cost of cell replacement, making it a more viable option. Research should focus on developing standardized and modular designs that facilitate easy replacement and minimize the need for specialized tools or procedures. Additionally, the durability and reliability of these new connection methods under various operating conditions and over extended periods should be thoroughly tested.

- Developing advanced fault prognosis/prediction algorithms using the extensive data available from cloud-based BMS is another promising area for future research. These algorithms can predict potential failures, especially thermal runaway, by analyzing patterns and anomalies in the data. A robust fault prognosis system can enhance battery safety and reliability, preventing catastrophic failures before they occur. The use of big data analytics and machine learning techniques can help in identifying early warning signs and understanding the underlying mechanisms of different types of faults. Moreover, real-time monitoring and continuous learning from the data can improve the accuracy and responsiveness of the prognosis system.
- The increased computational capabilities provided by cloud platforms should be utilized to improve state estimation algorithms, such as state of charge (SOC) and state of power (SOP) estimation. Future research should focus on developing more sophisticated models that can take advantage of real-time data and high computational power to deliver more accurate and reliable estimates. This includes exploring advanced filtering techniques, such as particle filters or unscented Kalman filters, and incorporating additional data sources, such as historical temperature and current measurements, to enhance the model accuracy. Furthermore, the development of adaptive algorithms that can adjust to changes in battery behavior over time can provide more robust state estimation.
- Leveraging historical battery data stored on the cloud, future research can devise better warranty strategies by understanding individual user behavior and usage patterns. This approach can lead to personalized warranty terms that reflect the actual conditions under which the batteries are used, ultimately improving customer satisfaction and reducing warranty costs. By analyzing the data, manufacturers and insurers can identify common failure modes and usage scenarios that lead to accelerated degradation. This information

can be used to develop guidelines for optimal battery usage and maintenance, as well as to design more resilient batteries. Additionally, predictive analytics can help in estimating the remaining useful life of batteries more accurately, allowing for more precise warranty provisions.

References

- [1] M.-K. Tran, A. DaCosta, A. Mevawalla, S. Panchal, and M. Fowler, “Comparative Study of Equivalent Circuit Models Performance in Four Common Lithium-Ion Batteries: LFP, NMC, LMO, NCA,” *Batteries*, vol. 7, no. 3, p. 51, Jul. 2021, doi: 10.3390/batteries7030051.
- [2] M.-K. Tran *et al.*, “A comprehensive equivalent circuit model for lithium-ion batteries, incorporating the effects of state of health, state of charge, and temperature on model parameters,” *J Energy Storage*, vol. 43, p. 103252, Nov. 2021, doi: 10.1016/j.est.2021.103252.
- [3] M.-K. Tran, S. Panchal, T. D. Khang, K. Panchal, R. Fraser, and M. Fowler, “Concept Review of a Cloud-Based Smart Battery Management System for Lithium-Ion Batteries: Feasibility, Logistics, and Functionality,” *Batteries*, vol. 8, no. 2, p. 19, Feb. 2022, doi: 10.3390/batteries8020019.
- [4] M.-K. Tran, C. Cunanan, S. Panchal, R. Fraser, and M. Fowler, “Investigation of Individual Cells Replacement Concept in Lithium-Ion Battery Packs with Analysis on Economic Feasibility and Pack Design Requirements,” *Processes*, vol. 9, no. 12, p. 2263, Dec. 2021, doi: 10.3390/pr9122263.
- [5] A. Evans, V. Strezov, and T. J. Evans, “Assessment of utility energy storage options for increased renewable energy penetration,” *Renewable and Sustainable Energy Reviews*, vol. 16, no. 6, pp. 4141–4147, Aug. 2012, doi: 10.1016/j.rser.2012.03.048.
- [6] D. S. Markovic, D. Zivkovic, I. Branovic, R. Popovic, and D. Cvetkovic, “Smart power grid and cloud computing,” *Renewable and Sustainable Energy Reviews*, vol. 24, pp. 566–577, Aug. 2013, doi: 10.1016/j.rser.2013.03.068.
- [7] B. K. Bose, “Power Electronics, Smart Grid, and Renewable Energy Systems,” *Proceedings of the IEEE*, vol. 105, no. 11, pp. 2011–2018, Nov. 2017, doi: 10.1109/JPROC.2017.2745621.
- [8] J. P. Barton and D. G. Infield, “Energy Storage and Its Use With Intermittent Renewable Energy,” *IEEE Transactions on Energy Conversion*, vol. 19, no. 2, pp. 441–448, Jun. 2004, doi: 10.1109/TEC.2003.822305.
- [9] A. Nasiri, “Integrating energy storage with renewable energy systems,” in *2008 34th Annual Conference of IEEE Industrial Electronics*, IEEE, Nov. 2008, pp. 17–18. doi: 10.1109/IECON.2008.4757918.
- [10] B. P. Roberts and C. Sandberg, “The Role of Energy Storage in Development of Smart Grids,” *Proceedings of the IEEE*, vol. 99, no. 6, pp. 1139–1144, Jun. 2011, doi: 10.1109/JPROC.2011.2116752.

- [11] B. Scrosati and J. Garche, “Lithium batteries: Status, prospects and future,” *J Power Sources*, vol. 195, no. 9, pp. 2419–2430, May 2010, doi: 10.1016/j.jpowsour.2009.11.048.
- [12] X. Li and C. Wang, “Engineering nanostructured anodes via electrostatic spray deposition for high performance lithium ion battery application,” *J. Mater. Chem. A*, vol. 1, no. 2, pp. 165–182, 2013, doi: 10.1039/C2TA00437B.
- [13] U.S. Energy Information Administration, “Battery Storage in the United States: An Update on Market Trends,” Washington, DC, Aug. 2021.
- [14] Y. Liu, H. Liu, L. An, X. Zhao, and G. Liang, “Blended spherical lithium iron phosphate cathodes for high energy density lithium–ion batteries,” *Ionics (Kiel)*, vol. 25, no. 1, pp. 61–69, Jan. 2019, doi: 10.1007/s11581-018-2566-7.
- [15] A. Fotouhi, D. J. Auger, K. Propp, S. Longo, and M. Wild, “A review on electric vehicle battery modelling: From Lithium-ion toward Lithium–Sulphur,” *Renewable and Sustainable Energy Reviews*, vol. 56, pp. 1008–1021, Apr. 2016, doi: 10.1016/j.rser.2015.12.009.
- [16] Statista Research Department, “Projected battery demand worldwide by application 2020-2030,” Hamburg, Oct. 2023.
- [17] D. Andrea, *Battery Management Systems for Large Lithium-Ion Battery Packs*. Artech House, 2010.
- [18] M.-K. Tran, M. Akinsanya, S. Panchal, R. Fraser, and M. Fowler, “Design of a Hybrid Electric Vehicle Powertrain for Performance Optimization Considering Various Powertrain Components and Configurations,” *Vehicles*, vol. 3, no. 1, pp. 20–32, Dec. 2020, doi: 10.3390/vehicles3010002.
- [19] A. Hauser and R. Kuhn, “High-voltage battery management systems (BMS) for electric vehicles,” in *Advances in Battery Technologies for Electric Vehicles*, Elsevier, 2015, pp. 265–282. doi: 10.1016/B978-1-78242-377-5.00011-X.
- [20] K. Liu, K. Li, Q. Peng, and C. Zhang, “A brief review on key technologies in the battery management system of electric vehicles,” *Frontiers of Mechanical Engineering*, vol. 14, no. 1, pp. 47–64, Mar. 2019, doi: 10.1007/s11465-018-0516-8.
- [21] M. T. Lawder *et al.*, “Battery Energy Storage System (BESS) and Battery Management System (BMS) for Grid-Scale Applications,” *Proceedings of the IEEE*, vol. 102, no. 6, pp. 1014–1030, Jun. 2014, doi: 10.1109/JPROC.2014.2317451.
- [22] H. Chaoui and H. Gualous, “Online parameter and state estimation of lithium-ion batteries under temperature effects,” *Electric Power Systems Research*, vol. 145, pp. 73–82, Apr. 2017, doi: 10.1016/j.epsr.2016.12.029.
- [23] Y. Cui *et al.*, “State of health diagnosis model for lithium ion batteries based on real-time impedance and open circuit voltage parameters identification method,” *Energy*, vol. 144, pp. 647–656, Feb. 2018, doi: 10.1016/j.energy.2017.12.033.

- [24] L. Lu, X. Han, J. Li, J. Hua, and M. Ouyang, “A review on the key issues for lithium-ion battery management in electric vehicles,” *J Power Sources*, vol. 226, pp. 272–288, Mar. 2013, doi: 10.1016/j.jpowsour.2012.10.060.
- [25] M. Kassem and C. Delacourt, “Postmortem analysis of calendar-aged graphite/LiFePO₄ cells,” *J Power Sources*, vol. 235, pp. 159–171, Aug. 2013, doi: 10.1016/j.jpowsour.2013.01.147.
- [26] M. Safari and C. Delacourt, “Aging of a Commercial Graphite/LiFePO₄ Cell,” *J Electrochem Soc*, vol. 158, no. 10, p. A1123, 2011, doi: 10.1149/1.3614529.
- [27] D. Linden, “Basic Concepts,” in *Handbook of Batteries*, 3rd ed., D. Linden and T. B. Reddy, Eds., New York: McGraw-Hill, 2002.
- [28] M. Winter and R. J. Brodd, “What Are Batteries, Fuel Cells, and Supercapacitors?,” *Chem Rev*, vol. 104, no. 10, pp. 4245–4270, Oct. 2004, doi: 10.1021/cr020730k.
- [29] J. Broadhead and H. C. Kuo, “Electrical Principles and Reactions,” in *Handbook of Batteries*, 3rd ed., D. Linden and T. B. Reddy, Eds., New York: McGraw-Hill, 2002.
- [30] S. Grolleau *et al.*, “Calendar aging of commercial graphite/LiFePO₄ cell – Predicting capacity fade under time dependent storage conditions,” *J Power Sources*, vol. 255, pp. 450–458, Jun. 2014, doi: 10.1016/j.jpowsour.2013.11.098.
- [31] R. Garcia-Valle and J. A. P. Lopes, *Electric Vehicle Integration into Modern Power Networks*. New York, NY: Springer New York, 2013. doi: 10.1007/978-1-4614-0134-6.
- [32] A. Barré, B. Deguilhem, S. Grolleau, M. Gérard, F. Suard, and D. Riu, “A review on lithium-ion battery ageing mechanisms and estimations for automotive applications,” *J Power Sources*, vol. 241, pp. 680–689, Nov. 2013, doi: 10.1016/j.jpowsour.2013.05.040.
- [33] T. D. Finley, “Battery Degradation Modeling for Vehicle Applications,” University of Waterloo, Waterloo, 2014.
- [34] I. Husain, *Electric and Hybrid Vehicles: Design Fundamentals*, 3rd ed. CRC Press, 2021.
- [35] Y. Che, X. Hu, X. Lin, J. Guo, and R. Teodorescu, “Health prognostics for lithium-ion batteries: mechanisms, methods, and prospects,” *Energy Environ Sci*, vol. 16, no. 2, pp. 338–371, 2023, doi: 10.1039/D2EE03019E.
- [36] S. Karagiannopoulos, A. Rigas, N. Hatzargyriou, G. Hug, and A. Oudalov, “Battery energy storage capacity fading and control strategies for deterministic and stochastic power profiles,” in *2016 Power Systems Computation Conference (PSCC)*, IEEE, Jun. 2016, pp. 1–7. doi: 10.1109/PSCC.2016.7540956.
- [37] L. He and K. G. Shin, “Fingerprinting Battery Health Using Relaxing Voltages,” in *Proceedings of the 14th ACM International Conference on Future Energy Systems*, New York, NY, USA: ACM, Jun. 2023, pp. 48–59. doi: 10.1145/3575813.3576875.

- [38] M. Kassem, J. Bernard, R. Revel, S. Pélissier, F. Duclaud, and C. Delacourt, “Calendar aging of a graphite/LiFePO₄ cell,” *J Power Sources*, vol. 208, pp. 296–305, Jun. 2012, doi: 10.1016/j.jpowsour.2012.02.068.
- [39] C. Lin, A. Tang, H. Mu, W. Wang, and C. Wang, “Aging Mechanisms of Electrode Materials in Lithium-Ion Batteries for Electric Vehicles,” *J Chem*, vol. 2015, pp. 1–11, 2015, doi: 10.1155/2015/104673.
- [40] C. Liu, Z. Deng, X. Zhang, H. Bao, and D. Cheng, “Battery state of health estimation across electrochemistry and working conditions based on domain adaptation,” *Energy*, vol. 297, p. 131294, Jun. 2024, doi: 10.1016/j.energy.2024.131294.
- [41] P. Keil *et al.*, “Calendar Aging of Lithium-Ion Batteries,” *J Electrochem Soc*, vol. 163, no. 9, pp. A1872–A1880, Jul. 2016, doi: 10.1149/2.0411609jes.
- [42] J. Schmalstieg, S. Kabitz, M. Ecker, and D. U. Sauer, “From accelerated aging tests to a lifetime prediction model: Analyzing lithium-ion batteries,” in *2013 World Electric Vehicle Symposium and Exhibition (EVS27)*, IEEE, Nov. 2013, pp. 1–12. doi: 10.1109/EVS.2013.6914753.
- [43] K. Ohue, T. Utsunomiya, O. Hatozaki, N. Yoshimoto, M. Egashira, and M. Morita, “Self-discharge behavior of polyacenic semiconductor and graphite negative electrodes for lithium-ion batteries,” *J Power Sources*, vol. 196, no. 7, pp. 3604–3610, Apr. 2011, doi: 10.1016/j.jpowsour.2010.12.073.
- [44] V. N. Bandla, L. Briot, J. Bernard, M. Petit, M. Morcrette, and C. Delacourt, “Modeling the internal inhomogeneous aging behavior within individual Li-ion cells – During cycle aging,” *J Energy Storage*, vol. 86, p. 111186, May 2024, doi: 10.1016/j.est.2024.111186.
- [45] A. W. Golubkov *et al.*, “Thermal-runaway experiments on consumer Li-ion batteries with metal-oxide and olivin-type cathodes,” *RSC Adv.*, vol. 4, no. 7, pp. 3633–3642, 2014, doi: 10.1039/C3RA45748F.
- [46] Q. Wang, B. Mao, S. I. Stolarov, and J. Sun, “A review of lithium ion battery failure mechanisms and fire prevention strategies,” *Prog Energy Combust Sci*, vol. 73, pp. 95–131, Jul. 2019, doi: 10.1016/j.pecs.2019.03.002.
- [47] X. Feng, Y. Pan, X. He, L. Wang, and M. Ouyang, “Detecting the internal short circuit in large-format lithium-ion battery using model-based fault-diagnosis algorithm,” *J Energy Storage*, vol. 18, pp. 26–39, Aug. 2018, doi: 10.1016/j.est.2018.04.020.
- [48] D. Lyu, B. Ren, and S. Li, “Failure modes and mechanisms for rechargeable Lithium-based batteries: a state-of-the-art review,” *Acta Mech*, vol. 230, no. 3, pp. 701–727, Mar. 2019, doi: 10.1007/s00707-018-2327-8.
- [49] X. Feng *et al.*, “Characterization of penetration induced thermal runaway propagation process within a large format lithium ion battery module,” *J Power Sources*, vol. 275, pp. 261–273, Feb. 2015, doi: 10.1016/j.jpowsour.2014.11.017.

- [50] Z. Liu, Q. Ahmed, G. Rizzoni, and H. He, "Fault Detection and Isolation for Lithium-Ion Battery System Using Structural Analysis and Sequential Residual Generation," in *Volume 2: Dynamic Modeling and Diagnostics in Biomedical Systems*, American Society of Mechanical Engineers, Oct. 2014. doi: 10.1115/DSCC2014-6101.
- [51] N. E. Galushkin, N. N. Yazvinskaya, and D. N. Galushkin, "Mechanism of Thermal Runaway in Lithium-Ion Cells," *J Electrochem Soc*, vol. 165, no. 7, pp. A1303–A1308, May 2018, doi: 10.1149/2.0611807jes.
- [52] H. Rahimi-Eichi, U. Ojha, F. Baronti, and M.-Y. Chow, "Battery Management System: An Overview of Its Application in the Smart Grid and Electric Vehicles," *IEEE Industrial Electronics Magazine*, vol. 7, no. 2, pp. 4–16, Jun. 2013, doi: 10.1109/MIE.2013.2250351.
- [53] M. Lelie *et al.*, "Battery Management System Hardware Concepts: An Overview," *Applied Sciences*, vol. 8, no. 4, p. 534, Mar. 2018, doi: 10.3390/app8040534.
- [54] C. Hendricks, N. Williard, S. Mathew, and M. Pecht, "A failure modes, mechanisms, and effects analysis (FMMEA) of lithium-ion batteries," *J Power Sources*, vol. 297, pp. 113–120, Nov. 2015, doi: 10.1016/j.jpowsour.2015.07.100.
- [55] F. Baronti, G. Fantechi, R. Roncella, and R. Saletti, "Intelligent cell gauge for a hierarchical battery management system," in *2012 IEEE Transportation Electrification Conference and Expo (ITEC)*, IEEE, Jun. 2012, pp. 1–5. doi: 10.1109/ITEC.2012.6243471.
- [56] A. Khaligh and Zhihao Li, "Battery, Ultracapacitor, Fuel Cell, and Hybrid Energy Storage Systems for Electric, Hybrid Electric, Fuel Cell, and Plug-In Hybrid Electric Vehicles: State of the Art," *IEEE Trans Veh Technol*, vol. 59, no. 6, pp. 2806–2814, Jul. 2010, doi: 10.1109/TVT.2010.2047877.
- [57] M. Uno and K. Tanaka, "Accelerated ageing testing and cycle life prediction of supercapacitors for alternative battery applications," in *2011 IEEE 33rd International Telecommunications Energy Conference (INTELEC)*, IEEE, Oct. 2011, pp. 1–6. doi: 10.1109/INTLEC.2011.6099720.
- [58] B. Saha, K. Goebel, and J. Christophersen, "Comparison of prognostic algorithms for estimating remaining useful life of batteries," *Transactions of the Institute of Measurement and Control*, vol. 31, no. 3–4, pp. 293–308, Jun. 2009, doi: 10.1177/0142331208092030.
- [59] V. Ramadesigan, P. W. C. Northrop, S. De, S. Santhanagopalan, R. D. Braatz, and V. R. Subramanian, "Modeling and Simulation of Lithium-Ion Batteries from a Systems Engineering Perspective," *J Electrochem Soc*, vol. 159, no. 3, pp. R31–R45, Jan. 2012, doi: 10.1149/2.018203jes.
- [60] IL-Song Kim, "A Technique for Estimating the State of Health of Lithium Batteries Through a Dual-Sliding-Mode Observer," *IEEE Trans Power Electron*, vol. 25, no. 4, pp. 1013–1022, Apr. 2010, doi: 10.1109/TPEL.2009.2034966.

- [61] K. S. Ng, C.-S. Moo, Y.-P. Chen, and Y.-C. Hsieh, “Enhanced coulomb counting method for estimating state-of-charge and state-of-health of lithium-ion batteries,” *Appl Energy*, vol. 86, no. 9, pp. 1506–1511, Sep. 2009, doi: 10.1016/j.apenergy.2008.11.021.
- [62] T. Huria, M. Ceraolo, J. Gazzarri, and R. Jackey, “High fidelity electrical model with thermal dependence for characterization and simulation of high power lithium battery cells,” in *2012 IEEE International Electric Vehicle Conference*, IEEE, Mar. 2012, pp. 1–8. doi: 10.1109/IEVC.2012.6183271.
- [63] N. Wassiliadis *et al.*, “A systematic approach for the parameter identification of electrochemical battery models enabling health-aware fast charging control of battery electric vehicles,” *J Energy Storage*, vol. 56, p. 105951, Dec. 2022, doi: 10.1016/j.est.2022.105951.
- [64] A. Mevawalla, S. Panchal, M.-K. Tran, M. Fowler, and R. Fraser, “Mathematical Heat Transfer Modeling and Experimental Validation of Lithium-Ion Battery Considering: Tab and Surface Temperature, Separator, Electrolyte Resistance, Anode-Cathode Irreversible and Reversible Heat,” *Batteries*, vol. 6, no. 4, p. 61, Dec. 2020, doi: 10.3390/batteries6040061.
- [65] X. Hu, S. Li, and H. Peng, “A comparative study of equivalent circuit models for Li-ion batteries,” *J Power Sources*, vol. 198, pp. 359–367, Jan. 2012, doi: 10.1016/j.jpowsour.2011.10.013.
- [66] H. L. Chan, “A new battery model for use with battery energy storage systems and electric vehicles power systems,” in *2000 IEEE Power Engineering Society Winter Meeting. Conference Proceedings (Cat. No.00CH37077)*, IEEE, pp. 470–475. doi: 10.1109/PESW.2000.850009.
- [67] K. A. Severson *et al.*, “Data-driven prediction of battery cycle life before capacity degradation,” *Nat Energy*, vol. 4, no. 5, pp. 383–391, Mar. 2019, doi: 10.1038/s41560-019-0356-8.
- [68] D. Wang, F. Yang, K.-L. Tsui, Q. Zhou, and S. J. Bae, “Remaining Useful Life Prediction of Lithium-Ion Batteries Based on Spherical Cubature Particle Filter,” *IEEE Trans Instrum Meas*, vol. 65, no. 6, pp. 1282–1291, Jun. 2016, doi: 10.1109/TIM.2016.2534258.
- [69] G. Ma, Y. Zhang, C. Cheng, B. Zhou, P. Hu, and Y. Yuan, “Remaining useful life prediction of lithium-ion batteries based on false nearest neighbors and a hybrid neural network,” *Appl Energy*, vol. 253, p. 113626, Nov. 2019, doi: 10.1016/j.apenergy.2019.113626.
- [70] M. A. Hannan, Md. M. Hoque, A. Hussain, Y. Yusof, and P. J. Ker, “State-of-the-Art and Energy Management System of Lithium-Ion Batteries in Electric Vehicle Applications: Issues and Recommendations,” *IEEE Access*, vol. 6, pp. 19362–19378, 2018, doi: 10.1109/ACCESS.2018.2817655.

- [71] M.-K. Tran and M. Fowler, “A Review of Lithium-Ion Battery Fault Diagnostic Algorithms: Current Progress and Future Challenges,” *Algorithms*, vol. 13, no. 3, p. 62, Mar. 2020, doi: 10.3390/a13030062.
- [72] C. Wu, C. Zhu, Y. Ge, and Y. Zhao, “A Review on Fault Mechanism and Diagnosis Approach for Li-Ion Batteries,” *J Nanomater*, vol. 2015, pp. 1–9, 2015, doi: 10.1155/2015/631263.
- [73] L. Tang, J. Dong, Y. Zhao, and L.-J. Zhang, “Enterprise Cloud Service Architecture,” in *2010 IEEE 3rd International Conference on Cloud Computing*, IEEE, Jul. 2010, pp. 27–34. doi: 10.1109/CLOUD.2010.10.
- [74] B. Varghese and R. Buyya, “Next generation cloud computing: New trends and research directions,” *Future Generation Computer Systems*, vol. 79, pp. 849–861, Feb. 2018, doi: 10.1016/j.future.2017.09.020.
- [75] C. Moretti, J. Bulosan, D. Thain, and P. J. Flynn, “All-pairs: An abstraction for data-intensive cloud computing,” in *2008 IEEE International Symposium on Parallel and Distributed Processing*, IEEE, Apr. 2008, pp. 1–11. doi: 10.1109/IPDPS.2008.4536311.
- [76] D. Agrawal, S. Das, and A. El Abbadi, “Big data and cloud computing,” in *Proceedings of the 14th International Conference on Extending Database Technology*, New York, NY, USA: ACM, Mar. 2011, pp. 530–533. doi: 10.1145/1951365.1951432.
- [77] J. B. Rothnie *et al.*, “Introduction to a system for distributed databases (SDD-1),” *ACM Transactions on Database Systems*, vol. 5, no. 1, pp. 1–17, Mar. 1980, doi: 10.1145/320128.320129.
- [78] J. Shamsi, M. A. Khojaye, and M. A. Qasmi, “Data-Intensive Cloud Computing: Requirements, Expectations, Challenges, and Solutions,” *J Grid Comput*, vol. 11, no. 2, pp. 281–310, Jun. 2013, doi: 10.1007/s10723-013-9255-6.
- [79] D. Agrawal, A. El Abbadi, S. Antony, and S. Das, “Data Management Challenges in Cloud Computing Infrastructures,” 2010, pp. 1–10. doi: 10.1007/978-3-642-12038-1_1.
- [80] T. D. Khang, N. D. Vuong, M.-K. Tran, and M. Fowler, “Fuzzy C-Means Clustering Algorithm with Multiple Fuzzification Coefficients,” *Algorithms*, vol. 13, no. 7, p. 158, Jun. 2020, doi: 10.3390/a13070158.
- [81] C. Barrington-Leigh and M. Ouliaris, “The renewable energy landscape in Canada: A spatial analysis,” *Renewable and Sustainable Energy Reviews*, vol. 75, pp. 809–819, Aug. 2017, doi: 10.1016/j.rser.2016.11.061.
- [82] M.-K. Tran *et al.*, “Environmental and Economic Benefits of a Battery Electric Vehicle Powertrain with a Zinc–Air Range Extender in the Transition to Electric Vehicles,” *Vehicles*, vol. 2, no. 3, pp. 398–412, Jun. 2020, doi: 10.3390/vehicles2030021.

- [83] M.-K. Tran *et al.*, “A Review of Range Extenders in Battery Electric Vehicles: Current Progress and Future Perspectives,” *World Electric Vehicle Journal*, vol. 12, no. 2, p. 54, Apr. 2021, doi: 10.3390/wevj12020054.
- [84] S. Panchal, K. Gudlanarva, M.-K. Tran, R. Fraser, and M. Fowler, “High Reynold’s Number Turbulent Model for Micro-Channel Cold Plate Using Reverse Engineering Approach for Water-Cooled Battery in Electric Vehicles,” *Energies (Basel)*, vol. 13, no. 7, p. 1638, Apr. 2020, doi: 10.3390/en13071638.
- [85] I. Veza, M. Z. Asy’ari, M. Idris, V. Epin, I. M. Rizwanul Fattah, and M. Spraggon, “Electric vehicle (EV) and driving towards sustainability: Comparison between EV, HEV, PHEV, and ICE vehicles to achieve net zero emissions by 2050 from EV,” *Alexandria Engineering Journal*, vol. 82, pp. 459–467, Nov. 2023, doi: 10.1016/j.aej.2023.10.020.
- [86] C. Cunanan, M.-K. Tran, Y. Lee, S. Kwok, V. Leung, and M. Fowler, “A Review of Heavy-Duty Vehicle Powertrain Technologies: Diesel Engine Vehicles, Battery Electric Vehicles, and Hydrogen Fuel Cell Electric Vehicles,” *Clean Technologies*, vol. 3, no. 2, pp. 474–489, Jun. 2021, doi: 10.3390/cleantechnol3020028.
- [87] Á. Porrás-Hermoso, S. Pindado, and J. Cubas, “Lithium-ion battery performance modeling based on the energy discharge level,” *Meas Sci Technol*, vol. 29, no. 11, p. 117002, Nov. 2018, doi: 10.1088/1361-6501/aae231.
- [88] E. K. Schwartz and M. Krarti, “Review of Adoption Status of Sustainable Energy Technologies in the US Residential Building Sector,” *Energies (Basel)*, vol. 15, no. 6, p. 2027, Mar. 2022, doi: 10.3390/en15062027.
- [89] B. Zou *et al.*, “A Review on the Fault and Defect Diagnosis of Lithium-Ion Battery for Electric Vehicles,” *Energies (Basel)*, vol. 16, no. 14, p. 5507, Jul. 2023, doi: 10.3390/en16145507.
- [90] C. Fleischer, W. Waag, H.-M. Heyn, and D. U. Sauer, “On-line adaptive battery impedance parameter and state estimation considering physical principles in reduced order equivalent circuit battery models,” *J Power Sources*, vol. 260, pp. 276–291, Aug. 2014, doi: 10.1016/j.jpowsour.2014.01.129.
- [91] X. Lai, Y. Zheng, and T. Sun, “A comparative study of different equivalent circuit models for estimating state-of-charge of lithium-ion batteries,” *Electrochim Acta*, vol. 259, pp. 566–577, Jan. 2018, doi: 10.1016/j.electacta.2017.10.153.
- [92] S. Nejad, D. T. Gladwin, and D. A. Stone, “A systematic review of lumped-parameter equivalent circuit models for real-time estimation of lithium-ion battery states,” *J Power Sources*, vol. 316, pp. 183–196, Jun. 2016, doi: 10.1016/j.jpowsour.2016.03.042.
- [93] S. Fletcher, V. J. Black, and I. Kirkpatrick, “A universal equivalent circuit for carbon-based supercapacitors,” *Journal of Solid State Electrochemistry*, vol. 18, no. 5, pp. 1377–1387, May 2014, doi: 10.1007/s10008-013-2328-4.

- [94] A. Mevawalla, S. Panchal, M.-K. Tran, M. Fowler, and R. Fraser, “One dimensional fast computational partial differential model for heat transfer in lithium-ion batteries,” *J Energy Storage*, vol. 37, p. 102471, May 2021, doi: 10.1016/j.est.2021.102471.
- [95] H. He, R. Xiong, H. Guo, and S. Li, “Comparison study on the battery models used for the energy management of batteries in electric vehicles,” *Energy Convers Manag*, vol. 64, pp. 113–121, Dec. 2012, doi: 10.1016/j.enconman.2012.04.014.
- [96] L. Zhang, H. Peng, Z. Ning, Z. Mu, and C. Sun, “Comparative Research on RC Equivalent Circuit Models for Lithium-Ion Batteries of Electric Vehicles,” *Applied Sciences*, vol. 7, no. 10, p. 1002, Sep. 2017, doi: 10.3390/app7101002.
- [97] K. C. Divya and J. Østergaard, “Battery energy storage technology for power systems—An overview,” *Electric Power Systems Research*, vol. 79, no. 4, pp. 511–520, Apr. 2009, doi: 10.1016/j.epsr.2008.09.017.
- [98] T. V. S. L. Satyavani, A. Srinivas Kumar, and P. S. V. Subba Rao, “Methods of synthesis and performance improvement of lithium iron phosphate for high rate Li-ion batteries: A review,” *Engineering Science and Technology, an International Journal*, vol. 19, no. 1, pp. 178–188, Mar. 2016, doi: 10.1016/j.jestch.2015.06.002.
- [99] A. K. Padhi, K. S. Nanjundaswamy, and J. B. Goodenough, “Phospho-olivines as Positive-Electrode Materials for Rechargeable Lithium Batteries,” *J Electrochem Soc*, vol. 144, no. 4, pp. 1188–1194, Apr. 1997, doi: 10.1149/1.1837571.
- [100] F. Forte, M. Pietrantonio, S. Pucciarmati, M. Puzone, and D. Fontana, “Lithium iron phosphate batteries recycling: An assessment of current status,” *Crit Rev Environ Sci Technol*, vol. 51, no. 19, pp. 2232–2259, Oct. 2021, doi: 10.1080/10643389.2020.1776053.
- [101] O. Capron, R. Gopalakrishnan, J. Jaguemont, P. Van Den Bossche, N. Omar, and J. Van Mierlo, “On the Ageing of High Energy Lithium-Ion Batteries—Comprehensive Electrochemical Diffusivity Studies of Harvested Nickel Manganese Cobalt Electrodes,” *Materials*, vol. 11, no. 2, p. 176, Jan. 2018, doi: 10.3390/ma11020176.
- [102] Z. Li *et al.*, “Comparative Study of the Capacity and Rate Capability of $\text{LiNi}_y\text{Mn}_y\text{Co}_{1-2y}\text{O}_2$ ($y = 0.5, 0.45, 0.4, 0.33$),” *J Electrochem Soc*, vol. 158, no. 5, p. A516, 2011, doi: 10.1149/1.3562212.
- [103] H. Yang, C. N. Savory, B. J. Morgan, D. O. Scanlon, J. M. Skelton, and A. Walsh, “Chemical Trends in the Lattice Thermal Conductivity of $\text{Li}(\text{Ni}, \text{Mn}, \text{Co})\text{O}_2$ (NMC) Battery Cathodes,” *Chemistry of Materials*, vol. 32, no. 17, pp. 7542–7550, Sep. 2020, doi: 10.1021/acs.chemmater.0c02908.
- [104] M. V. Reddy, A. Mauger, C. M. Julien, A. Paolella, and K. Zaghib, “Brief History of Early Lithium-Battery Development,” *Materials*, vol. 13, no. 8, p. 1884, Apr. 2020, doi: 10.3390/ma13081884.

- [105] H. Zhu *et al.*, “Key technologies for smart energy systems: Recent developments, challenges, and research opportunities in the context of carbon neutrality,” *J Clean Prod*, vol. 331, p. 129809, Jan. 2022, doi: 10.1016/j.jclepro.2021.129809.
- [106] M.-J. Lee, S. Lee, P. Oh, Y. Kim, and J. Cho, “High Performance LiMn_2O_4 Cathode Materials Grown with Epitaxial Layered Nanostructure for Li-Ion Batteries,” *Nano Lett*, vol. 14, no. 2, pp. 993–999, Feb. 2014, doi: 10.1021/nl404430e.
- [107] Y. Miao, P. Hynan, A. von Jouanne, and A. Yokochi, “Current Li-Ion Battery Technologies in Electric Vehicles and Opportunities for Advancements,” *Energies (Basel)*, vol. 12, no. 6, p. 1074, Mar. 2019, doi: 10.3390/en12061074.
- [108] H. He, R. Xiong, and J. Fan, “Evaluation of Lithium-Ion Battery Equivalent Circuit Models for State of Charge Estimation by an Experimental Approach,” *Energies (Basel)*, vol. 4, no. 4, pp. 582–598, Mar. 2011, doi: 10.3390/en4040582.
- [109] G. L. Plett, “Extended Kalman filtering for battery management systems of LiPB-based HEV battery packs,” *J Power Sources*, vol. 134, no. 2, pp. 262–276, Aug. 2004, doi: 10.1016/j.jpowsour.2004.02.032.
- [110] D. Li, J. Ouyang, H. Li, and J. Wan, “State of charge estimation for LiMn_2O_4 power battery based on strong tracking sigma point Kalman filter,” *J Power Sources*, vol. 279, pp. 439–449, Apr. 2015, doi: 10.1016/j.jpowsour.2015.01.002.
- [111] Y. Li, C. Wang, and J. Gong, “A combination Kalman filter approach for State of Charge estimation of lithium-ion battery considering model uncertainty,” *Energy*, vol. 109, pp. 933–946, Aug. 2016, doi: 10.1016/j.energy.2016.05.047.
- [112] J. Moskon, J. Jamnik, and M. Gaberscek, “In depth discussion of selected phenomena associated with intrinsic battery hysteresis: Battery electrode versus rubber balloons,” *Solid State Ion*, vol. 238, pp. 24–29, May 2013, doi: 10.1016/j.ssi.2013.02.018.
- [113] T. Kalogiannis *et al.*, “Comparative Study on Parameter Identification Methods for Dual-Polarization Lithium-Ion Equivalent Circuit Model,” *Energies (Basel)*, vol. 12, no. 21, p. 4031, Oct. 2019, doi: 10.3390/en12214031.
- [114] M.-K. Tran, A. Mevawala, S. Panchal, K. Raahemifar, M. Fowler, and R. Fraser, “Effect of integrating the hysteresis component to the equivalent circuit model of Lithium-ion battery for dynamic and non-dynamic applications,” *J Energy Storage*, vol. 32, p. 101785, Dec. 2020, doi: 10.1016/j.est.2020.101785.
- [115] A. Li, S. Pelissier, P. Venet, and P. Gyan, “Fast Characterization Method for Modeling Battery Relaxation Voltage,” *Batteries*, vol. 2, no. 2, p. 7, Apr. 2016, doi: 10.3390/batteries2020007.
- [116] V. Schwarzer and R. Ghorbani, “Drive Cycle Generation for Design Optimization of Electric Vehicles,” *IEEE Trans Veh Technol*, vol. 62, no. 1, pp. 89–97, Jan. 2013, doi: 10.1109/TVT.2012.2219889.

- [117] B. Y. Liaw, G. Nagasubramanian, R. G. Jungst, and D. H. Doughty, "Modeling of lithium ion cells?A simple equivalent-circuit model approach," *Solid State Ion*, vol. 175, no. 1–4, pp. 835–839, Nov. 2004, doi: 10.1016/j.ssi.2004.09.049.
- [118] J. Jiang, Y. Liang, Q. Ju, L. Zhang, W. Zhang, and C. Zhang, "An Equivalent Circuit Model for Lithium-sulfur Batteries," *Energy Procedia*, vol. 105, pp. 3533–3538, May 2017, doi: 10.1016/j.egypro.2017.03.810.
- [119] X. Hu, H. Yuan, C. Zou, Z. Li, and L. Zhang, "Co-Estimation of State of Charge and State of Health for Lithium-Ion Batteries Based on Fractional-Order Calculus," *IEEE Trans Veh Technol*, vol. 67, no. 11, pp. 10319–10329, Nov. 2018, doi: 10.1109/TVT.2018.2865664.
- [120] L. He, M. Hu, Y. Wei, B. Liu, and Q. Shi, "State of charge estimation by finite difference extended Kalman filter with HPPC parameters identification," *Sci China Technol Sci*, vol. 63, no. 3, pp. 410–421, Mar. 2020, doi: 10.1007/s11431-019-1467-9.
- [121] J. Li, K. Adewuyi, N. Lotfi, R. G. Landers, and J. Park, "A single particle model with chemical/mechanical degradation physics for lithium ion battery State of Health (SOH) estimation," *Appl Energy*, vol. 212, pp. 1178–1190, Feb. 2018, doi: 10.1016/j.apenergy.2018.01.011.
- [122] J. Vetter *et al.*, "Ageing mechanisms in lithium-ion batteries," *J Power Sources*, vol. 147, no. 1–2, pp. 269–281, Sep. 2005, doi: 10.1016/j.jpowsour.2005.01.006.
- [123] R. Hausbrand *et al.*, "Fundamental degradation mechanisms of layered oxide Li-ion battery cathode materials: Methodology, insights and novel approaches," *Materials Science and Engineering: B*, vol. 192, pp. 3–25, Feb. 2015, doi: 10.1016/j.mseb.2014.11.014.
- [124] Y. Li, P. Chattopadhyay, A. Ray, and C. D. Rahn, "Identification of the battery state-of-health parameter from input–output pairs of time series data," *J Power Sources*, vol. 285, pp. 235–246, Jul. 2015, doi: 10.1016/j.jpowsour.2015.03.068.
- [125] F. Feng, R. Lu, G. Wei, and C. Zhu, "Online Estimation of Model Parameters and State of Charge of LiFePO₄ Batteries Using a Novel Open-Circuit Voltage at Various Ambient Temperatures," *Energies (Basel)*, vol. 8, no. 4, pp. 2950–2976, Apr. 2015, doi: 10.3390/en8042950.
- [126] T. Feng, L. Yang, X. Zhao, H. Zhang, and J. Qiang, "Online identification of lithium-ion battery parameters based on an improved equivalent-circuit model and its implementation on battery state-of-power prediction," *J Power Sources*, vol. 281, pp. 192–203, May 2015, doi: 10.1016/j.jpowsour.2015.01.154.
- [127] C. Zhang, W. Allafi, Q. Dinh, P. Ascencio, and J. Marco, "Online estimation of battery equivalent circuit model parameters and state of charge using decoupled least squares technique," *Energy*, vol. 142, pp. 678–688, Jan. 2018, doi: 10.1016/j.energy.2017.10.043.

- [128] X. Lai, S. Wang, S. Ma, J. Xie, and Y. Zheng, “Parameter sensitivity analysis and simplification of equivalent circuit model for the state of charge of lithium-ion batteries,” *Electrochim Acta*, vol. 330, p. 135239, Jan. 2020, doi: 10.1016/j.electacta.2019.135239.
- [129] J. Gomez, R. Nelson, E. E. Kalu, M. H. Weatherspoon, and J. P. Zheng, “Equivalent circuit model parameters of a high-power Li-ion battery: Thermal and state of charge effects,” *J Power Sources*, vol. 196, no. 10, pp. 4826–4831, May 2011, doi: 10.1016/j.jpowsour.2010.12.107.
- [130] A. Farmann and D. U. Sauer, “A study on the dependency of the open-circuit voltage on temperature and actual aging state of lithium-ion batteries,” *J Power Sources*, vol. 347, pp. 1–13, Apr. 2017, doi: 10.1016/j.jpowsour.2017.01.098.
- [131] S. J. Bazinski and X. Wang, “The Influence of Cell Temperature on the Entropic Coefficient of a Lithium Iron Phosphate (LFP) Pouch Cell,” *J Electrochem Soc*, vol. 161, no. 1, pp. A168–A175, Dec. 2014, doi: 10.1149/2.082401jes.
- [132] Y. Li, M. Vilathgamuwa, T. Farrell, S. S. Choi, N. T. Tran, and J. Teague, “A physics-based distributed-parameter equivalent circuit model for lithium-ion batteries,” *Electrochim Acta*, vol. 299, pp. 451–469, Mar. 2019, doi: 10.1016/j.electacta.2018.12.167.
- [133] M. Akdere *et al.*, “Hardware and software framework for an open battery management system in safety-critical applications,” in *IECON 2016 - 42nd Annual Conference of the IEEE Industrial Electronics Society*, IEEE, Oct. 2016, pp. 5507–5512. doi: 10.1109/IECON.2016.7793001.
- [134] M. İnci, Ö. Çelik, A. Lashab, K. Ç. Bayındır, J. C. Vasquez, and J. M. Guerrero, “Power System Integration of Electric Vehicles: A Review on Impacts and Contributions to the Smart Grid,” *Applied Sciences*, vol. 14, no. 6, p. 2246, Mar. 2024, doi: 10.3390/app14062246.
- [135] Y. Xing, E. W. M. Ma, K. L. Tsui, and M. Pecht, “Battery Management Systems in Electric and Hybrid Vehicles,” *Energies (Basel)*, vol. 4, no. 11, pp. 1840–1857, Oct. 2011, doi: 10.3390/en4111840.
- [136] S. M. Rezvanianiani, Z. Liu, Y. Chen, and J. Lee, “Review and recent advances in battery health monitoring and prognostics technologies for electric vehicle (EV) safety and mobility,” *J Power Sources*, vol. 256, pp. 110–124, Jun. 2014, doi: 10.1016/j.jpowsour.2014.01.085.
- [137] M. Shen and Q. Gao, “A review on battery management system from the modeling efforts to its multiapplication and integration,” *Int J Energy Res*, vol. 43, no. 10, pp. 5042–5075, Aug. 2019, doi: 10.1002/er.4433.
- [138] V. Myilsamy, S. Sengan, R. Alroobaea, and M. Alsafyani, “State-of-Health Prediction for Li-ion Batteries for Efficient Battery Management System Using Hybrid Machine Learning Model,” *Journal of Electrical Engineering & Technology*, vol. 19, no. 1, pp. 585–600, Jan. 2024, doi: 10.1007/s42835-023-01564-2.

- [139] Z. Li, Y. Zhou, C. Guo, Y. Dang, X. Ji, and G. He, “Uneven Usage Battery State of Health Estimation via Fractional-Order Equivalent Circuit Model and AutoML Fusion,” *J Electrochem Soc*, vol. 171, no. 4, p. 040543, Apr. 2024, doi: 10.1149/1945-7111/ad3eb9.
- [140] J. Li, L. Wang, C. Lyu, E. Liu, Y. Xing, and M. Pecht, “A parameter estimation method for a simplified electrochemical model for Li-ion batteries,” *Electrochim Acta*, vol. 275, pp. 50–58, Jun. 2018, doi: 10.1016/j.electacta.2018.04.098.
- [141] S. C. Chen, C. C. Wan, and Y. Y. Wang, “Thermal analysis of lithium-ion batteries,” *J Power Sources*, vol. 140, no. 1, pp. 111–124, Jan. 2005, doi: 10.1016/j.jpowsour.2004.05.064.
- [142] E. Prada, D. Di Domenico, Y. Creff, J. Bernard, V. Sauvant-Moynot, and F. Huet, “Simplified Electrochemical and Thermal Model of LiFePO₄-Graphite Li-Ion Batteries for Fast Charge Applications,” *J Electrochem Soc*, vol. 159, no. 9, pp. A1508–A1519, Jan. 2012, doi: 10.1149/2.064209jes.
- [143] X. Hu, F. Feng, K. Liu, L. Zhang, J. Xie, and B. Liu, “State estimation for advanced battery management: Key challenges and future trends,” *Renewable and Sustainable Energy Reviews*, vol. 114, p. 109334, Oct. 2019, doi: 10.1016/j.rser.2019.109334.
- [144] Y. Song, D. Liu, C. Yang, and Y. Peng, “Data-driven hybrid remaining useful life estimation approach for spacecraft lithium-ion battery,” *Microelectronics Reliability*, vol. 75, pp. 142–153, Aug. 2017, doi: 10.1016/j.microrel.2017.06.045.
- [145] Z. Deng, L. Yang, Y. Cai, H. Deng, and L. Sun, “Online available capacity prediction and state of charge estimation based on advanced data-driven algorithms for lithium iron phosphate battery,” *Energy*, vol. 112, pp. 469–480, Oct. 2016, doi: 10.1016/j.energy.2016.06.130.
- [146] L. Su, M. Wu, Z. Li, and J. Zhang, “Cycle life prediction of lithium-ion batteries based on data-driven methods,” *eTransportation*, vol. 10, p. 100137, Nov. 2021, doi: 10.1016/j.etrans.2021.100137.
- [147] H. Pang, K. Chen, Y. Geng, L. Wu, F. Wang, and J. Liu, “Accurate capacity and remaining useful life prediction of lithium-ion batteries based on improved particle swarm optimization and particle filter,” *Energy*, vol. 293, p. 130555, Apr. 2024, doi: 10.1016/j.energy.2024.130555.
- [148] X. Chen, Z. Liu, H. Sheng, J. Mi, X. Tang, and Q. Li, “A data reconstruction-based Monte Carlo method for remaining useful life prediction of lithium-ion battery with few historical samples,” *J Power Sources*, vol. 589, p. 233760, Jan. 2024, doi: 10.1016/j.jpowsour.2023.233760.
- [149] J. Zhao, X. Feng, M.-K. Tran, M. Fowler, M. Ouyang, and A. F. Burke, “Battery safety: Fault diagnosis from laboratory to real world,” *J Power Sources*, vol. 598, p. 234111, Apr. 2024, doi: 10.1016/j.jpowsour.2024.234111.

- [150] R. Xiong, W. Sun, Q. Yu, and F. Sun, “Research progress, challenges and prospects of fault diagnosis on battery system of electric vehicles,” *Appl Energy*, vol. 279, p. 115855, Dec. 2020, doi: 10.1016/j.apenergy.2020.115855.
- [151] Q. Wang, P. Ping, X. Zhao, G. Chu, J. Sun, and C. Chen, “Thermal runaway caused fire and explosion of lithium ion battery,” *J Power Sources*, vol. 208, pp. 210–224, Jun. 2012, doi: 10.1016/j.jpowsour.2012.02.038.
- [152] J. Marcicki, S. Onori, and G. Rizzoni, “Nonlinear Fault Detection and Isolation for a Lithium-Ion Battery Management System,” in *ASME 2010 Dynamic Systems and Control Conference, Volume 1*, ASMEDC, Jan. 2010, pp. 607–614. doi: 10.1115/DSCC2010-4085.
- [153] C. Zheng, Y. Ge, Z. Chen, D. Huang, J. Liu, and S. Zhou, “Diagnosis Method for Li-Ion Battery Fault Based on an Adaptive Unscented Kalman Filter,” *Energies (Basel)*, vol. 10, no. 11, p. 1810, Nov. 2017, doi: 10.3390/en10111810.
- [154] Z. Liu, H. He, Q. Ahmed, and G. Rizzoni, “Structural Analysis Based Fault Detection and Isolation Applied for A Lithium-Ion Battery Pack,” *IFAC-PapersOnLine*, vol. 48, no. 21, pp. 1465–1470, 2015, doi: 10.1016/j.ifacol.2015.09.731.
- [155] Y. Shang, G. Lu, Y. Kang, Z. Zhou, B. Duan, and C. Zhang, “A multi-fault diagnosis method based on modified Sample Entropy for lithium-ion battery strings,” *J Power Sources*, vol. 446, p. 227275, Jan. 2020, doi: 10.1016/j.jpowsour.2019.227275.
- [156] A. Naha *et al.*, “Internal short circuit detection in Li-ion batteries using supervised machine learning,” *Sci Rep*, vol. 10, no. 1, p. 1301, Jan. 2020, doi: 10.1038/s41598-020-58021-7.
- [157] Y. Zhao, P. Liu, Z. Wang, L. Zhang, and J. Hong, “Fault and defect diagnosis of battery for electric vehicles based on big data analysis methods,” *Appl Energy*, vol. 207, pp. 354–362, Dec. 2017, doi: 10.1016/j.apenergy.2017.05.139.
- [158] R. Xiong, L. Li, and J. Tian, “Towards a smarter battery management system: A critical review on battery state of health monitoring methods,” *J Power Sources*, vol. 405, pp. 18–29, Nov. 2018, doi: 10.1016/j.jpowsour.2018.10.019.
- [159] T. Kim, D. Makwana, A. Adhikaree, J. Vagdoda, and Y. Lee, “Cloud-Based Battery Condition Monitoring and Fault Diagnosis Platform for Large-Scale Lithium-Ion Battery Energy Storage Systems,” *Energies (Basel)*, vol. 11, no. 1, p. 125, Jan. 2018, doi: 10.3390/en11010125.
- [160] W. Li, M. Rentemeister, J. Badeda, D. Jöst, D. Schulte, and D. U. Sauer, “Digital twin for battery systems: Cloud battery management system with online state-of-charge and state-of-health estimation,” *J Energy Storage*, vol. 30, p. 101557, Aug. 2020, doi: 10.1016/j.est.2020.101557.

- [161] S. Yang *et al.*, “Implementation for a cloud battery management system based on the CHAIN framework,” *Energy and AI*, vol. 5, p. 100088, Sep. 2021, doi: 10.1016/j.egyai.2021.100088.
- [162] A. L. Beam and I. S. Kohane, “Big Data and Machine Learning in Health Care,” *JAMA*, vol. 319, no. 13, p. 1317, Apr. 2018, doi: 10.1001/jama.2017.18391.
- [163] A. Nuhic, T. Terzimehic, T. Soczka-Guth, M. Buchholz, and K. Dietmayer, “Health diagnosis and remaining useful life prognostics of lithium-ion batteries using data-driven methods,” *J Power Sources*, vol. 239, pp. 680–688, Oct. 2013, doi: 10.1016/j.jpowsour.2012.11.146.
- [164] X. Li, C. Yuan, X. Li, and Z. Wang, “State of health estimation for Li-Ion battery using incremental capacity analysis and Gaussian process regression,” *Energy*, vol. 190, p. 116467, Jan. 2020, doi: 10.1016/j.energy.2019.116467.
- [165] R. Yang, R. Xiong, S. Ma, and X. Lin, “Characterization of external short circuit faults in electric vehicle Li-ion battery packs and prediction using artificial neural networks,” *Appl Energy*, vol. 260, p. 114253, Feb. 2020, doi: 10.1016/j.apenergy.2019.114253.
- [166] H. Dai, G. Zhao, M. Lin, J. Wu, and G. Zheng, “A Novel Estimation Method for the State of Health of Lithium-Ion Battery Using Prior Knowledge-Based Neural Network and Markov Chain,” *IEEE Transactions on Industrial Electronics*, vol. 66, no. 10, pp. 7706–7716, Oct. 2019, doi: 10.1109/TIE.2018.2880703.
- [167] P. Singh, R. Vinjamuri, X. Wang, and D. Reisner, “Fuzzy logic modeling of EIS measurements on lithium-ion batteries,” *Electrochim Acta*, vol. 51, no. 8–9, pp. 1673–1679, Jan. 2006, doi: 10.1016/j.electacta.2005.02.143.
- [168] S. Ould Amrouche, D. Rekioua, T. Rekioua, and S. Bacha, “Overview of energy storage in renewable energy systems,” *Int J Hydrogen Energy*, vol. 41, no. 45, pp. 20914–20927, Dec. 2016, doi: 10.1016/j.ijhydene.2016.06.243.
- [169] M. Tran *et al.*, “Python-based scikit-learn machine learning models for thermal and electrical performance prediction of high-capacity lithium-ion battery,” *Int J Energy Res*, vol. 46, no. 2, pp. 786–794, Feb. 2022, doi: 10.1002/er.7202.
- [170] J. Xie and Y.-C. Lu, “A retrospective on lithium-ion batteries,” *Nat Commun*, vol. 11, no. 1, p. 2499, May 2020, doi: 10.1038/s41467-020-16259-9.
- [171] S. Barcellona and L. Piegari, “Effect of current on cycle aging of lithium ion batteries,” *J Energy Storage*, vol. 29, p. 101310, Jun. 2020, doi: 10.1016/j.est.2020.101310.
- [172] M. Dubarry, N. Vuillaume, and B. Y. Liaw, “From single cell model to battery pack simulation for Li-ion batteries,” *J Power Sources*, vol. 186, no. 2, pp. 500–507, Jan. 2009, doi: 10.1016/j.jpowsour.2008.10.051.

- [173] L. Zhou, Y. Zheng, M. Ouyang, and L. Lu, “A study on parameter variation effects on battery packs for electric vehicles,” *J Power Sources*, vol. 364, pp. 242–252, Oct. 2017, doi: 10.1016/j.jpowsour.2017.08.033.
- [174] D. J. Rogers, L. J. M. Aslett, and M. C. M. Troffaes, “Modelling of modular battery systems under cell capacity variation and degradation,” *Appl Energy*, vol. 283, p. 116360, Feb. 2021, doi: 10.1016/j.apenergy.2020.116360.
- [175] K. M. Winslow, S. J. Laux, and T. G. Townsend, “A review on the growing concern and potential management strategies of waste lithium-ion batteries,” *Resour Conserv Recycl*, vol. 129, pp. 263–277, Feb. 2018, doi: 10.1016/j.resconrec.2017.11.001.
- [176] E. Hossain, D. Murtaugh, J. Mody, H. M. R. Faruque, Md. S. Haque Sunny, and N. Mohammad, “A Comprehensive Review on Second-Life Batteries: Current State, Manufacturing Considerations, Applications, Impacts, Barriers & Potential Solutions, Business Strategies, and Policies,” *IEEE Access*, vol. 7, pp. 73215–73252, 2019, doi: 10.1109/ACCESS.2019.2917859.
- [177] S. B. Peterson, J. F. Whitacre, and J. Apt, “The economics of using plug-in hybrid electric vehicle battery packs for grid storage,” *J Power Sources*, vol. 195, no. 8, pp. 2377–2384, Apr. 2010, doi: 10.1016/j.jpowsour.2009.09.070.
- [178] M. Foster, P. Isely, C. R. Standridge, and M. M. Hasan, “Feasibility assessment of remanufacturing, repurposing, and recycling of end of vehicle application lithium-ion batteries,” *Journal of Industrial Engineering and Management*, vol. 7, no. 3, Jun. 2014, doi: 10.3926/jiem.939.
- [179] A. Kampker, S. Wessel, F. Fiedler, and F. Maltoni, “Battery pack remanufacturing process up to cell level with sorting and repurposing of battery cells,” *Journal of Remanufacturing*, vol. 11, no. 1, pp. 1–23, Apr. 2021, doi: 10.1007/s13243-020-00088-6.
- [180] M. Mathew, Q. H. Kong, J. McGrory, and M. Fowler, “Simulation of lithium ion battery replacement in a battery pack for application in electric vehicles,” *J Power Sources*, vol. 349, pp. 94–104, May 2017, doi: 10.1016/j.jpowsour.2017.03.010.
- [181] N. G. Nenadic, T. A. Trabold, and M. G. Thurston, “Cell Replacement Strategies for Lithium Ion Battery Packs,” *Batteries*, vol. 6, no. 3, p. 39, Jul. 2020, doi: 10.3390/batteries6030039.
- [182] Y. Lu *et al.*, “A method of cell-to-cell variation evaluation for battery packs in electric vehicles with charging cloud data,” *eTransportation*, vol. 6, p. 100077, Nov. 2020, doi: 10.1016/j.etrans.2020.100077.
- [183] Z. B. Omariba, L. Zhang, and D. Sun, “Review of Battery Cell Balancing Methodologies for Optimizing Battery Pack Performance in Electric Vehicles,” *IEEE Access*, vol. 7, pp. 129335–129352, 2019, doi: 10.1109/ACCESS.2019.2940090.

- [184] M. M. U. Rehman, F. Zhang, M. Evzelman, R. Zane, K. Smith, and D. Maksimovic, “Advanced cell-level control for extending electric vehicle battery pack lifetime,” in *2016 IEEE Energy Conversion Congress and Exposition (ECCE)*, IEEE, Sep. 2016, pp. 1–8. doi: 10.1109/ECCE.2016.7854827.
- [185] Y. Zheng, M. Ouyang, L. Lu, and J. Li, “Understanding aging mechanisms in lithium-ion battery packs: From cell capacity loss to pack capacity evolution,” *J Power Sources*, vol. 278, pp. 287–295, Mar. 2015, doi: 10.1016/j.jpowsour.2014.12.105.
- [186] Jeffrey R. Belt, “Battery Test Manual For Plug-In Hybrid Electric Vehicles,” Dec. 2010. doi: 10.2172/1010675.
- [187] Z. Deng, X. Hu, X. Lin, L. Xu, Y. Che, and L. Hu, “General Discharge Voltage Information Enabled Health Evaluation for Lithium-Ion Batteries,” *IEEE/ASME Transactions on Mechatronics*, vol. 26, no. 3, pp. 1295–1306, Jun. 2021, doi: 10.1109/TMECH.2020.3040010.
- [188] J. Schmalstieg, S. Käbitz, M. Ecker, and D. U. Sauer, “A holistic aging model for Li(NiMnCo)O₂ based 18650 lithium-ion batteries,” *J Power Sources*, vol. 257, pp. 325–334, Jul. 2014, doi: 10.1016/j.jpowsour.2014.02.012.
- [189] H. Gabbar, A. Othman, and M. Abdussami, “Review of Battery Management Systems (BMS) Development and Industrial Standards,” *Technologies (Basel)*, vol. 9, no. 2, p. 28, Apr. 2021, doi: 10.3390/technologies9020028.
- [190] S. S. Lee, T. H. Kim, S. J. Hu, W. W. Cai, and J. A. Abell, “Joining Technologies for Automotive Lithium-Ion Battery Manufacturing: A Review,” in *ASME 2010 International Manufacturing Science and Engineering Conference, Volume 1*, ASMEDC, Jan. 2010, pp. 541–549. doi: 10.1115/MSEC2010-34168.
- [191] M. Wentker, M. Greenwood, and J. Leker, “A Bottom-Up Approach to Lithium-Ion Battery Cost Modeling with a Focus on Cathode Active Materials,” *Energies (Basel)*, vol. 12, no. 3, p. 504, Feb. 2019, doi: 10.3390/en12030504.
- [192] M. Bercibar, I. Gandiaga, I. Villarreal, N. Omar, J. Van Mierlo, and P. Van den Bossche, “Critical review of state of health estimation methods of Li-ion batteries for real applications,” *Renewable and Sustainable Energy Reviews*, vol. 56, pp. 572–587, Apr. 2016, doi: 10.1016/j.rser.2015.11.042.
- [193] L. Ungurean, G. Cârstoiu, M. V. Micea, and V. Groza, “Battery state of health estimation: a structured review of models, methods and commercial devices,” *Int J Energy Res*, vol. 41, no. 2, pp. 151–181, Feb. 2017, doi: 10.1002/er.3598.
- [194] L. Fan, P. Wang, and Z. Cheng, “A remaining capacity estimation approach of lithium-ion batteries based on partial charging curve and health feature fusion,” *J Energy Storage*, vol. 43, p. 103115, Nov. 2021, doi: 10.1016/j.est.2021.103115.

- [195] M. Cao, Y. Liu, T. Zhang, Y. Wang, R. Wang, and Z. Shi, “A flexible battery capacity estimation method based on partial voltage curves and polynomial fitting,” *Energy Build*, vol. 290, p. 113045, Jul. 2023, doi: 10.1016/j.enbuild.2023.113045.
- [196] J. Yao and T. Han, “Data-driven lithium-ion batteries capacity estimation based on deep transfer learning using partial segment of charging/discharging data,” *Energy*, vol. 271, p. 127033, May 2023, doi: 10.1016/j.energy.2023.127033.
- [197] Z. Lyu, R. Gao, and X. Li, “A partial charging curve-based data-fusion-model method for capacity estimation of Li-Ion battery,” *J Power Sources*, vol. 483, p. 229131, Jan. 2021, doi: 10.1016/j.jpowsour.2020.229131.
- [198] J. Tian, R. Xiong, W. Shen, J. Lu, and F. Sun, “Flexible battery state of health and state of charge estimation using partial charging data and deep learning,” *Energy Storage Mater*, vol. 51, pp. 372–381, Oct. 2022, doi: 10.1016/j.ensm.2022.06.053.
- [199] Q. Xue, J. Li, Z. Chen, Y. Zhang, Y. Liu, and J. Shen, “Online Capacity Estimation of Lithium-Ion Batteries Based on Deep Convolutional Time Memory Network and Partial Charging Profiles,” *IEEE Trans Veh Technol*, vol. 72, no. 1, pp. 444–457, Jan. 2023, doi: 10.1109/TVT.2022.3205439.
- [200] J. He, S. Meng, X. Li, and F. Yan, “Partial Charging-Based Health Feature Extraction and State of Health Estimation of Lithium-Ion Batteries,” *IEEE J Emerg Sel Top Power Electron*, vol. 11, no. 1, pp. 166–174, Feb. 2023, doi: 10.1109/JESTPE.2022.3143831.
- [201] J. Schmitt, M. Rehm, A. Karger, and A. Jossen, “Capacity and degradation mode estimation for lithium-ion batteries based on partial charging curves at different current rates,” *J Energy Storage*, vol. 59, p. 106517, Mar. 2023, doi: 10.1016/j.est.2022.106517.
- [202] Y. Wu and J. Feng, “Development and Application of Artificial Neural Network,” *Wirel Pers Commun*, vol. 102, no. 2, pp. 1645–1656, Sep. 2018, doi: 10.1007/s11277-017-5224-x.
- [203] W. Loh, “Fifty Years of Classification and Regression Trees,” *International Statistical Review*, vol. 82, no. 3, pp. 329–348, Dec. 2014, doi: 10.1111/insr.12016.
- [204] H. Tyralis and G. Papacharalampous, “Boosting algorithms in energy research: a systematic review,” *Neural Comput Appl*, vol. 33, no. 21, pp. 14101–14117, Nov. 2021, doi: 10.1007/s00521-021-05995-8.
- [205] Z. Arif Ali, Z. H. Abduljabbar, H. A. Tahir, A. Bibo Sallow, and S. M. Almufti, “eXtreme Gradient Boosting Algorithm with Machine Learning: a Review,” *Academic Journal of Nawroz University*, vol. 12, no. 2, pp. 320–334, May 2023, doi: 10.25007/ajnu.v12n2a1612.
- [206] J. T. Hancock and T. M. Khoshgoftaar, “CatBoost for big data: an interdisciplinary review,” *J Big Data*, vol. 7, no. 1, p. 94, Dec. 2020, doi: 10.1186/s40537-020-00369-8.

- [207] G. Biau and E. Scornet, “A random forest guided tour,” *TEST*, vol. 25, no. 2, pp. 197–227, Jun. 2016, doi: 10.1007/s11749-016-0481-7.
- [208] F. von Bülow and T. Meisen, “A review on methods for state of health forecasting of lithium-ion batteries applicable in real-world operational conditions,” *J Energy Storage*, vol. 57, p. 105978, Jan. 2023, doi: 10.1016/j.est.2022.105978.